HYDRAULIC TESTS ON A XBLOCPLUS ARMOURED COASTAL REVETMENT

A THESIS SUBMITTED TO
THE GRADUATE SCHOOL OF NATURAL AND APPLIED SCIENCES
OF
MIDDLE EAST TECHNICAL UNIVERSITY

BY

ALPEREN MÜLAYİM KORKMAZ

IN PARTIAL FULFILLMENT OF THE REQUIREMENTS
FOR
THE DEGREE OF MASTER OF SCIENCE
IN
CIVIL ENGINEERING

SEPTEMBER 2024

Approval of the thesis:

HYDRAULIC TESTS ON A XBLOCPLUS ARMOURED COASTAL REVETMENT

submitted by **ALPEREN MÜLAYİM KORKMAZ** in partial fulfillment of the requirements for the degree of **Master of Science** i**n Civil Engineering, Middle East Technical University** by,

Prof. Dr. Naci Emre Altun
Dean, **Graduate School of Natural and Applied Sciences** _____

Prof. Dr. Erdem Canbay
Head of the Department, **Civil Engineering** _____

Assist. Prof. Dr. Hasan Gökhan Güler
Supervisor, **Civil Engineering, METU** _____

Assist. Prof. Dr. Cüneyt Baykal
Co-Supervisor, **Civil Engineering, METU** _____

Examining Committee Members:

Assist. Prof. Dr. Gülizar Özyurt Tarakcıoğlu
Civil Engineering, METU _____

Assist. Prof. Dr. Hasan Gökhan Güler
Civil Engineering, METU _____

Assist. Prof. Dr. Cüneyt Baykal
Civil Engineering, METU _____

Assoc. Prof. Dr. Elif Oğuz
Civil Engineering, METU _____

Prof. Dr. Kubilay Cihan
Civil Engineering, Kırıkkale University _____

Date: 02.09.2024

I hereby declare that all information in this document has been obtained and presented in accordance with academic rules and ethical conduct. I also declare that, as required by these rules and conduct, I have fully cited and referenced all material and results that are not original to this work.

Name Last name: Alperen Mülayim Korkmaz

Signature:

ABSTRACT

HYDRAULIC TESTS ON A XBLOCPLUS ARMOURED COASTAL REVETMENT

Korkmaz, Alperen Mülayim
Master of Science, Civil Engineering
Supervisor: Assist. Prof. Dr. Hasan Gökhan Güler
Co-Supervisor: Assist. Prof. Dr. Cüneyt Baykal

September 2024, 111 pages

In the present study, the performance of recently developed XblocPlus® and XblocPlusOvertop® units is investigated by physical model experiments for different coastal revetment cross-sections at METU Coastal and Ocean Engineering Laboratory. The interlocking of XblocPlus® units is primarily designed to improve armour layer stability compared to Xbloc® units, whereas XblocPlusOvertop® units aim to reduce wave overtopping discharges. The cross-sections are constructed in the wave flume on a flat region following a 1:30 foreshore bottom slope. The face slopes of the revetment sections are kept constant as 1:1.5 for all cases. Different water depths, crest heights, crest widths, toe units, and armour layer configurations are tested under eight different wave conditions to observe the performance of a coastal revetment in detail. During the physical model experiments, the stability of the armour and toe layer, forces acting on the crown wall, mean wave overtopping discharges, and overtopping-induced scour at the lee side of the structure are observed simultaneously. Differences in the hydraulic performances of cross-

sections constructed with and without XblocPlusOvertop® units under various experimental conditions are discussed, highlighting the effects on the toe region.

Keywords: Coastal Revetment, XblocPlus®, XblocPlusOvertop®, Hydraulic Stability, Overtopping

ÖZ

XBLOCPLUS KORUMA TABAKALI BİR KIYI TAHKİMATININ HİDROLİK TESTLERİ

Korkmaz, Alperen Mülayim
Yüksek Lisans, İnşaat Mühendisliği
Tez Yöneticisi: Dr. Öğr. Üyesi Hasan Gökhan Güler
Ortak Tez Yöneticisi: Dr. Öğr. Üyesi Cüneyt Baykal

Eylül 2024, 111 sayfa

Bu çalışmada, yeni geliştirilen XblocPlus® ve XblocPlusOvertop® birimlerinin performansı, ODTÜ Kıyı ve Deniz Mühendisliği Laboratuvarı'nda farklı kıyı tahkimatı kesitleri için fiziksel model deneyleri ile araştırılmıştır. XblocPlus® ünitelerinin birbirine kenetlenmesi öncelikle Xbloc® ünitelerine kıyasla koruma tabakası stabilitesini artırmak için tasarlanmıştır; XblocPlusOvertop® üniteleri ise dalga aşma debisini azaltmayı amaçlamaktadır. Kesitler, kıyıya doğru 1:30'luk bir taban eğimini takip eden düz bir bölgedeki dalga kanalında inşa edilmiştir. Kıyı tahkimatlarının yüz eğimleri tüm durumlarda 1:1,5 oranında sabit tutulmuştur. Kıyı tahkimatının performansını ayrıntılı olarak gözlemlemek için farklı su derinlikleri, kret yükseklikleri, kret genişlikleri, topuk birimleri ve koruma tabakası konfigürasyonları sekiz farklı dalga koşulu altında test edilmiştir. Fiziksel model deneyleri sırasında, koruma ve topuk tabakasının stabilitesi, kronman duvarına etki eden kuvvetler, ortalama dalga aşmaları ve yapının arka tarafında dalga aşması kaynaklı oyulma eş zamanlı olarak gözlemlenmiştir. Çeşitli deney koşulları altında XblocPlusOvertop® üniteleri ile ve XblocPlusOvertop® üniteleri olmadan inşa edilen

kesitlerin hidrolik performanslarındaki farklılıklar tartışılarak topuk bölgesi üzerindeki etkiler vurgulanmıştır.

Anahtar Kelimeler: Kıyı Tahkimatı, XblocPlus®, XblocPlusOvertop®, Hidrolik Stabilite, Dalga Aşması

To the heroes who keep the homeland alive…

ACKNOWLEDGMENTS

I would like to express my deepest gratitude and respect to my supervisor, Assist. Prof. Dr. Hasan Gökhan Güler for his guidance, advice, criticism, encouragement, and insight throughout the research. I am also grateful to him for sharing his experiences and guiding me in my future plans. I also thank him for trusting me in my work and supporting me under all circumstances. I want to thank him for being there for me and teaching me whenever I needed help, not only in my academic career but also in my life. I also thank him for supporting me and patiently providing me many opportunities.

I would also like to thank my co-supervisor, Assist. Prof. Dr. Cüneyt Baykal for his guidance, advice, criticism, encouragement, and insight throughout the research. I would like to thank him for providing me with many opportunities, supporting me, and patiently teaching me many things to improve myself. Also, I would like to thank him for trusting me with the projects and teaching me how to think like an engineer.

I would like to thank Prof. Dr. Ayşen Ergin for teaching the fundamentals of coastal and ocean engineering and contributing to my interest in this field. I would also like to thank her for the visions she brought to us. Thank her for teaching us not only how to be engineers but also how to be good individuals. It is a privilege and pride to be her student.

I would like to thank Assist. Prof. Dr. Gülizar Özyurt Tarakcıoğlu for imparting her knowledge and experience from my undergraduate courses and for increasing my interest in the field of coastal and ocean engineering. I would also like to thank her for supporting and guiding me throughout my graduate studies.

I would like to thank Dr. Işıkhan Güler for his contributions and teaching throughout the lessons I took from him. I would also like to thank him for sharing his experiences.

I would like to thank Prof. Dr. Ahmet Cevdet Yalçıner for helping me improve myself with the lessons I took from him and the international projects I had the opportunity to participate in as one of his students.

I would like to thank Assoc. Prof. Dr. Onur Pekcan very much for helping me in every aspect as my advisor during my undergraduate education and for adding vision to me by sharing his experiences and knowledge. He always supported me and offered me opportunities to make the right decisions for my future. I am also grateful to him for always being by my side, supporting and guiding me throughout my graduate education.

I would like to thank Zeynep Kut for being with me at every moment, supporting me, and understanding me. I am so lucky that I can share everything with her, and she always makes me feel better with her ideas. She always supported me to achieve better. She gave me all the help she could. I thank her for everything.

I would like to thank Furkan Demir for sharing his experiences and knowledge with me since the beginning of my laboratory work. During the good times we spent, I learned a lot from him and had a delightful time. I am pleased about this friendship, which I believe will continue throughout my life. I would also like to thank Berkay Erler for always being there for me, helping me, and sharing his knowledge. Another person I want to thank is Cem Sevindik, who helped me a lot during the difficult times I went through. He always tried to make my work easier during my long and intense working period. I would also like to thank him for the conversations and sharing we had during the time we spent together in the laboratory day and night. I would also like to thank Mert Yaman and Barış Ufuk Şentürk, who helped me and were there when I needed help. I feel thrilled to have met such valuable people and to call them my friends.

I would like to thank Arif Çağatay Uysal for the beautiful friendship we have established. He was always with me during my thesis writing process, and we worked together. We shared our feelings and supported each other. I thank him for

this beautiful friendship and always being there for me. I would also like to thank Görkem Kılıç for never leaving me alone, for his help, and for his friendship. I am grateful to him for making the environment we work in better for all of us and for taking care of us. I would also like to thank Ayşenur Gökdağ, who believed in me, supported me, and stood by me both in my work and in my daily life. I thank her for everything and her friendship during my undergraduate and graduate studies.

I would like to thank my friends Bilge Karakütük, Akdeniz İnce, Setenay Özaslan, and İremnaz Kösem, with whom I worked in the laboratory.

I would like to thank Yusuf Korkut, Servet Şeherli, Eyüp Uğur, Nuray Çimen Emre, and Ayhan Karadeniz for the help they gave me throughout my thesis work.

I would like to thank my family, Serpil Korkmaz, Nadir Korkmaz, Sena Yılmaz, Turhan Yılmaz, and İnci Güneş Yılmaz. They were with me and trusted me at every moment of my life. I thank them for always supporting me in becoming better. I would like to express my gratitude to my family, to whom I owe everything I have achieved. I am very lucky and happy to have them.

I would like to thank my friends Doğukan Kaya, Ömer Karakaya, and Ümit Korkunç, whom I met during my undergraduate education and whom I have always trusted since this process. I thank them for always being there for me and understanding me. I would also like to thank Hüseyin Mert Alkan, Melis Sayın, Ahmet Emir Pir, Eren Volkan Küçük, İbrahim Gider, and Emir Yavuz for supporting me and being by my side during this process.

This thesis study is partially funded by METU-DOSIM (Project No: 2023-03-03-2-02-174) in the scope of a consultancy project.

TABLE OF CONTENTS

LIST OF TABLES

TABLES

LIST OF FIGURES

FIGURES

LIST OF ABBREVIATIONS

ABBREVIATIONS

AYGM	General Directorate of Infrastructure Investments
CERC	Coastal Engineering Research Center
CIRIA	Construction Industry Research and Information Association
DMC	DMC Marine Consultants
HWL	High water level
IPCC	Intergovernmental Panel on Climate Change
LWL	Low water level
MAE	Mean absolute error
MALE	Mean absolute logarithmic error
RMSE	Root mean square error
RMSLE	Root mean square logarithmic error
SPM	Shore Protection Manual
SSP	Shared socio-economic pathways
SWL	Still water level
UK	United Kingdom
WG	Wave gauge
WOS	Wave overtopping simulator
XP	XblocPlus®
XP-OT	XblocPlusOvertop®

LIST OF SYMBOLS

SYMBOLS

α	Angle of breakwater armour slope
γ_β	Obliquity factor
γ_f	Roughness factor
γ_z	Correction factor for crest width
λ_L	Length scale
λ_t	Time scale
λ_w	Weight scale
Δ	Relative buoyant density
ξ_m	Local surf similarity parameter corresponding to mean wave period
η	Water surface profile
ρ_r	Density of rock
ρ_w	Density of water
A_c	Armour crest freeboard
B	Crest berm width
CO_2	Carbon dioxide
D_{n50}	Mean nominal diameter of the stone
d_{50}	Mean diameter of the sand
f	Friction coefficient

f_c	Unprotected part of the crown wall front face
F_G	Weight of buoyancy-reduced crown wall structure
F_H	Wave-induced horizontal force on crown wall
$F_{H,0.1\%}$	Horizontal wave force per meter acting on crown wall exceeded by 0.1% of the waves
F_r	Froud number
F_U	Wave-induced uplift force
G_c	Crest width
g	Gravitational acceleration
h	Water depth
H	Wave height
$H_{1/10}$	Wave height exceeded by 10% of waves in a storm
H_{m0}	Spectral significant wave height
H_{max}	Maximum wave height
H_s	Significant wave height
h_f	Crown wall height
h_{prot}	Protected part of the crown wall front face
h_t	Depth of the toe
H_s	Significant wave height
Hz	Hertz
K_D	Stability coefficient
kHz	Kilohertz

L_m	Length in the model scale
L_{om}	Deep water wavelength corresponding to mean wave period
L_p	Length in the prototype scale
M_{50}	Median armour unit mass
M_G	Moment due to the weight of the crown wall
M_H	Moment due to horizontal forces
$M_{H,0.1\%}$	Overturning moment exceeded by 0.1% of the waves
$M_{prototype}$	Weight of the unit in prototype scale
M_U	Moment due to uplift force
N	Number of waves
N_d	Percentage damage number
N_{od}	Damage number
N_s	Stability number
N_f	Number of relocated units
N_{total}	Total number of units
p_m	Stagnation pressure at crown wall face due to wave impact
$p_{U,0.1\%}$	Uplift wave pressure at crown wall base exceeded by 0.1% of the waves
q	Overtopping discharge
q^*	Densimetric overtopping discharge
q_{mean}	Mean overtopping discharge

R_c	Crest freeboard of structure
$R_{u,0.1\%}$	Wave run-up level exceeded by 0.1% of incident waves
S	Scour depth
$T_{m-1,0}$	Spectral mean wave period defined by m_{-1}/m_0
t_m	Time in model scale
t_p	Time in prototype scale
T_p	Peak wave period
T_s	Significant wave period
V	Pedersen reduction factor for wave impact
$V_{XblocPlus}$	Volume of XblocPlus®
y	Vertical run-up wedge thickness
y_{eff}	Effective wave pressure impact zone height

CHAPTER 1

INTRODUCTION

Coastal regions are crucial for societies because of their economic, ecological, and social values. Fisheries, oil and gas potential underneath the seas, and mineral extraction activities provide additional economic opportunities to people near the coastline. In addition, tourism and cultural and historical places enhance the economic potential of coastal regions. On the other hand, marine animals and plants create an environment in these regions. These living beings play a critical role in the food chain. By considering these aspects, coastal regions become more important for human beings. Thus, protecting coasts against disasters and extreme events is important for both economic and social activities.

Breakwaters, coastal revetments, dikes, jetties, and groins are some examples of coastal structures constructed to protect coastal areas and properties. Understanding wave action on these structures is an important and difficult task to design these coastal structures more efficiently and safely.

Coastal revetments are one of the most widely used structures in coastal engineering applications, briefly summarized above. This type of structure is generally used to prevent coastal erosion and flooding. Moreover, coastal revetments protect the infrastructure and residential areas near the shoreline from wave attacks. Increasing water levels due to climate change makes coastal regions more vulnerable to wave overtopping and creates additional risks for society near the coastline. According to the IPCC report (Calvin et al., 2023), the global sea level rise is predicted to be up to 1 meter by the year 2100, which is the SSP5-8.5 scenario. This significant change makes the coastal revetment design process more important for future projects. Thus,

understanding the hydraulic performance and design details of coastal revetments plays a crucial role in providing safety and availability to society.

There are different aspects in the design of coastal revetments. The armour layer is one of the most important sections for coastal revetment stability, serviceability, and performance. Increasing wave heights and water levels increase the demand for armour unit sizes. Thus, using artificial concrete armour units is becoming more popular and necessary for coastal structures. Different artificial units perform differently in terms of stability due to changing interlocking properties. Differences between concrete armour units cause different overtopping performances. This situation affects the serviceability of the structure. Armour layer design and performance analyses for coastal revetments can be considered similar to breakwater trunk sections. Numerous different artificial units are being used in the coastal structures. These units are being developed and new units are designed to enhance the performance of coastal structures.

Xbloc® and XblocPlus® units are examples of recently developed armour units for coastal engineering applications. These units are developed by DMC Marine Consultants to provide more resilient structures against climate change by lowering the CO_2 footprint (Xbloc, 2024). Less concrete consumption and less unit need for a project can be achieved by using this new type of unit (Jacobs et al., 2018). Thus, this unit is more economical and environmentally friendly unit than traditional units. XblocPlus® units are designed for straight sections such as coastal revetments. Due to the geometry of these units, increasing the armour stability performance is aimed. Also, the overtopping performance of the structure is enhanced with XblocPlus® and XbloxPlusOvertop® units. XbloxPlusOvertop® units are specially designed to reduce the overtopping discharge and increase the serviceability performance of the structure. Geometrical properties and differences between these two concrete units are described in Chapter 2.

Contrary to more common artificial units such as Antifer and tetrapod, there is limited research on Xbloc® and XblocPlus® units. Because of this limitation, this

thesis focuses on the performance of XblocPlus® units. The stability of armour and toe sections, forces acting on the crown wall, mean overtopping discharge, and overtopping induced scour at the lee side of the revetment are investigated to determine the effects and performance of this recently developed artificial unit type. Investigations are carried out in the scope of a consultancy project for a coastal revetment located in the Black Sea Region in Türkiye. Thus, all investigations are evaluated within a case study.

In the scope of this study, the performance of recently developed XblocPlus® and XblocPlusOvertop® units is investigated, and the following research questions are tried to be answered:

i. How do XblocPlus® and XblocPlusOvertop® units perform on armour stability?
ii. What is the effect of using XblocPlusOvertop® units on toe stability?
iii. How do XblocPlus® and XblocPlusOvertop® units perform on forces acting on the crown wall?
iv. How do XblocPlus® units perform on mean overtopping discharge? How do XblocPlusOvertop® units affect the overtopping performance of the structure?
v. What is the effect of the L-type crown wall on overtopping-induced scour at the lee side compared to the I-type crown wall used in Yıldırım et al. (2024)?

In Chapter 2, the literature review is presented under three sections to provide detailed information. In the first part of this chapter, the properties of XblocPlus® and XblocPlusOvertop® units are explained. In addition, existing studies on these units are summarized, and gaps in the literature about this subject are discussed. In the second part, general information about coastal revetment design, which is mainly about armour design, crown wall design, and toe design, is overviewed, and related studies are briefly described. In the third part of this chapter, experimental studies that use similar setups to the experimental setup used in the present study are

introduced focusing on the related measurement systems. Similar studies that exist in the literature are presented and described.

In Chapter 3, the selected methodologies for measuring and analyzing the stability of armour and toe layers, forces acting on the crown wall, mean overtopping discharge, and overtopping induced scour at the lee side of the structure. This chapter is presented in two main sections. In the first section, the design of cross-sections of the coastal revetment and wave conditions created in the wave flume are presented in detail. Furthermore, the experimental setup and measurement devices are presented in this part. In the second part of the chapter, the measurement procedure and analysis methods are described in detail.

In Chapter 4, the results and discussions are presented in two sections. The results of all experimental studies and analyses are presented in the first section of this chapter. In the second part of the chapter, findings about the research questions and limitations of this thesis study are discussed.

In Chapter 5, conclusions and suggestions for future studies are given.

CHAPTER 2

LITERATURE REVIEW

In this thesis study, the hydraulic performance of recently developed XblocPlus® and XblocPlusOvertop® units are evaluated in terms of the stability of armour layers and toe regions, forces acting on the crown wall, mean overtopping discharge, and overtopping induced scour at the lee side of the structure. These various types of experimental measurements require different methodologies. Thus, this chapter is divided into three main subsections. In the first part of this chapter, the geometry and properties of recently developed armour units are explained with the design objectives. As stated in Chapter 1, there are limited studies on coastal revetments utilizing the XblocPlus® and XblocPlusOvertop® units. In this part of this chapter, these studies are presented, and gaps in the literature on this subject are discussed. In the second part, studies exist in literature about armour design, crown wall design, and toe design of a coastal revetment are summarized and presented. Description of studies on armour layer design and performance consists of not only standard design processes but also the design and performance of XblocPlus® and XblocPlusOvertop® units. In the third part, the studies on the abovementioned subjects are overviewed.

2.1 Studies on XblocPlus® and XblocPlusOvertop® Units

XblocPlus® units were developed between 2015 and 2018, and the first application of this unit is the Afsluitdijk Project in the Netherlands (Xbloc, 2024). XblocPlusOvertop® units are designed to be placed close to the crest, and reducing the overtopping by reflecting the wave is aimed by using these modified units. These

units are designed to provide enhanced interlocking performance for regular placement by DMC. Geometries of XblocPlus® and XblocPlusOvertop® units are presented in Figure 2.1.

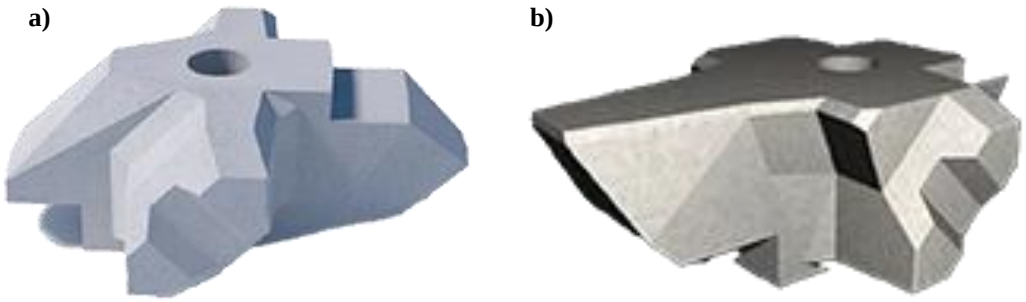

Figure 2.1. Geometry of units; a) XblocPlus® (Adopted from Reedijk et al., 2018), b) XblocPlusOvertop® (Adopted from Bakker et al., 2022)

Due to the unique geometry of recently developed units shown in the figure above, units can be placed with a single placement method which provides ease of placement and same orientation for all units different than Xbloc® units. During the development of these units, openings are used and preventing the water pressure build-up is aimed (Reedijk et al., 2018). This hole is also designed to provide fast construction with a specially designed clamp (Jacobs et al., 2018). XblocPlusOvertop® units are designed to reduce wave overtopping, and curvature is introduced by observing caissons and crown wall structures (Bakker et al., 2022). Due to the similar geometry of XblocPlusOvertop® units with XblocPlus® units provides high interlocking between different unit types while enhancing the desired overtopping performance of coastal structures.

Being a relatively new armour unit, research on the performance of coastal structures constructed using these units is limited, but these studies can be summarized as follows.

Moreno (2017) completed physical modeling experiments by using XblocPlus® to observe the overtopping performance of this unit and estimate the roughness coefficient of this new unit. Overtopping measurements are completed by implementing a chute and an overtopping tank at the back side of the structure. By

implementing this system, Moreno (2017) was able to measure the mean wave overtopping discharge. Measurements are completed on structures with 3:4 and 1:2 slopes. A foreshore slope of 1:30 is also constructed for these experimental studies. As a result, Moreno (2017) presents overtopping volume and roughness coefficient suggestions for different structure slopes and discusses the existing formulas and parameters that affect the overtopping volume. This research only focuses on XblocPlus® units for two different structure slopes in terms of overtopping performance.

Reedijk et al. (2018) present 2D and 3D experimental studies on XblocPlus® armoured structure to investigate the roughness coefficient of this artificial unit and the stability of the armour layer. Model tests are performed with a structure slope of 1:2 and 3:4 and a seabed slope of 1:30. In this study, Reedijk et al. (2018) present the hydraulic stability of the armour units and overtopping performance for only XblocPlus®. Reedijk et al. (2018) state that there is no observation, and further investigations should be carried out for the transition from the structure slope to the crest. Similarly, Bakker et al. (2019) evaluated the hydraulic stability of the XblocPlus® armoured structure through 2D and 3D physical model experiments.

Different than the stability investigations presented above, Broos (2019) completed a study on stability investigations of the first row of the XblocPlus® armoured structure. It is stated that there are fewer interlocking points for the first row of the armour units, and failure of this row can lead to a massive failure of the structure. Thus, a physical model is utilized, and the stability performance of the first row in different conditions is evaluated.

Janssen (2018) focused on the transition to crest elements of XblocPlus® armoured structures. Understanding the failure behavior of the units at the transition is crucial to model and predict the solutions. Thus, physical model tests are conducted, and a numerical model is utilized in this study. Janssen (2018) used video camera recording to determine the failure modes of the crest elements. For numerical simulations, OpenFOAM is utilized. However, only XblocPlus® units are evaluated

in this study. Ruwiel (2020) states the same problem for this unit. In these studies, instabilities at the top of the structure and crest are emphasized and physical model experiments are conducted to see the crest performance of XblocPlus® units. A modified design is provided and tested to eliminate this problem.

Van den Berg et al. (2020) investigated the effects of rock underlayer on the stability of the armour layer in their studies. It is emphasized that the weight of the armour unit and hydraulic pressure cause the armour layer to be pushed out. Due to this situation, Van den Berg et al. (2020) investigated the irregularities by physical model experiments. At the end of these experimental studies, it is shown that irregularities in the underlayer cause another failure mechanism.

Although the abovementioned studies focus on different aspects of the XblocPlus® unit, there are limited studies on XblocPlusOvertop® units. Bakker et al. (2022) evaluate the modified units in terms of reducing the overtopping amount by physical model experiments. They provide roughness coefficients for these units and compare the overtopping performances of different units. Also, Bakker et al. (2022) discuss overtopping reductions when these new units are placed. Moreover, the hydraulic stability of recently developed XblocPlusOvertop® units is tested for different freeboards. The study shows also that this new unit creates similar effects with bullnose and similarities are discussed in the study.

In summary, hydraulic stability, overtopping performance, and roughness coefficient of the XblocPlus® unit have been investigated by different studies. However, there are limited studies on XblocPlusOvertop® units compared to XblocPlus® units. Therefore, more investigations on XblocPlus® and XblocPlusOvertop® armoured coastal revetment should be conducted. The present thesis study primarily aims to investigate the performances of XblocPlus® with and without XblocPlusOvertop® units under different testing conditions and utilizing different cross-sections.

2.2 General Information About Coastal Revetment Design

2.2.1 Armour Design

Providing a stable and safe design for the armour layer of rubble mound structures is a widely studied subject in the literature. The most widely used formulations for designing an armour layer are provided by Hudson (1959), Van der Meer (1988), and Van Gent (2004). However, the Hudson formulation is modified and applied to the design of Xbloc® and XblocPlus® armoured structures by DMC. Modifications are implemented to the formula by considering the characteristics of the artifical units. Due to this situation, Hudson's methodology to design an armour layer is presented in this section. Moreover, modifications and assumptions presented by DMC are explained.

The Hudson equation was developed by physical model experiments in 1959, and it provides the median mass of armour units as an output (CIRIA et al., 2007). This method can be applied to deep water and shallow water regions with different breaking conditions. However, it covers only regular wave properties without considering wave period and storm duration (CIRIA et al., 2007). Also, this equation does not explicitly cover damage level and is applicable only to permeable coastal structures. Although this equation has some limitations, it is widely used for design purposes with some modifications in design processes. The equation is presented in Equation 2.1.

$$M_{50} = \frac{\rho_r g H^3}{K_D \Delta^3 cot\alpha} \qquad (2.1)$$

The parameters given in the equation above are presented and explained in Table 2.1.

Table 2.1 Parameters in the Hudson equation.

Parameter	**Symbol**	**Unit**
Median Armour Unit Mass	M_{50}	kg
Density of Rock	ρ_r	kg/m^3
Gravitational Acceleration	g	m/s^2
Wave Height	H	m
Stability Coefficient	K_D	-
Relative Buoyant Density	Δ	-
Slope Angle of the Structure	α	-

The Rock Manual (CIRIA et al., 2007) states that design wave height is specified as wave height at the toe of the structure. Since the Hudson method covers only regular waves, the Shore Protection Manual (SPM) suggests the use of significant wave height (H_s) for irregular wave conditions in 1977 (CERC, 1977). Later, SPM (CERC, 1984) suggests the use of the wave height exceeded by 10% of waves ($H_{1/10}$).

The stability coefficient (K_D) changes for different armour units due to different shapes and interlocking properties (CERC, 1984). This shows that the shapes and interlocking properties of the armour unit determine the weight of the unit. Increasing K_D enables engineers to decrease weight and concrete consumption. Different values of K_D for different armour units are presented in the SPM (CERC, 1984), but Xbloc® and XblocPlus® units are not included in the table. On the other hand, (Xbloc, 2023) provides K_D as 16 and 12 for Xbloc® and XblocPlus®, respectively, based on the studies summarized in Section 2.1.

The ratio of the density of the armour unit and water gives the relative buoyant density (Δ). The formula to calculate Δ value is presented in Equation 2.2.

$$\Delta = \left(\frac{\rho_{armor}}{\rho_{water}}\right) - 1 \qquad (2.2)$$

In the Xbloc and XblocPlus Design Guidelines (Xbloc, 2023), a modified version of the Hudson equation is suggested to determine the unit size. In the guideline, modifications are presented by assuming the face slope of the structure as 3:4, concrete density in the range of 2350-2500 kg/m^3 and using the K_D value as given above. This modified equation for XblocPlus® units is presented in Equation 2.3.

$$V_{XblocPlus} = \left[\frac{H_s}{2.5x\Delta}\right]^3 \quad (2.3)$$

In certain circumstances, correction factors to the Equation 2.3 are suggested (Xbloc, 2023). These circumstances are presented in Table 2.2 below.

Table 2.2 Correction factors for different circumstances (Adopted from Xbloc, 2023)

Phenomenon	**Correction factor on unit weight**
Frequent occurrence of near-design wave height during the lifetime of the structure	Not applicable (as rocking was not observed during XblocPlus model tests)
The foreshore in front of the structure is steep	1.10 for a steepness between 1:30 and 1:20
	1.25 for a steepness between 1:20 and 1:15
	1.50 for a steepness between 1:15 and 1:10
	2.00 for a steepness greater than 1:10
The structure is low crested	1.50 for a relative freeboard < 0.5
	1.25 for a relative freeboard < 1
The water depth is large	Not applicable [as stability was demonstrated in model tests with deep water conditions for stability numbers > 2.5]
The core permeability is low	1.25 for low core permeability
	1.50 for an impermeable core
The armour slope is mild (<1:1.5)	Not applicable [as model tests showed no decrease in stability for milder slopes]

2.2.2 Toe Design

The stability of the toe section has a great impact on armour stability in coastal structures, and different studies have been conducted on toe design formulations. Xbloc (2023) suggests using the Van der Meer et al. (1995) formulation to determine the weight of rock in the toe section. Due to this situation, the methodology proposed by Van der Meer et al. (1995) is explained in this section. The equation is presented in Equation 2.4.

$$\frac{H_s}{\Delta D_{n50}} = \left(2 + 6.2\left(\frac{h_t}{h}\right)^{2.7}\right) N_{od}^{0.15} \qquad (2.4)$$

The parameters given in the equation above are presented in Table 2.3, and these parameters are explained below.

Table 2.3 Parameters in the Van der Meer equation

Parameter	**Symbol**	**Unit**
Significant Wave Height	H_s	m
Relative Buoyant Density	Δ	-
Nominal Diameter of the Stone	D_{n50}	m
Depth of the Toe	h_t	m
Water Depth	h	m
Damage Number	N_{od}	-

As presented in Equation 2.4 and Table 2.3, design wave parameter, relative buoyant density (see Equation 2.2), water depth in front of the toe, and water depth above the toe are important parameters to determine the D_{n50} of the toe units. It is noted that the h_t/h ratio determines the suitability of the formula. If this ratio is smaller than 0.4, the structure tends to behave as a berm structure. Thus, this formula can be applied when h_t/h ratio is between 0.4 and 0.9.

Another important parameter, N_{od}, which corresponds to the number of displaced units in a section, is implemented in the formula (CIRIA et al., 2007). The following equation represents the N_{od} parameter.

$$N_{od} = \frac{N_s D_{n50}}{B} \qquad (2.5)$$

As shown above, the number of replaced units during the experiment (N_s), the width of the cross-section (B), and the nominal diameter of the unit (D_{n50}) are used to determine the stability number.

CIRIA et al. (2007) state that three different values of N_{od} are identified to explain the start of damage (N_{od} = 0.5), damage (N_{od} = 2), and failure (N_{od} = 4). Designers should determine the N_{od} value that is applicable to the specific project.

According to this information, Xbloc (2023) suggests using the condition of the start of damage in the section design. The producer also suggests using a minimum of $3D_{n50}$ toe berm width and $2D_{n50}$ toe height while designing a toe of an XblocPlus® armoured coastal structure.

2.2.3 Crown Wall Design

Crown walls provide access to coastal structures for different operations while increasing the overtopping performance of structures (CIRIA et al., 2007). AYGM (2016) also states that crown wall structures enhance the stability of the crest, decrease the wave overtopping discharge by increasing the crest height, and provide inspection pats.

Thus, the stability of this structure plays a crucial role in coastal structure design. Two main stability criteria are being investigated to provide a safe and stable crown wall design. These criteria are sliding and overturning, and CIRIA et al. (2007) explain the stability criteria against sliding (see Equation 2.6) and overturning (see Equation 2.7) conditions.

$$f(F_G - F_U) \geq F_H \quad (2.6)$$

$$M_G - M_U \geq M_H \quad (2.7)$$

Parameters given in the stability formulations are given in Table 2.4.

Table 2.4 Parameters in the stability conditions

Parameter	**Symbol**	**Unit**
Friction Coefficient	f	-
Weight of the Crown Wall	F_G	N
Uplift Force	F_U	N
Horizontal Force	F_H	N
Moment due to the Weight of the Crown Wall	M_G	Nm
Moment due to Uplift Force	M_U	Nm
Moment due to Horizontal Force	M_H	Nm

To evaluate the stability criteria presented above, different experimental studies and formulations exist in the literature to determine forces acting on the crown wall structures. CIRIA et al. (2007) emphasize that these different studies and formulations on determining forces show significant variations. Demir (2023) listed the most widely used studies on this subject and emphasized that Jensen (1984), Bradbury et al. (1988), and Pedersen (1996) are the leading studies. These studies give higher results than other formulations in literature by implementing H_s, and the formula proposed by Pedersen (1996) is accepted as the most accurate formula to determine forces (CIRIA et al., 2007). Moreover, AYGM (2016) utilizes Pedersen (1996) in the Turkish National Design Manual. Thus, the formula developed by Pedersen (1996) is explained in this section.

Pedersen (1996) focused on developing a design equation for crown walls by conducting 373 physical model tests. During these tests, different significant wave height (H_s), peak wave period (T_p), water depth (h), crown wall height (h_f), armour

crest freeboard (A_c), crest freeboard (R_c), crest berm width (B), slope of the structure ($cot\alpha$), and armour units are evaluated to obtain a global equation. These parameters and pressure distributions are identified and presented in Figure 2.2.

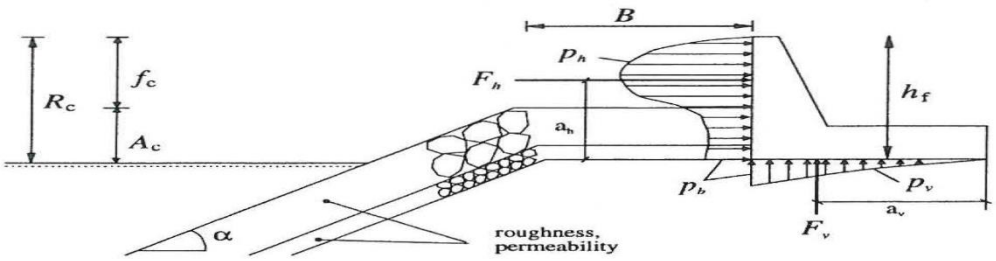

Figure 2.2. Definition of parameters (Taken from Pedersen, 1996)

Moreover, different ranges of ratios are investigated during these physical model experiments. The variation of these different parameters and ratios is presented in Table 2.5.

Table 2.5 Variations of different parameters and ratios of the study (Pedersen, 1996)

Parameter / Ratio	Range	Unit
H_s	0.10 – 0.18	m
T_p	1.20 – 2.20	s
h	0.51 – 0.59	m
h_f	0.15 – 0.33	m
A_c	0.11 – 0.19	m
R_c	0.11 – 0.37	m
B	0.18 – 0.36	m
$cot\alpha$	1.5 – 3.5	-
Armour Unit	Rock, Dolos, Cubes	-
ξ_m	1.1 – 5.1	-
H_s/A_c	0.5 – 1.7	-
R_c/A_c	1.0 – 2.6	-
A_c/B	0.3 – 1.1	-

Measurements (see Section 2.3.2) of forces for these different parameters have been analyzed, and pressure distribution and hypothetical wedge are presented in the study as shown in Figure 2.3.

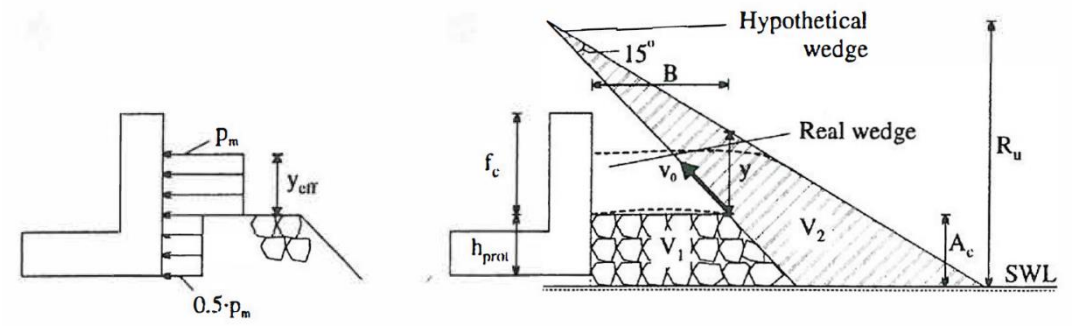

Figure 2.3. Pressure distribution and hypothetical wedge (Taken from Pedersen, 1996)

To obtain the maximum forces, an exceedance probability of 0.1% is utilized in this study, and formulas are developed in this concern. CIRIA et al. (2007) present the formulas suggested by Pedersen (1996) of total horizontal force ($F_{H,0.1\%}$) and related parameters in the Rock Manual, and these formulas are presented in Equations 2.8 – 2.12.

To provide consistency, all formulas (Equations 2.8 – 2.14) and parameters given in Table 2.6 are given by following the same notation as Pedersen (1996).

$$p_m = g\rho_w\left(R_{u,0.1\%} - A_c\right) \quad (2.8)$$

$$y = \frac{R_{u,0.1\%} - A_c}{sin\alpha}\frac{sin15^\circ}{cos(\alpha - 15^\circ)} \quad (2.9)$$

$$y_{eff} = min\{y/2, f_c\} \quad (2.10)$$

$$V = min\{V_1, V_2\} \quad (2.11)$$

$$F_{H,0.1\%} = 0.21\sqrt{\frac{L_{om}}{B}}\left(1.6p_m y_{eff} + V\frac{p_m}{2}h_{prot}\right) \quad (2.12)$$

Turning moment calculation procedures are also available in this study. Pedersen (1996) provides these formulas as presented in Equations 2.13 and 2.14.

$$M_{H,0.1\%} = 0.55F_{H,0.1\%}\left(h_{prot} - y_{eff}\right) \quad (2.13)$$

$$p_{U,0.1\%} = 1.0\ V\ p_m \quad (2.14)$$

Pedersen (1996) states that these formulas are valid in certain ranges of different parameters. These ranges are presented in Table 2.6.

Table 2.6 Limitations of parameters for Pedersen (1996) methodology (CIRIA et al., 2007)

Parameter	Symbol	Range
Breaker Parameter	ξ_m	1.1 – 4.2
Relative Wave Height	H_s/A_c	0.5 – 1.5
Relative Run-up Level	R_c/A_c	1.0 – 2.6
Relative Berm Width	A_c/B	0.3 – 1.0
Structure Slope	$cot\alpha$	1.5 – 3.5

2.2.4 Mean Wave Overtopping Calculation

Wave overtopping is one of the most important parameters to determine the serviceability of coastal structures. In the literature, the most widely used formula to determine dimensionless overtopping discharge is provided by EurOtop (2018) and presented in Equation 2.15.

$$\frac{q}{\sqrt{gH_{m0}^3}} = 0.09exp\left[-\left(1.5\frac{R_c}{H_{m0}\gamma_f\gamma_\beta\gamma^*}\right)^{1.3}\right] \quad (2.15)$$

Dimensionless overtopping discharge ($q/\sqrt{gH_{m0}^3}$) value is predicted by using the nearshore H_{m0}, roughness factor (γ_f), influence factor for oblique wave (γ_β), influence factor (γ^*), and R_c. Measured wave height and different R_c values are directly implemented in the formula. Roughness factors differ for different armour units, and this factor is determined by experimental studies presented in the literature. Roughness factors for XblocPlus and XblocPlusOvertop units are provided by DMC and discussed in Section 3.2.3.3.

2.3 Experimental Measurement and Analysis Techniques

2.3.1 Armour and Toe Stability

The stability of the armour layer plays a crucial role in the safety and sustainability of coastal structures. Different armour units perform differently. This situation is being investigated widely through physical model experiments. Visual analysis with photos taken before and after the experiments (Bakker et al., 2019; Reedijk et al., 2018; Van Gent & van der Werf, 2014) and assessment of video recordings are widely used methods in the literature to assess the stability. As Hofland et al. (2023) stated in their study, Garcia et al. (2013) emphasize the reason behind this situation as difficulties in measuring stresses on a physical model. However, Hofland et al. (2023) propose a new novel approach for rocking measurement with embedded sensors. According to Hofland et al. (2023), determining rocking by visual methods can be possible when the rocking angle is higher than 5°. On the other hand, less than 0.1° rocking angle can be detected by using embedded sensors (Hofland et al., 2023). However, placing the unit with sensors on the armour layer has some

limitations. A new unit should be prepared with space inside of it to place sensors, which is challenging.

Another method to determine rocking and extracting in the armour layer is profile measurements. Laser meter measurements are used to record profiles before and after the experiments to observe damage in the armour layer. However, this method is applicable to rock layers, it cannot be used for artificial concrete units accurately.

The toe section of a coastal structure provides support for the armour layer, increases the stability of this layer, and protects the structure against damage due to scour at the toe location (Van Gent & van der Werf, 2014). Generally, quarry rocks are used to provide safe toe design in coastal engineering applications. Damage criteria and formulas (see. Section 2.2.2) are being evaluated by physical model experiments. Similar methodologies with armour stability measurement techniques can be used for the toe section.

Although recently developed measurement techniques provide high accuracy, these studies have some limitations regarding the unit types and require the usage of special equipment. Therefore, most of the studies in the literature on stability and rocking conditions of armour and toe layers utilize the assessment of visual recordings and profile measurements.

2.3.2 Pressure Measurements on Crown Wall

As stated in Section 2.2.3, crown walls are important sections of coastal structures due to wave overtopping and stability performances. Thus, understanding the design procedures with forces acting on these structures is widely studied in the literature.

Bradbury et al. (1988) conducted physical model experiments to measure overtopping discharge and wave forces acting on the crown wall. A physical model with a crown wall structure and impermeable core is installed in front of a 1:52 slope. Different crown wall heights are tested during the experiments. Pressure transducers are used to obtain pressure distribution on the front face of the crown wall.

Horizontal forces acting on the crown wall are measured by the force table designed with four foil strain gauges. Measured forces are averaged along the test section to obtain a distribution and low-pass Butterworth filter with a cut-off frequency of 5 *Hz*. As a final result, Bradbury et al. (1988) present pressure and force distribution on a crown wall for different wave conditions and cross sections.

Pedersen (1996) introduced the most widely used formula on crown walls by his physical model experiments. With the different cross-sections and different parameters explained in Section 2.2.3, pressure measurements are conducted in this study. Four different aluminum plates with different heights are selected as crown wall material in these experiments. Pedersen (1996) states that using a dynamometer to measure the forces on the crown wall causes errors, so using pressure transducers is preferred. Pressure sensors are placed in the holes in front of the aluminum crown wall models. 256 *Hz* of sampling rate is applied to be able to record all events. A small mesh is implemented in front of the sensors for protection. Three of the largest wave impacts are recorded and analyzed during the experiments.

Martin et al. (1999) focused on the effects of breaking waves on the forces acting on crown walls and designed the model such that the wave-breaking phenomenon occurs on the structure slope. Monochromatic waves are applied to the experimental setup, and additional experiments are conducted with irregular wave series. Strain gauges with the 120 *Hz* sampling rate are used to record pressure, and four gauges are placed on the crown wall basement, while eight gauges are placed at the front face of the crown wall. Martin et al. (1999) explain the pressure distribution characteristics in the study and present horizontal and vertical distributions with the gauge placement configurations.

Nørgaard et al. (2013) emphasize that Pedersen (1996) is not applicable for shallow water conditions and determines the wave loads higher than the natural conditions in shallow water. Thus, Norgaard et al. (2013) proposed a modified version of the existing formulas in the literature by physical model experiments. Similar to previous

studies, both horizontal and vertical pressure distributions are recorded. The layout of the sensor placements is presented in Figure 2.4.

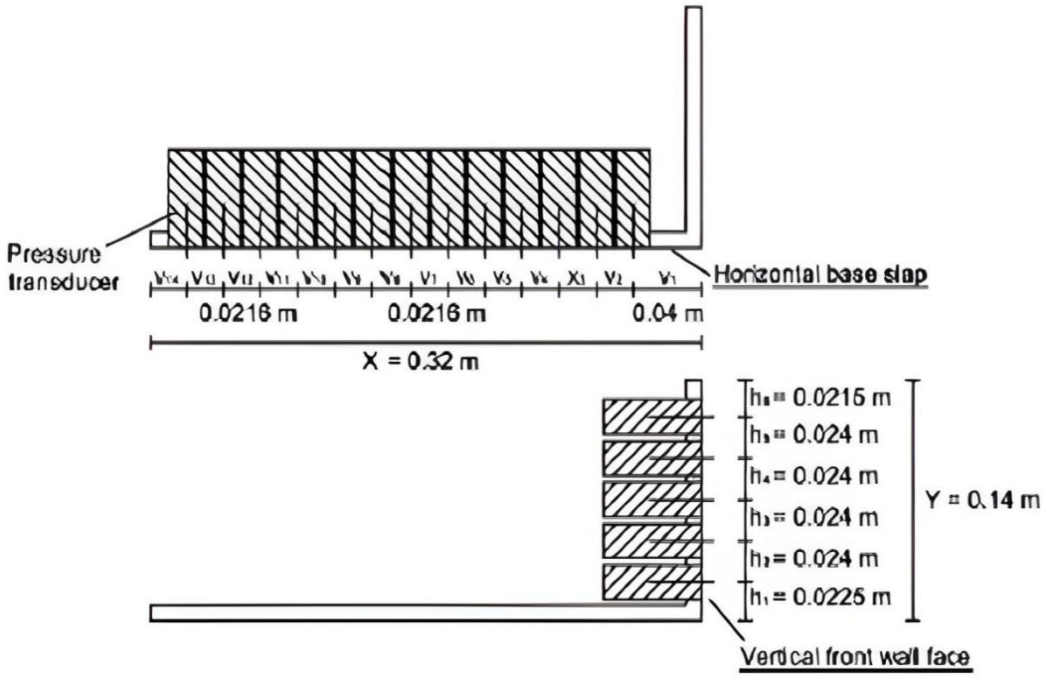

Figure 2.4. Pressure sensor placement (Taken from Nørgaard et al., 2013)

Pressure sensors are located as shown in the figure above, and records are obtained with a sampling frequency of 1.5 *kHz*. Similar to the other studies low pass filter is applied to the row data with a cut-off frequency of 250 *Hz*.

Demir (2023) evaluated the effects of different armour unit configurations on forces acting on the crown wall. Similar to the other studies, pressure sensors with a sampling rate of 12.5 *kHz* are placed on the crown wall. The placement of these sensors is similar to the locations given by Nørgaard et al. (2013) (see Figure 2.4). The crown wall model is designed with spaces to locate the pressure sensor group, and the mechanism allows researchers to change the location of sensors. Also, a thin mesh is used to protect the pressure sensors from external damage similar to Pedersen (1996). Three different crown wall heights are evaluated while changing armour layer units as rock, Antifer and tetrapods.

In summary, crown walls enhance the overtopping performance of a coastal structure and provides usage area on a structure. Thus, researchers emphasize the importance of the design process of crown walls. However, knowledge of the effects of different artificial units is limited in the literature. Measurement methods are similar and consistent for different studies.

2.3.3 Wave Overtopping

The overtopping performance of a coastal structure determines the serviceability performance of the structure. There are widely used methodologies to measure overtopping in literature.

Pillai et al. (2017) introduced an overtopping collection system with a chute and a collecting box at the back side of the structure. Pillai et al. (2017) are able to transport the overtopped water from the chute to the collecting box, and the amount of water is measured with relative ease. This setup is applied to a berm breakwater, but measuring the wave overtopping can be considered similar for any coastal structure.

Schoonees et al. (2021) conducted wave overtopping measurements for a full-scale stepped revetment model. A chute is installed to collect the overtopped water in the bin located at the back side of the structure. Load cells are used to determine the weight of the total overtopped water. Measuring the weight of the total overtopped water enabled Schoonees et al. (2021) to calculate the mean overtopping discharge.

Nørgaard et al. (2014) focus on the wave overtopping phenomenon. A ramp and a collecting box for overtopped water are installed at the back side of the structure, similar to the mean overtopping measurement methods explained above. The measurement setup of this study is presented in Figure 2.5.

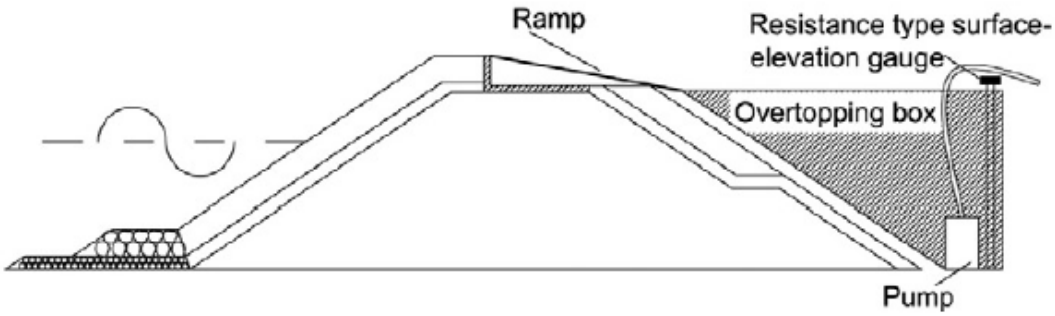

Figure 2.5. Measurement setup for wave overtopping volume (Taken from Nørgaard et al., 2014)

The overtopped water is collected in the overtopping box by using a ramp, and wave overtopping volumes are measured by wave gauges placed in the collecting box.

Molines et al. (2019) focus on wave overtopping, crown wall stability, and armour layer stability in their research. A similar setup with Nørgaard et al. (2014) is implemented, and the setup is shown in Figure 2.6.

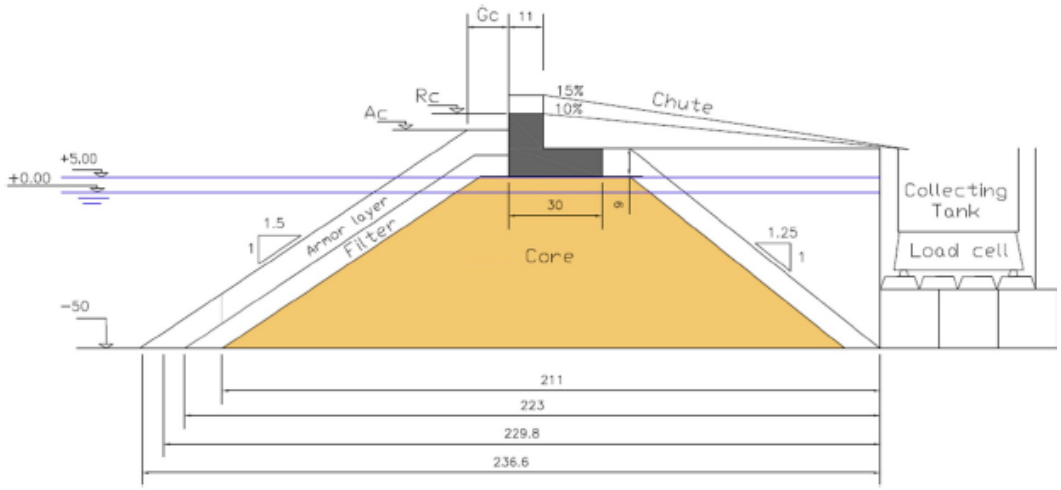

Figure 2.6. Measurement setup for wave overtopping events (Taken from Molines et al., 2019)

As shown in Figure 2.6, a chute and a collecting box are implemented. Contrary to Nørgaard et al. (2014), Molines et al. (2019) used load cells to observe wave

overtopping events. In this study, these events are determined by evaluating the changes in load cell measurements.

Similar to these studies, Koosheh et al. (2022) installed a chute and a collecting box on the physical model to measure individual wave overtopping volumes and mean overtopping discharge. Two wave gauges (see Figure 2.7, WG6 and WG7) are installed at the collecting box to measure cumulative wave overtopping volume. The wave overtopping measurement system proposed by this study is similar to other studies, but it is modified and more recent. Details of this system are shown in Figure 2.7.

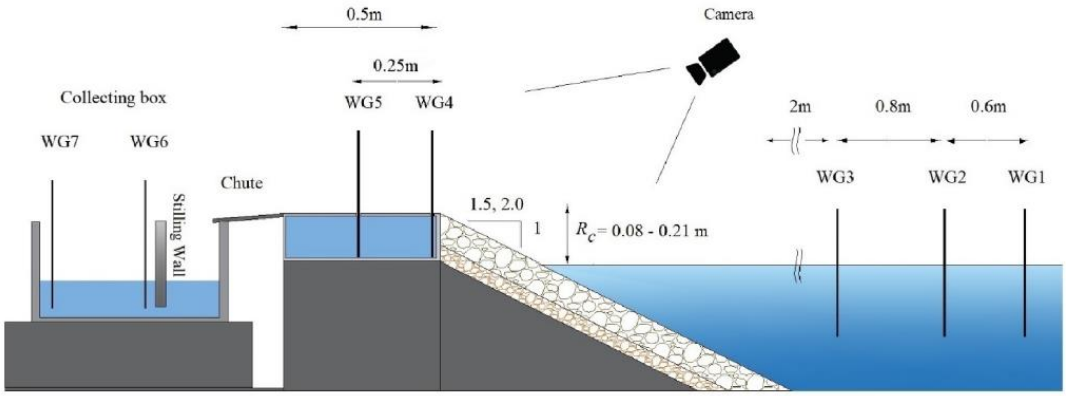

Figure 2.7. Wave overtopping measurement system (Taken from Koosheh et al., 2022).

By this experimental setup, Koosheh et al. (2022) measured the mean overtopping and individual wave overtopping events. Modifications such as additional wave gauges and modified chute are shown in the figure. On the other hand, chute and collecting box systems are utilized in other studies mentioned above. Also, Koosheh et al. (2022) emphasize that camera recordings are useful to control the quality of the recordings.

Erler (2023) also used a similar method to Koosheh et al. (2022) in terms of wave gauge locations, box and chute properties, and camera positioning. Erler (2023)

observed mean overtopping and individual wave overtopping events with this experimental setup.

In summary, measuring wave overtopping and understanding the interaction between this phenomenon and structure plays a crucial role in providing a safe, serviceable, and sustainable design. The methodologies utilized in the literature are mostly similar and consistent.

2.3.4 Wave Overtopping Induced Scour at the Lee Side

Excessive scour at the lee side of coastal revetments might cause different types of damages. As Yıldırım et al. (2024) explain in their study, Guler et al. (2024) emphasize that the scour at the lee side causes a reduction of support for crest elements, and this situation leads to failure on the crown wall and crest units. Also, Thomas & Hall (2015) state that about 5% of damages on seawalls in the UK are caused by wave overtopping induced scour at the lee side of structures (Yıldırım et al., 2024). Due to the importance of this phenomenon on structure stability, different studies on overtopping-induced scour and erosion have been conducted in the literature. However, Senturk et al. (2023) state that scour at the rear side of coastal revetments is studied limitedly in the literature. These studies are presented in this section as follows.

Senturk et al. (2023) conducted numerical simulations on scour at the uncovered rear side of a coastal revetment. The numerical simulations are conducted based on the physical model experiments (Yaman, 2022) performed for three different wave conditions. The mean overtopping volumes and backfill profiles are measured to observe the scour at the lee side of the structure.

Möller et al. (2002) investigated the failure mechanism of sea dikes with large-scale experiments and stated that damages due to wave overtopping also depend on soil properties. Thus, the relation between wave overtopping, wave overtopping-induced scour, soil properties, and the failure mechanism of a structure is investigated in this

study. Overtopping measurements and damage analyses are conducted at the same time in this large-scale experiment. Overtopping measurements are conducted by similar methodologies presented in Section 2.3.3.

Van Der Meer et al. (2006) developed a new approach to evaluate wave overtopping-induced damages on dikes, and state that sufficient information about the wave overtopping phenomenon exists in the literature. Thus, they propose using the wave overtopping simulator to create an artificial wave overtopping event without creating waves in a laboratory environment. This system is presented in Figure 2.8.

Figure 2.8. The wave overtopping simulator (Taken from Van Der Meer et al., 2006)

Van Der Meer et al. (2006) state that realistic overtopping events can be simulated by this device. Moreover, studies can be conducted with less experiment budget than completing these experiments in large wave flumes by using WOS.

Bomers et al. (2018) state that understanding the behavior of road structure on erosion due to wave overtopping is important. Bomers et al. (2018) show that existing road structure increases the erosion rates of the grass-covered dikes. To

show the relation between asphalt cover and erosion, hydraulic and erosion experiments are conducted seperately. In this study, the wave overtopping simulator (see Figure 2.8) introduced by Van Der Meer et al. (2006) is implemented to simulate the overtopping event. Laser scanning devices are implemented to determine erosions during the experiments. These physical model experiments are also numerically modeled by computational fluid dynamics simulations.

Yıldırım et al. (2024) focus on scour at the lee side of a coastal revetment by physical model experiments, and measured mean overtopping discharge and scour at the lee side at the same time.

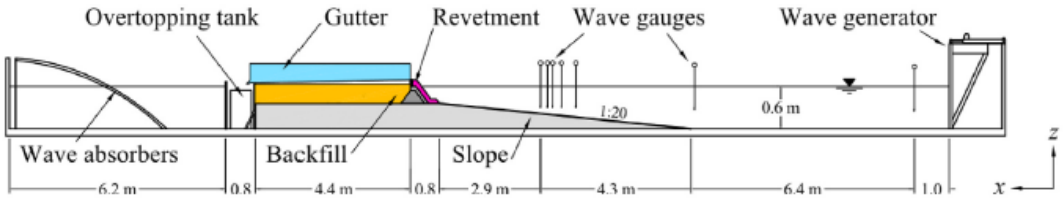

Figure 2.9. Experimental setup to measure mean wave overtopping discharge and scour (Taken from Yıldırım et al., 2024)

As shown in Figure 2.9, Yıldırım et al. (2024) created waves by a piston-type wave generator and measured mean overtopping by implementing a gutter similar to the methods presented in Section 2.3.3. The scour at the lee side is measured by laser sensors.

In addition to laser distance meter measurements, measuring the scour depth by implementing metric sticks in the backfill region is a common and accepted method in the literature.

In summary, understanding the scour mechanism is important to enhance the stability performance of coastal structures in terms of scour. Using laser sensors is a common application in literature. On the other hand, using metric sticks is applicable to measure the maximum scour depth and scour at the regular intervals of the wave series.

CHAPTER 3

METHODOLOGY

In this chapter, the design procedure of the structure, experimental setup, measurement methods, and analysis methods are explained in three parts. In the first part of this chapter, the design procedures of the armour layer, toe section, and crown wall are explained. Moreover, storm conditions for the project area are presented. The determination of scale is described in the second part of this chapter. As stated in Chapter 2, the stability of the armour layer and toe section, forces acting on the crown wall, mean overtopping volume, and overtopping induced scour at the lee side of the structure are evaluated in this study. Measurement and analysis methods of these different types of tests are introduced in the second part. The wave conditions created in the wave flume are also presented in this part. In the third part of this chapter, the experimental program and cross-sections of the physical model are presented.

3.1 Design of the Coastal Revetment Sections and Wave Conditions

Three different cross-sections, armoured with XblocPlus® units, are considered in this study, namely AA, AA2, and BB (two sections with different G_c values). The designs of AA and BB cross-sections are carried out by Dolfen Consultancy Engineering Inc. at different water depths. On the other hand, the cross-section AA2 is a variation of the cross-section AA, where the crest height (R_c) is decreased. The designs of the cross-sections are presented in terms of armour, toe, and crown wall design in this section. All information in this part is provided by Dolfen Consultancy Engineering Inc. for this consultancy project.

The mass of the armour unit is determined by the formula provided by DMC (see Equation 2.3). The density of XblocPlus® and water are used as 2.4 t/m^3 and 1.025

t/m^3 relatively. As a result, the calculated armour unit mass for the prototype ($M_{prototype}$) given by Dolfen is presented in Table 3.1 for different cross-sections.

Table 3.1 Armour unit sizes for prototype

	AA and AA2	***BB***
$M_{prototype}$ (tons)	43.2	33.6

Toe design is conducted by following the Van der Meer (1995) methodology presented in Equation 2.4. The density of the rock and water are used as 2.65 t/m^3 and 1.00 t/m^3, respectively. The stability number, N_{od} (see Section 2.2.2), mean nominal diameter (D_{n50}), and mass of the toe unit (M) are presented in Table 3.2.

Table 3.2 Parameters for the toe section

	AA and AA2	***BB***
N_{od}	0.50	0.70
D_{n50} (m)	1.39	1.39
M (tons)	7.10	7.10

It is decided to use (4 – 6) tons of rock for the toe section for all cross-sections to provide continuity of the cross-sections along the coastal revetment. Additionally, evaluating the performance of 10 tons of cube blocks is decided during the experiments for different cross-sections, as explained in the forthcoming sections. The mass of the cube blocks as toe units is determined by following the same procedure explained above.

The design of the crown wall is completed by following the suggestions of Xbloc (2023) and AYGM (2016). The methodologies are given in Section 2.2.3 and utilized for the crown wall design.

Storm conditions of the project site are determined by conducting wave statistics analyses previously conducted by METU (2020). For each cross-section, wave heights with a 10-hour exceedance probability per year (*D1*) and wave heights with

a 5-year (*D2*), 50-year (*D3*), and 100-year return period (LWL: *D4.1,* HWL: *D4.2*) are specified. *D1* and *D2* represent relatively frequent storm conditions, *D3* represents a significant storm condition, and *D4.1* and *D4.2* represent the design storm conditions. Additionally, a 90% upper confidence level for the wave with a 100-year return period (*D5*) is determined for the tests, which is referred to as an overloading condition. Moreover, an additional three waves (*D6, D7, D8*) with higher wave heights are selected during the planning of the experiments in order to increase the data for the experimental studies, which are actually out of the scope of the design of the cross-sections. Storm conditions and additional waves for the region are given in Table 3.3.

Table 3.3 Wave conditions for the region in prototype scale

	Exceedance Probability/ Return Period	H_{m0} **(m)**	T_s **(s)**	**Storm Duration (*h*)**
D1	10 hours/year	5.4	9.65	6
D2	5 years	6.9	10.32	8
D3	50 years	8.1	11.21	10
D4.1	100 years	8.6	11.52	10
D4.2	100 years	8.6	11.52	10
D5	100 years	9.2	12.00	10
D6	-	11.4	11.13	-
D7	-	12.6	11.84	-
D8	-	13.5	12.42	-

3.2 Physical Model Experiments

Mainly, three different sections (Section AA, Section AA2, and Section BB) are observed in this study. Different cases by changing the crest berm width (G_c), crest freeboard (R_c), toe units, and armour configurations are introduced and explained in

this section. Moreover, details on scale, model wave conditions, experimental setup, and measurement methods are presented.

3.2.1 Scaling of Coastal Revetment Cross-Sections

Froude Law is used to model the coastal revetment in the wave flume, as suggested by e.g. Hughes (1993). Froude number is a nondimensional parameter that shows the ratio between water particle velocity and shallow water group velocity and is identified as the ratio between water particle velocity (u) and the multiplication of gravitational acceleration (g) and water depth (h). This relation is presented in Equation 3.1.

$$F_r = \frac{u}{\sqrt{gh}} \qquad (3.1)$$

According to this law, Froude numbers for the prototype and model should be equal to each other. The geometrical similarity between the prototype and model is obtained by using the model scale (λ_L), and the time scale (λ_t) is obtained by the square root of the length scale. The length scale and time scale of a physical model are presented in Equations 3.2a and 3.2b.

$$\lambda_L = \frac{L_m}{L_p} \qquad (3.2a)$$

$$\lambda_t = \frac{t_m}{t_p} = \sqrt{\lambda_L} \qquad (3.2b)$$

To determine the weight scale (λ_w), Hudson's (1979) methodology is used for this study by equating the stability numbers of the prototype and model of the coastal revetment. The weight scale of a physical model is presented in Equation 3.3.

$$\lambda_w = \lambda_L^3 \frac{\gamma_{r,m}}{\gamma_{r,p}} \left[\frac{\gamma_{r,p}/\gamma_{w,p} - 1}{\gamma_{r,m}/\gamma_{w,m} - 1} \right] \qquad (3.3)$$

In Equation 3.3, $\gamma_{r,m}$ and $\gamma_{r,p}$ unit weights of stone in model and prototype scales, $\gamma_{w,p}$ and $\gamma_{w,m}$ unit weights of water in model and prototype scales. In addition, Burcharth (1999) is used to scale the core layer to minimize the scale effects due to viscosity.

By following these methodologies, two different length scales are selected for different cross-sections and presented in Table 3.4, considering the wave conditions and flume characteristics which are discussed later in this chapter. Thus, the same XblocPlus® units are used in the experiments.

Table 3.4 Model scales

	AA and AA2	**BB**
$\boldsymbol{\lambda_L}$	65.693	60.414
$\boldsymbol{\lambda_t}$	8.105	7.773
$\boldsymbol{\lambda_w}$	$3.19 * 10^{-5}$	$2.51 * 10^{-5}$

Selected scales are used to design the model based on the parameters given in Section 3.1.

3.2.2 Experimental Setup

The physical model experiments are conducted at Middle East Technical University, Department of Civil Engineering, Coastal and Ocean Engineering Laboratory. The flume is 26.9 meters long, 6.0 meters wide and 1.0 meter deep. For the experimental setup, the flume is divided into two 0.9-meter-wide parts, and a cross-section of the coastal revetment is built in one of these narrower inner channels of the flume. Irregular wave series are created by a piston-type wave generator, and a passive absorption system is installed at the end of the flume. The general view of the flume is presented in Figure 3.1.

Figure 3.1. General view of the wave flume at Middle East Technical University.

A foreshore slope of 1:30 is constructed to represent the bathymetry of the project site. A total of 10 wave gauges (*WG*) are placed to record water surface elevations (η). The coordinate system is identified to symbolize the experimental setup more systematically. As shown in Figure 3.2, the x-direction represents the horizontal distance, and the z-direction represents the vertical distance from the starting point. The starting point is determined as the wave generator for the x-direction and the still water level for the z-direction.

As stated above, three different cross sections are built in the wave flume. However, Sections AA and AA2 are applied to the same experimental layout, and two different setups are designed by decreasing the R_c for Section AA2 for this study. Side views of the physical models are shown in Figure 3.2.

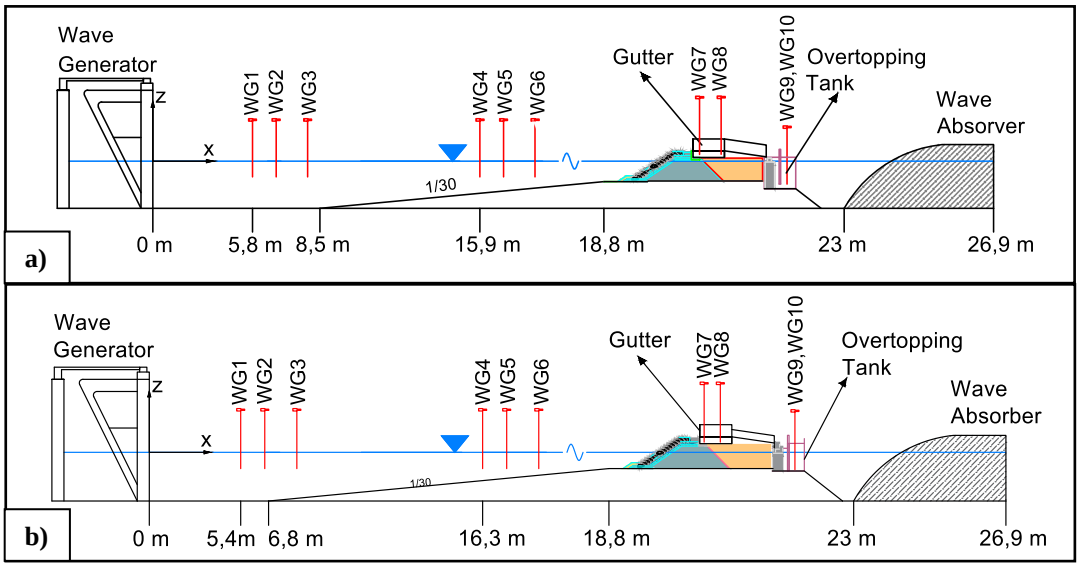

Figure 3.2. Side view of the physical models in the wave flume; a) Cross sections AA and AA2, b) Cross section BB.

The irregular wave series are measured by using *WG1*, *WG2*, *WG3* for offshore conditions and *WG4*, *WG5*, *WG6* for nearshore conditions. The location of wave gauges located nearshore is determined as 1.5 wavelength (*L*) far away from the toe of the structure, and wave gauges located offshore are placed 1.5 *L* away from the wave generator (Goda & Suzuki, 1976). With the data obtained from these wave gauge groups, reflection analyses are conducted by following the method suggested by Baldock and Simmonds (1999). Probe spacing is an important parameter for reflection analyses, and spacings are determined by following the methodology provided by Goda and Suzuki (1976). Spacings are given in Table 3.5.

Table 3.5 Probe spacings

WG	***WG1-WG2***	***WG2-WG3***
Distance (cm)	30.0	32.0
WG	***WG4-WG5***	***WG5-WG6***
Distance (cm)	33.0	35.0

Six irregular wave series are generated for Section AA and nine irregular wave series are utilized for Section AA2. A total of eight irregular wave series are applied to

Section BB. Wave conditions are selected to reflect the storm conditions of the region presented in Table 3.3.

By using the length scale values given in Section 3.2.1, model wave parameters are created, and experiment durations are determined by using the time scale with storm duration information given in Table 3.3. The targeted values of the model waves to reflect the wave conditions in the project site are presented in Table 3.6.

Table 3.6 Desired wave parameters in the wave flume

Section	Wave Cond.	H_{m0} (m)	T_s (s)	Duration (s)
AA ***AA2***	D1	0.082	1.191	2664.98
	D2	0.105	1.273	3553.31
	D3	0.123	1.383	4441.64
	D4.1	0.131	1.421	4441.64
	D4.2	0.131	1.421	4441.64
	D5	0.140	1.481	4441.64
BB	D1	0.089	1.242	2778.98
	D2	0.114	1.328	3705.30
	D3	0.134	1.442	4631.63
	D4.1	0.142	1.482	4631.63
	D4.2	0.142	1.482	4631.63
	D5	0.152	1.544	4631.63

For the additional wave conditions (*D6, D7, D8*), wave series are created with more than 1000 waves. The measured wave parameters for offshore conditions by *WG1*, *WG2*, and *WG3* are presented in Table 3.7 (Section AA), Table 3.8 (Section AA2), and Table 3.9 (Section BB).

Table 3.7 Measured incident wave parameters for Section AA

	H_{m0}	H_{max}	$T_{m-1.0}$	T_s	N
D1	0.092	0.162	1.085	1.065	2557
D2	0.108	0.180	1.103	1.093	3422
D3	0.128	0.199	1.191	1.180	3978
D4.1	0.137	0.200	1.232	1.226	3809
D4.2	0.137	0.200	1.233	1.226	3786
D5	0.154	0.241	1.296	1.299	3640

Table 3.8 Measured incident wave parameters for Section AA2

	H_{m0}	H_{max}	$T_{m-1.0}$	T_s	N
D1	0.099	0.178	1.101	1.059	2564
D2	0.115	0.196	1.127	1.094	3413
D3	0.134	0.203	1.219	1.183	3930
D4.1	0.148	0.218	1.262	1.230	3792
D4.2	0.147	0.213	1.267	1.229	3787
D5	0.163	0.239	1.334	1.305	3610
D6	0.173	0.244	1.385	1.373	1089
D7	0.192	0.254	1.463	1.461	1098
D8	0.205	0.257	1.495	1.532	1097

Table 3.9 Measured incident wave parameters for Section BB

	H_{m0}	H_{max}	$T_{m-1.0}$	T_s	N
D1	0.098	0.180	1.300	1.295	2550
D2	0.114	0.197	1.349	1.334	3157
D3	0.136	0.233	1.401	1.433	3841
D4.1	0.143	0.245	1.416	1.432	3791
D4.2	0.141	0.245	1.463	1.494	3720
D5	0.157	0.220	1.525	1.539	1076
D6	0.191	0.248	1.556	1.578	1401
D7	0.216	0.262	1.582	1.629	1401

All generated waves presented in the tables above are compared with Rayleigh distribution by non-dimensional histograms of the recorded wave heights. In general, the measured time series are in reasonably good agreement with the Rayleigh distribution. More deviations between histograms and Rayleigh distribution are

observed for additional waves (D6, D7, D8). During the generation of *D6*, *D7*, and *D8* waves, breaking in front of the wave generator is observed. This situation causes deviations between the histogram and Rayleigh distribution. An example analysis is presented in Figure 3.3 for the *D5* irregular wave series for Section BB. The results for other wave conditions are given in Appendix A.

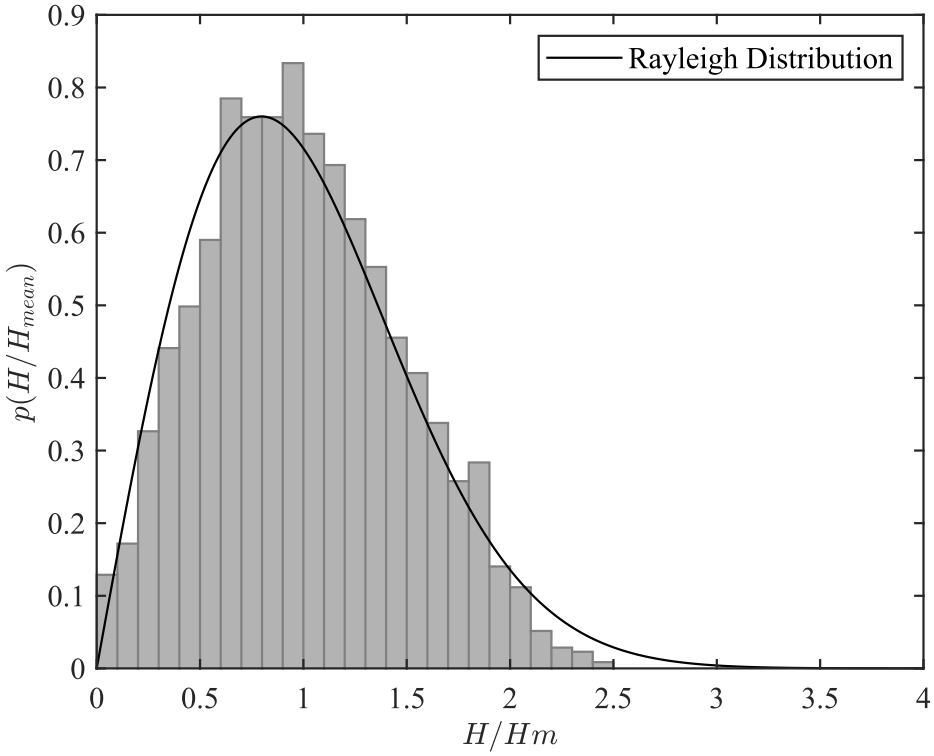

Figure 3.3. Non-dimensional histogram: Section BB, *D5* irregular wave condition

Mean overtopping volume measurements are conducted using *WG7-8-9-10*, gutter, and overtopping tank shown in Figure 3.2.

Since different measurements are completed during experiments, a lighting system is placed into the experimental setup to follow the different measurements more systematically. Four different colors are used to represent camera recordings, wave gauge recordings, pressure recordings, and the initiation of the wave generator. In addition, all experiments are recorded by using cameras placed in two different locations. The lighting system and cameras are presented in Figure 3.4.

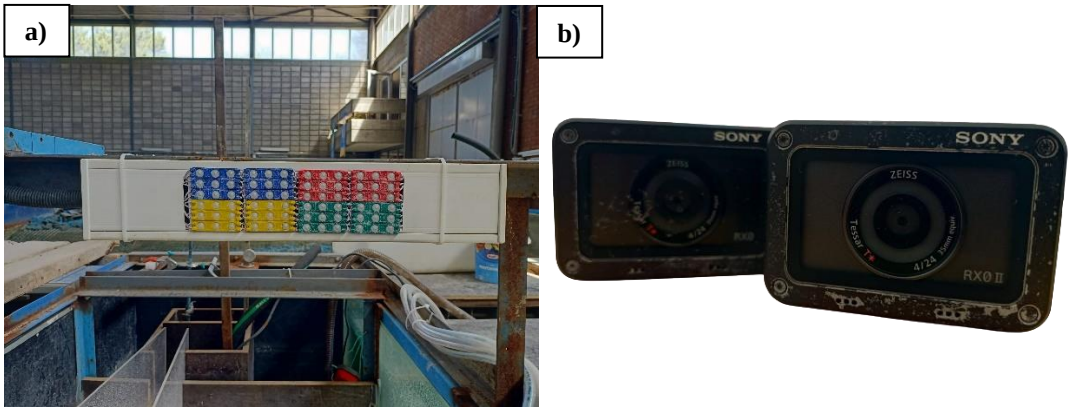

Figure 3.4. Instruments used in experiments; a) Lighting system, b) Cameras.

3.2.3 Measurement and Analysis Methods

3.2.3.1 Stability Measurements and Analyses

There are different methods to observe the stability performance of the structure (see Section 2.3.1). In this study, the visual inspection of the toe and armour layer is conducted by placing two cameras to analyze the stability conditions. Although the profile measurements and embedded sensor methods give more accurate results, implementing these methodologies is not applicable to this study.

During the stability tests, cumulative damages on the toe and armour units are observed. Storm conditions for the region (see Table 3.3) are applied and the model is not repaired between the experiments. As stated in Section 3.1, additional wave conditions are tested separately. The model is reconstructed between the storm conditions and additional waves. The same procedure is followed for the additional waves; between these experiments, the model is not repaired, and cumulative damages are determined.

As stated in Chapter 2, damage level can be represented by damage number (N_{od}) or percentage damage (N_d). In this study, both parameters are calculated by following the formulas presented in Equations 3.4 and 3.5.

$$N_{od} = \frac{N_f D_{n50}}{B} \quad (3.4)$$

$$N_d = \frac{N_f}{N_{total}} \quad (3.5)$$

In Equations 3.4 and 3.5, N_f is the number of replaced units during the experiment, B is the width of the cross-section, N_{total} is the total number of units, and D_{n50} is the nominal diameter of the unit. Different N_f values are observed during the tests and these values are presented in Chapter 4. The width of the cross-section is 0.9 meters, and the total number of units used in different sets of experiments is presented in Table 3.10. An example procedure to determine the number of replaced units is shown in Figure 3.5.

Table 3.10 Number of units used in experiments

Cross-Section	**Armour Unit**		**Toe Unit**	
	XP	XP-OT	Rock	Cube
AA	161	23	713	-
	184	-	713	-
AA2	161	23	693	-
	184	-	693	-
BB	173	-	-	385
	173	-	-	402
	173	-	697	-

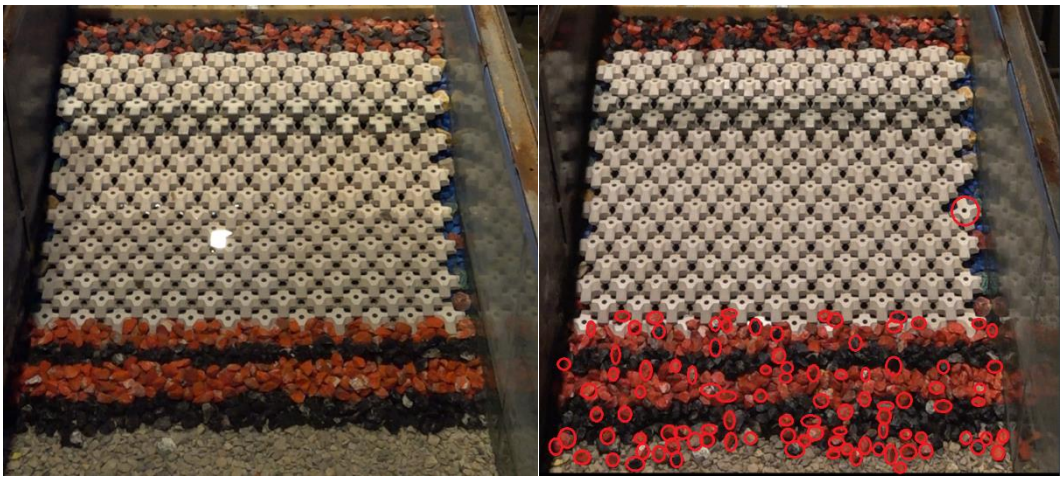

Figure 3.5. An example stability analysis for section AA

All detected damages, results, and discussions are presented in Chapter 4.

3.2.3.2 Pressure Measurements and Analyses

Forces acting on the crown wall are measured by Kistler Type 601C Piezoelectric Pressure Sensors. To obtain reliable measurements and avoid changing pressure values, no damage on the crown wall should be observed during the experiments. Due to this situation, the crown wall model is fixed to take relevant pressure measurements. Moreover, the crown wall model is manufactured with a material named kestamite. This material provides corrosion resistance and durability for long experiment durations. The crown wall model is presented in Figure 3.6.

Figure 3.6. Crown wall model

Horizontal (face of the crown wall) pressure measurements are conducted during the experiments. Four locations for horizontal forces are determined to measure pressures. Pressure sensors are calibrated by the producer by default, and sensor locations are determined by following the Demir (2023). All sensor locations and distances between pressure sensors are presented in Figure 3.7.

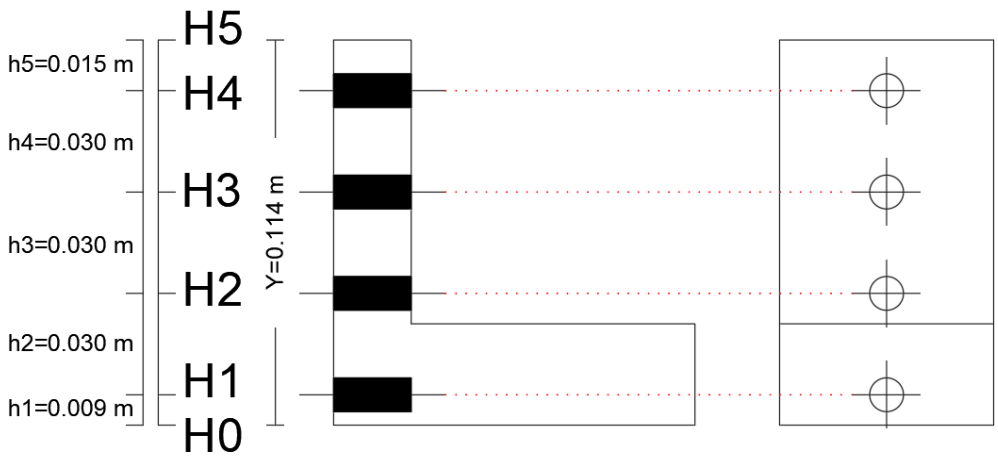

Figure 3.7. Pressure sensor locations

Because of these different measurement locations, spaces for the pressure sensor block on the face and bottom of the crown wall are created. The spaces are closed with aluminum blocks to preserve the geometry of the crown wall, as shown in Figure 3.6. Four pressure sensors are grouped in an aluminum apparatus to place the sensors on the crown wall easily.

Kistler suggests using a minimum of 12.5 kHz of the sampling rate, and this suggestion is applied to the experimental measurements. Analyzing the pressure measurements requires filtering and downsampling the raw data recorded with a 12.5 *kHz* sampling rate. Lamberti et al. (2011) emphasize that using high-frequency pressure data may cause the overestimation of the forces acting on the structure. Recording the data with high-frequency sampling rates shows the local effects on the individual pressure sensor. This local effect should not be taken into account while integrating the overall force acting on the structure.

As applied in similar experimental studies by Nørgaard et al. (2013) and Demir (2023) based on the discussions of Lamberti et al. (2011), the downsampling frequency is selected as 1250 Hz. Another filter is applied to the row data to eliminate noise. Spectral distributions are evaluated and the noise at a frequency of 50 Hz and multiples of this frequency (eg. 100 Hz, 150 Hz, 200 Hz…) is observed. Thus,

Butterworth low-pass filter is applied to the data with 50 Hz to avoid noises during analyses.

For the analyses and comparison of the pressure data, Nørgaard et al. (2013) and Pedersen (1996) formulations are selected. The pressure data is converted to force and momentum values by following Nørgaard et al. (2013) methodology. Extrapolation determines pressures acting on the bottom and top points of the crown wall, according to this methodology. Total forces and momentum are calculated by following the Equations 3.6– 3.9.

$$\Delta F_H = \frac{1}{2} h_n (H_{n-1} - H_n) \quad (3.6)$$

$$F_H = \sum_{n=1}^{5} \Delta F_H \quad (3.7)$$

$$\Delta M_H = \frac{1}{2} h_n \left[h_n \left(\frac{1}{3} H_{n-1} + \frac{2}{3} H_n \right) + (H_{n-1} + H_n) \sum_{i=1}^{n-1} h_i \right] \quad (3.8)$$

$$M_{F_H} = \sum_{n=1}^{5} \Delta M_H \quad (3.9)$$

Parameters given in the equations above are presented in Table 3.11.

Table 3.11 Parameters used in Equations 3.6 – 3.9

Parameter	**Symbol**	**Unit**
Pressure	H_n	*kPa*
Distance Between Sensors	h_n	*m*
Force per Unit Width	ΔF_H	*kN/m*
Total Force per Unit Width	F_H	*kN/m*
Moment	ΔM_H	*kN.m/m*
Moment of the Total Force	M_{F_H}	*kN.m/m*

Pedersen (1996) and Demir (2023) state that determining vertical forces acting on a crown wall has some limitations due to the high variations of the scatter obtained by experimental measurements. Moreover, these forces are generally determined by triangular distribution based on a value at the bottom corner of the crown wall. Due to the experimental limitations, vertical forces are not measured, and horizontal forces acting on the crown wall are evaluated in this study. All results and discussions are presented in Chapter 4.

3.2.3.3 Overtopping Measurements and Analyses

Mean overtopping volume measurements are conducted by implementing a gutter and an overtopping tank, similar to other studies in the literature (see Section 2.3.3). The collecting system of overtopped water is presented in Figure 3.8.

Figure 3.8. The collecting system for wave overtopping

As shown in Figure 3.8, a gutter is placed on the crown wall at the same level. The width of the gutter is determined as 15 cm. Overtopped water is collected by this equipment, and transferred to the overtopping tank. The overtopping tank is placed in a protected area, and a pump is placed inside the tank. Due to the long experiment durations, collected water is transferred to the measurement box when the capacity of the overtopping tank is full. The total overtopped water during the experiments is

calculated by weighting the collected water and measuring the water level changes inside the overtopping tank. Moreover, two cameras are placed on the cross-section to control the quality of the experiments, as Koosheh et al. (2022) suggest.

Since the design formulas in the literature require the determination of mean overtopping discharge (q) values for the region, results are presented by converting the measured data to q. With the overtopped water volume, experiment duration, and width of the gutter information, the mean overtopping discharge is calculated for each experiment.

Overtopping performances of XblocPlus® and XblocPlusOvertop® units are evaluated by following the measurement methodology explained above and following the methodology suggested by Bakker et al. (2022).

The prediction formula in EurOtop (2018) is utilized to compare the measurement results. The formula is presented in Equation 2.15. Since there is no oblique wave attack during the experiments, γ_β value is used as 1. factors are given by Bakker et al. (2022), as shown in Figure 3.9.

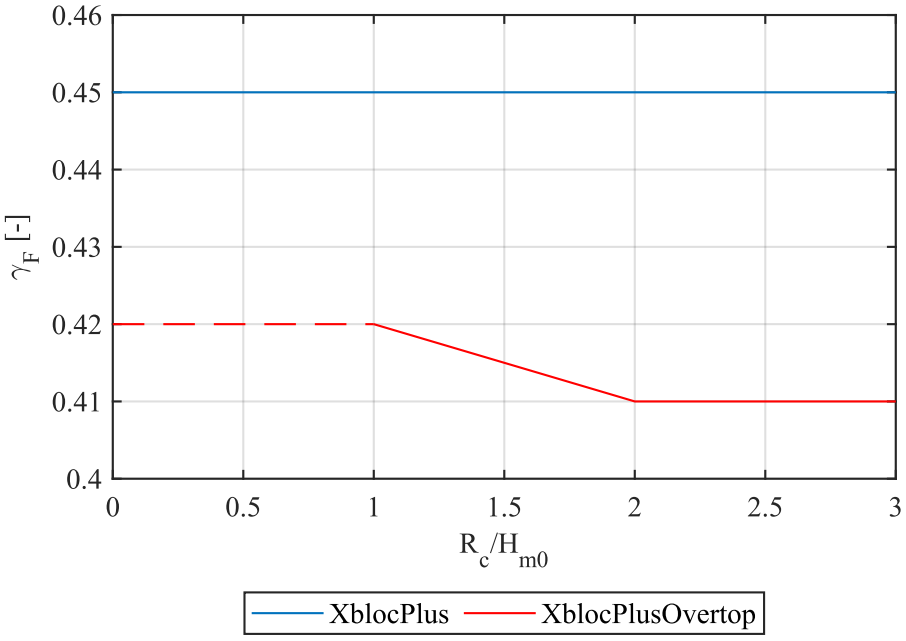

Figure 3.9. Roughness factors (γ_f) for XblocPlus® and XblocPlusOvertop® units (Adopted from Bakker et al., 2022)

As shown in Figure 3.9, γ_f value is given as 0.45 for XblocPlus®, and the varying values of γ_f is between 0.42 and 0.41 for XblocPlusOvertop® units. By considering the study, γ_f values are selected as 0.45 and 0.415 for XblocPlus® and XblocPlusOvertop®, respectively.

Bakker et al. (2022) state that a good fit is obtained by using the roughness coefficients presented above. Thus, theoretical overtopping discharge values are calculated by using these factors to compare the measurement results. All results are presented in Chapter 4.

3.2.3.4 Scour Measurements and Analyses

Overtopping-induced scour at the lee side of the coastal revetment is evaluated by profile measurements with a Bosch GLM 100C laser distance meter. As stated in Section 3.2.2, the width of the cross-section is 90 cm. Five profiles are measured within the cross-section width. The profile sections are determined within a 15-cm intervals, and measurement points are presented in Figure 3.10.

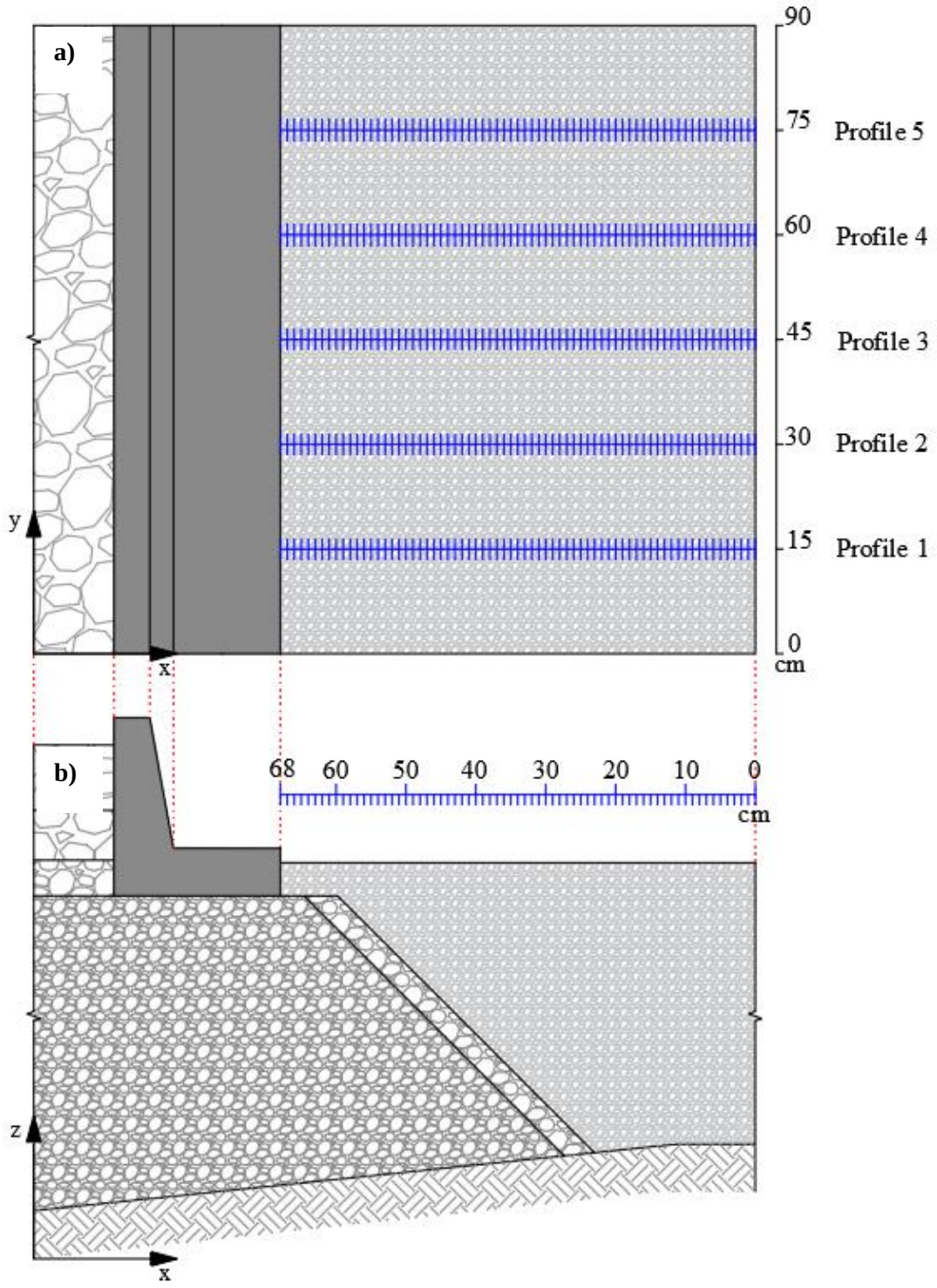

Figure 3.10. Scour measurement profiles; a) Top-view, b) Side-view (The figure is not to scaled)

Blue lines represent the measurement points of each profile in Figure 3.10, and it is shown that measurements are conducted with the Δx = 1 cm intervals along the profiles before and after the experiments. The measurement setup is presented in Figure 3.11.

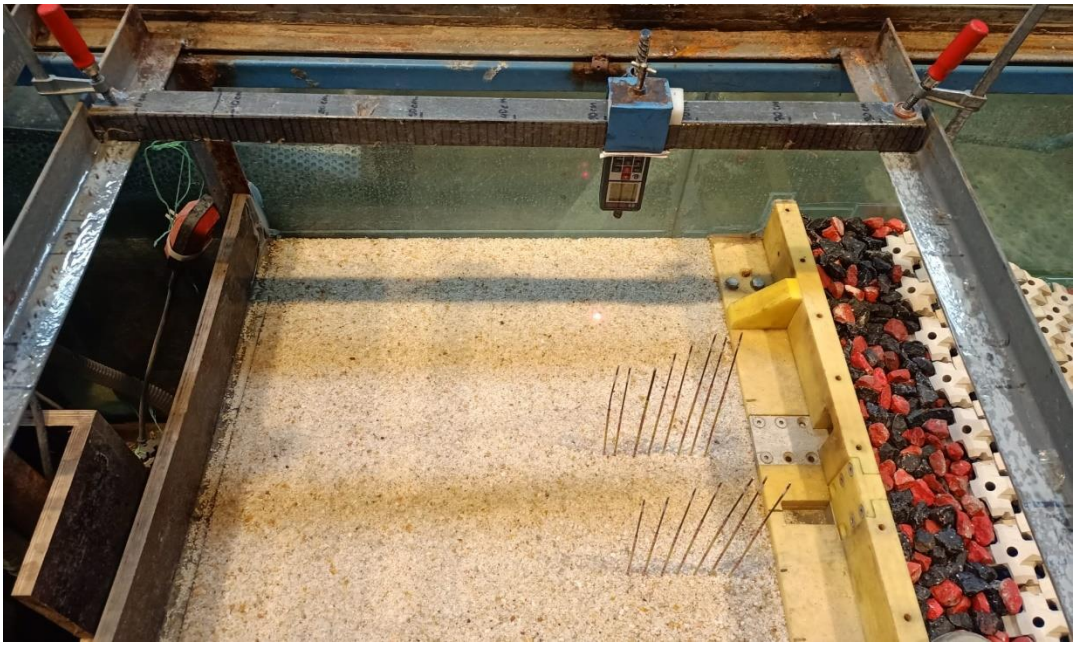

Figure 3.11. Profile measurement setup

All measurement data is visualized and analyzed using homemade MATLAB routines. Scour depths for different profiles are computed individually and on average for different wave conditions and cross-sections (see Section 3.1). An example visualization of experimental data is presented in Figure 3.12.

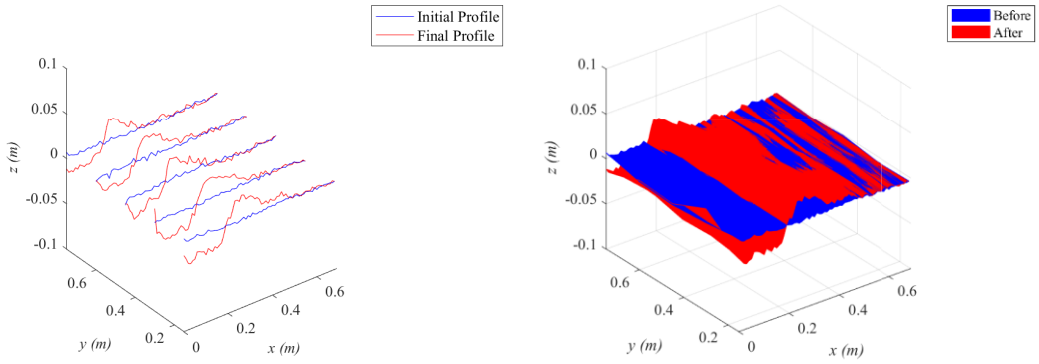

Figure 3.12. Visualization of experimental data for Section BB, D8

Silica sand with a mean diameter of 1.63 mm and a backfill depth of 22.98 cm is used to reflect the backfill material that will be placed in the project. Measured scour depths using the L-shaped crown wall for different wave conditions are compared with the equation proposed by Yıldırım et al. (2024) given for an I-shaped crown wall. The crown wall shapes tested in Yıldırım et al. (2024) and in this study are described in Figure 3.13, and the equation is presented in Equation 3.10.

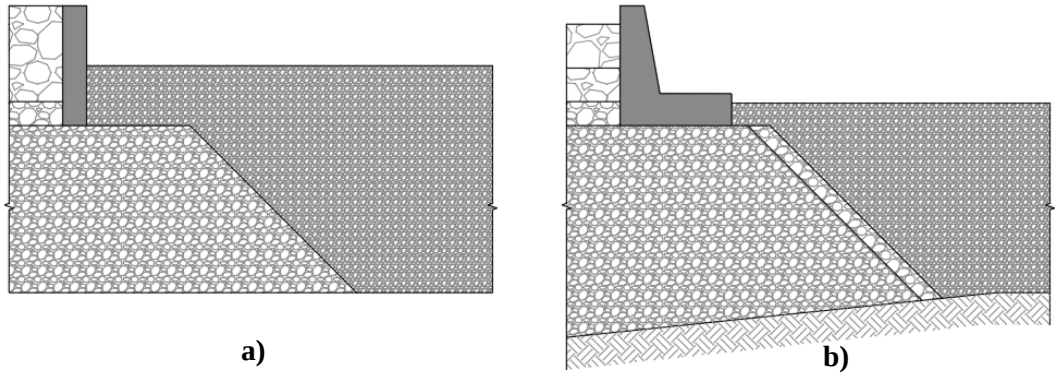

Figure 3.13. Crown wall shapes tested in; a) Yıldırım et al. (2024), b) Present study

$$ln\left(\frac{S}{d_{50}}\right) = B_0 + B_1 ln(q^*) + B_2 ln(N) + B_3 \frac{h_c}{d_{50}} + B_4 ln(q^*)^2 \quad (3.10)$$

As shown in the equation above, dimensionless scour depth is calculated by the densimetric overtopping discharge (q*), number of waves in the wave series (N), and dimensionless backfill depth (h_c/d_{50}). The densimetric overtopping discharge is calculated by following the Equation 3.11.

$$q^* = \frac{q_{mean}^2}{\Delta g d_{50}^2} \quad (3.11)$$

Coefficients shown in Equation 3.11 are presented in Table 3.12.

Table 3.12 Coefficients for Equation 3.10 (Adopted from Yıldırım et al., 2024)

Condition	N < 3000	N < 7000
B0	0.201	0.196
B1	0.893	0.909
B2	0.119	0.222
B3	0.163	0.168
B4	-0.204	-0.197

In summary, dimensionless scour depths for the experimental setup are calculated by utilizing the mean overtopping discharge results, number of waves, backfill depth, and diameter of the backfill material for the different cross-sections. The resulting computations and comparisons with experiments are presented in Chapter 4.

3.3 Details of the Cross-Sections and Experimental Program

A summary of the physical properties and scale of different cross-sections is presented in Table 3.13.

Table 3.13 Summary of scales and stone sizes for all cross-sections

Cross-section	**AA and AA2**		**BB**	
	Prototype	**Model**	**Prototype**	**Model**
$\boldsymbol{\rho_w}$ **(*kg/m³*)**	1025	1000	1025	1000
$\boldsymbol{\rho_{unit}}$ **(*kg/m³*)**	2400	2360	2400	2360
$\boldsymbol{M_{XblocPlus}}$*****	43.2	154	33.6	154
Filter 1*	4-6	12.5-18.7	4-6	16.0-23.9
Filter 2*	2-4	6.2-12.5	2-4	8.0-16.0
Filter 3*	1-2	3.1-6.2	1-2	4.0-8.0
Filter 4*	0.4-2	1.3-6.2	0.4-2	1.6-8.0
Core*	0.001-0.4	0.02-1.3	0.001-0.4	0.2-1.6
$\boldsymbol{\lambda_L}$	65.693		60.414	
$\boldsymbol{\lambda_t}$	8.105		7.773	
$\boldsymbol{\lambda_w}$	$3.19 * 10^{-5}$		$2.51 * 10^{-5}$	
**Tons in prototype, grams in model scale*				

By using the information provided above, cross-sections are constructed for different test configurations. An example cross-section for the experiments is presented in Figure 3.14.

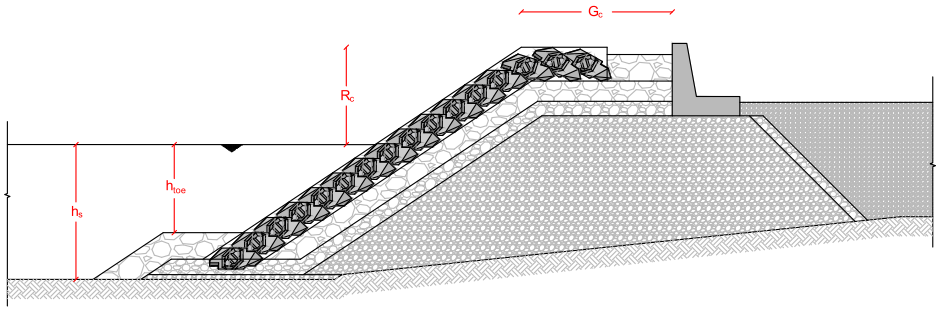

Figure 3.14. Example cross-section for the experiments

Due to the different test conditions explained above, different cross sections are constructed in the wave flume. Two cross-sections for section AA, two sections for AA2, and three sections for BB are tested in this study. These different cross-sections are presented in Appendix B, and different parameters used for the sections are explained in Table 3.14.

Table 3.14 Cross-section variations

Section	**Exp. Set**	**Armour Unit**	**Toe Unit**	h_s **(m)**	h_{toe} **(m)**	R_c **(m)**	G_c **(m)**
AA	1, 3	XP XP-OT	Rock	0.228	0.158	0.166	0.235
AA	2, 4	XP	Rock	0.228	0.158	0.166	0.235
AA2	1, 2, 3, 6	XP XP-OT	Rock	0.260	0.190	0.134	0.235
AA2	4, 5	XP	Rock	0.260	0.190	0.134	0.235
BB	1, 2, 4, 5	XP	Cube	0.175	0.092	0.159	0.235
BB	3	XP	Rock	0.175	0.102	0.159	0.235
BB	6	XP	Cube	0.175	0.092	0.159	0.120

A total of 127 experiments are conducted for three different cross-sections with seven variations and 16 sets. During these tests, different configurations are considered, as shown in Table 3.14. In Section AA, wave overtopping and stability analyses are conducted with and without XblocPlusOvertop® units. Effects of different toe units and G_c on stability, forces acting on the crown wall, and overtopping performance of the structure are observed in section BB. Moreover, overtopping induced scour at the lee side of the structure is observed in this section. Section AA and AA2 represent a deeper structure depth than Section BB. Different armour layer configurations are observed in section AA2. Moreover, the effects of different R_c values on the performance of the structure are observed by comparing section AA and section AA2.

The experimental programs and explanations for different cross-sections are presented in Table 3.15 (Section AA), Table 3.16 (Section AA2), and Table 3.17 (Section BB). XblocPlus® and XblocPlusOvertop® units are indicated as XP and XP-OT in these tables.

Table 3.15 Experiment program for section AA

Cross-Section	Set	Armour Unit	Toe Unit	Wave Conditions	Test
AA	1	XP, XP-OT	Rock	D1, D2, D3 D4.1, D4.2, D5	Wave Overtopping Stability
	2	XP	Rock	D1, D2, D3 D4.1, D4.2, D5	Wave Overtopping Stability
	3	XP, XP-OT	Rock	D1, D2, D3 D4.1, D4.2, D5	Wave Overtopping Stability
	4	XP	Rock	D1, D2, D3 D4.1, D4.2, D5	Wave Overtopping Stability

Table 3.16 Experiment program for section AA2

Cross-Section	Set	Armour Unit	Toe Unit	Wave Conditions	Test
AA-2	1	XP, XP-OT	Rock	D1, D2, D3, D4.1, D4.2, D5, D6, D7, D8	Pressure Wave Overtopping Stability
	2	XP, XP-OT	Rock	D1, D2, D3, D4.1, D4.2, D5, D6, D7, D8	Pressure Wave Overtopping
	3	XP, XP-OT	Rock	D1, D2, D3, D4.1, D4.2, D5, D6, D7, D8	Pressure Wave Overtopping Stability
	4	XP	Rock	D1, D2, D3, D4.1, D4.2, D5, D6, D7, D8	Pressure Wave Overtopping Stability
	5	XP	Rock	D1, D2, D3, D4.1, D4.2, D5, D6, D7, D8	Pressure Wave Overtopping Stability
	6	XP, XP-OT	Rock	D4.1, D4.2, D5 D6, D7, D8	Scour

Table 3.17 Experiment program for section BB

Cross-Section	Set	Armour Unit	Toe Unit	Wave Conditions	Test
BB	1	XP	Cube	D1, D2, D3, D4.1, D4.2, D5, D6, D7	Pressure Wave Overtopping Stability
	2	XP	Cube	D1, D2, D3, D4.1, D4.2, D5, D6, D7	Pressure Wave Overtopping Stability
	3	XP	Rock	D1, D2, D3, D4.1, D4.2, D5, D6, D7	Pressure Wave Overtopping Stability
	4	XP	Cube	D5, D6, D7	Scour
	5	XP	Cube	D1, D2, D3 D4.1, D4.2, D5	Wave Overtopping Stability
	6*	XP	Cube	D1, D2, D3, D4.1, D4.2, D5, D6, D7	Wave Overtopping

**G_c is shortened in this experiment set*

CHAPTER 4

RESULTS AND DISCUSSIONS

In this chapter, the results of the experiments are presented and discussed based on armour layer stability, toe stability, forces acting on the crown wall, mean overtopping volume, and overtopping induced scour at the lee side of the structure. This chapter is divided into four parts. In the first part of this chapter, results on armour and toe stability measurements are presented. Moreover, the effects of different armour units, toe units, and water depths on the stability performance of the structure are discussed. The second part presents results and discussions of pressure measurements and calculated forces acting on the crown wall. Mean overtopping discharge calculations and comparisons between the existing formulas are discussed in the third part of this chapter. Finally, results and discussions of overtopping-induced scour measurements are presented in the fourth part.

4.1 Stability Test Results

As stated in Chapter 3, damage assessments are carried out by visual inspection method for the armour and toe layers of the coastal revetment model. The number of replaced units is presented for all sections, and stability results are obtained by using the total number of units information previously provided in Table 3.10. The results of design waves (*D1, D2, D3, D4.1, D4.2, D5*) and additional waves (*D6, D7, D8*) are presented separately for all experiment sets. Overall, no damage is observed in the armour layer of the tested cross-sections constructed with either XblocPlus® or XblocPlusOvertop® units under any wave conditions. Therefore, the discussions in this section are based on the damage observations/measurements in the toe region.

The number of displaced units (N_f), stability number (N_{od}), and percentage damage (N_d) are given for each wave condition in the experimental set individually, and cumulative values are given between the beginning and final conditions of the model.

As previously indicated in Table 3.15, four sets of stability tests are conducted with the toe unit of quarry rocks (4-6 tons in prototype scale) for Section AA under D1 to D5 wave conditions. No damages are observed in the armour layer during the experiments. On the other hand, significant damage on the toe layer is observed. Stability analysis results of the toe layer for Section AA are presented in Table 4.1, and cumulative damage results are visualized in Figure 4.1. In Figure 4.1, red curves indicate the cases where XblocPlus® units are used together with XblocPlusOvertop® units, and blue curves indicate the cases where only XblocPlus® units are used when constructing the cross-sections in the experiments.

Table 4.1 Toe layer stability analysis results for Section AA

Wave Cond.		**D1**	**D2**	**D3**	**D4.1**	**D4.2**	**D5**	**D1-D5**
N_s		2.50	2.91	3.31	3.56	3.46	3.73	-
SET 1	$N_{f,\,toe}$	12	11	32	29	7	21	112
	$N_{d,\,toe}$ **(%)**	1.68	1.54	4.49	4.07	0.98	2.95	15.71
	$N_{od,\,toe}$	0.24	0.22	0.64	0.58	0.14	0.42	2.24
SET 2	$N_{f,\,toe}$	8	5	17	21	9	19	79
	$N_{d,\,toe}$ **(%)**	1.12	0.70	2.38	2.95	1.26	2.66	11.08
	$N_{od,\,toe}$	0.16	0.10	0.34	0.42	0.18	0.38	1.58
SET 3	$N_{f,\,toe}$	13	13	23	27	10	20	106
	$N_{d,\,toe}$ **(%)**	1.82	1.82	3.23	3.79	1.40	2.81	14.87
	$N_{od,\,toe}$	0.26	0.26	0.46	0.54	0.20	0.40	2.12
SET 4	$N_{f,\,toe}$	15	16	15	19	11	24	100
	$N_{d,\,toe}$ **(%)**	2.10	2.24	2.10	2.66	1.54	3.37	14.03
	$N_{od,\,toe}$	0.30	0.32	0.30	0.38	0.22	0.48	2.00

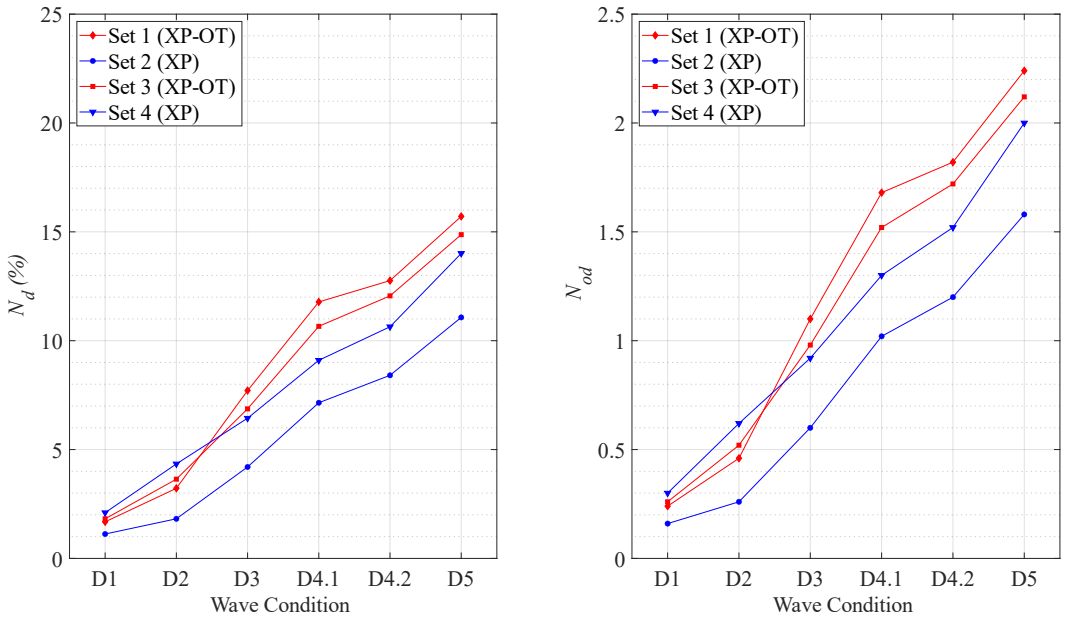

Figure 4.1. Cumulative damage results on the toe layer for Section AA

A negative impact of XblocPlusOvertop® units on toe stability is observed, as presented in Table 4.1 and Figure 4.1. However, these units did not affect the toe stability performance of the structure for smaller wave heights (D1, D2) due to the limited run-up heights. Moreover, the same wave conditions with different depths (D4.1, D4.2) showed significant differences. The wave condition D4.1, which corresponds to LWL, caused more damage compared to D4.2, which corresponds to HWL. Overall, a 21.8% increase in cumulative damage is observed for the experiments conducted with XblocPlusOvertop® units.

Four stability tests are conducted with and without XblocPlusOvertop® units and the toe layer with quarry rock (4-6 tons in prototype scale) for Section AA2 (see Table 3.16) for all wave conditions from D1 to D8. No damages are observed in the armour layer during the experiments, and stability analysis results only on the toe layer for Section AA2 are presented in Table 4.2 for design wave conditions (*D1-D5*) and Table 4.3 for additional waves (*D6-D8*), and cumulative damage results are visualized in Figure 4.2 (*D1-D5*) and Figure 4.3 (*D6-D8*) separately for design and additional wave conditions. In these figures, red curves indicate the cases where XblocPlus® units are used together with XblocPlusOvertop® units, and blue curves

indicate the cases where only XblocPlus® units are used when constructing the cross-sections in the experiments.

Table 4.2 Toe layer stability analysis results for Section AA2 (*D1-D5*)

Wave Cond.		D1	D2	D3	D4.1	D4.2	D5	D1-D5
N_s		2.87	3.30	3.77	3.91	3.98	4.28	-
SET 1	$N_{f,\,toe}$	6	3	10	27	3	12	61
	$N_{d,\,toe}$ (%)	0.87	0.43	1.44	3.90	0.43	1.73	8.80
	$N_{od,\,toe}$	0.12	0.06	0.20	0.54	0.06	0.24	1.22
SET 3	$N_{f,\,toe}$	7	5	15	22	7	19	75
	$N_{d,\,toe}$ (%)	1.01	0.72	2.16	3.17	1.01	2.74	10.82
	$N_{od,\,toe}$	0.14	0.10	0.30	0.44	0.14	0.38	1.50
SET 4	$N_{f,\,toe}$	3	1	7	18	3	16	48
	$N_{d,\,toe}$ (%)	0.43	0.14	1.01	2.60	0.43	2.31	6.93
	$N_{od,\,toe}$	0.06	0.02	0.14	0.36	0.06	0.32	0.96
SET 5	$N_{f,\,toe}$	6	2	8	12	5	9	42
	$N_{d,\,toe}$ (%)	0.87	0.29	1.15	1.73	0.72	1.30	6.06
	$N_{od,\,toe}$	0.12	0.04	0.16	0.24	0.10	0.18	0.84

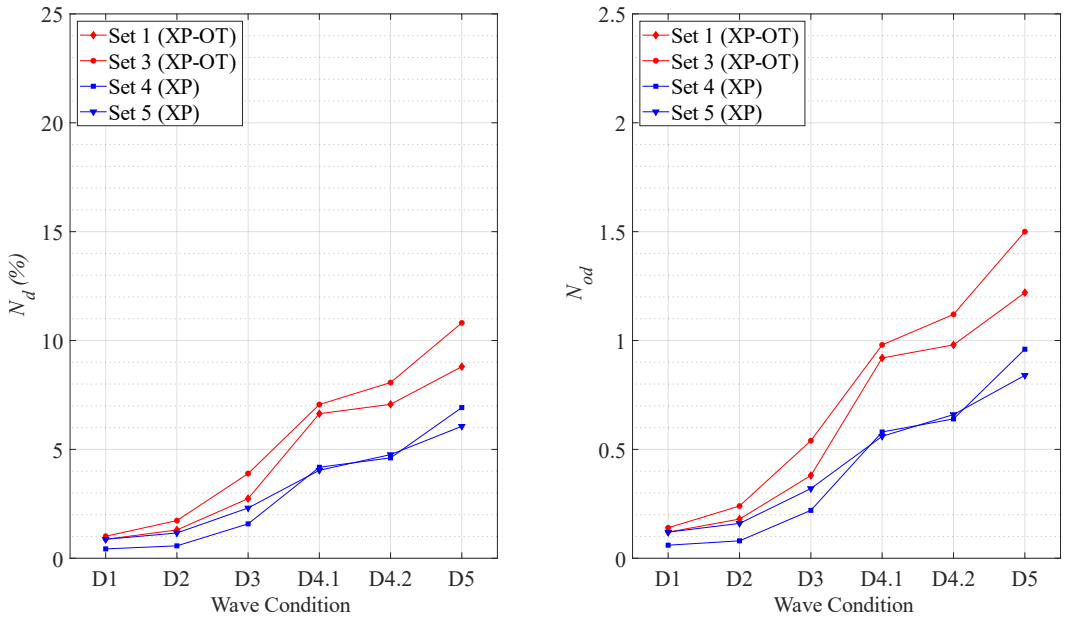

Figure 4.2. Cumulative damage results on the toe layer for Section AA2 (*D1-D5*)

Similar to Section AA, more damage on the toe layer is observed when the XblocPlusOvertop® units are placed on the structure. On average, a 51% increase in

the cumulative damages is observed, as shown in the table above. This situation is observed for the relatively high wave heights significantly. For the smaller waves (D1, D2), consistent results are observed for the cases constructed with and without XblocPlusOvertop® units. The water level effect shows consistency with Section AA such that the LWL condition for the same wave properties (D4.1) caused more damage with respect to the HWL condition (D4.2) on the toe layer.

Table 4.3 Toe layer stability analysis results for Section AA2 (*D6-D8*)

Wave Cond.		**D6**	**D7**	**D8**	**D6-D8**
	N_s	4.51	4.86	5.17	-
SET 1	$N_{f,\,toe}$	44	39	44	127
	$N_{d,\,toe}$ **(%)**	6.35	5.63	6.35	18.33
	$N_{od,\,toe}$	0.88	0.78	0.88	2.54
SET 3	$N_{f,\,toe}$	39	28	29	96
	$N_{d,\,toe}$ **(%)**	5.63	4.04	4.18	13.85
	$N_{od,\,toe}$	0.78	0.56	0.58	1.92
SET 4	$N_{f,\,toe}$	31	32	39	102
	$N_{d,\,toe}$ **(%)**	4.47	4.62	5.63	14.72
	$N_{od,\,toe}$	0.62	0.64	0.78	2.04
SET 5	$N_{f,\,toe}$	29	38	39	106
	$N_{d,\,toe}$ **(%)**	4.18	5.48	5.63	15.30
	$N_{od,\,toe}$	0.58	0.76	0.78	2.12

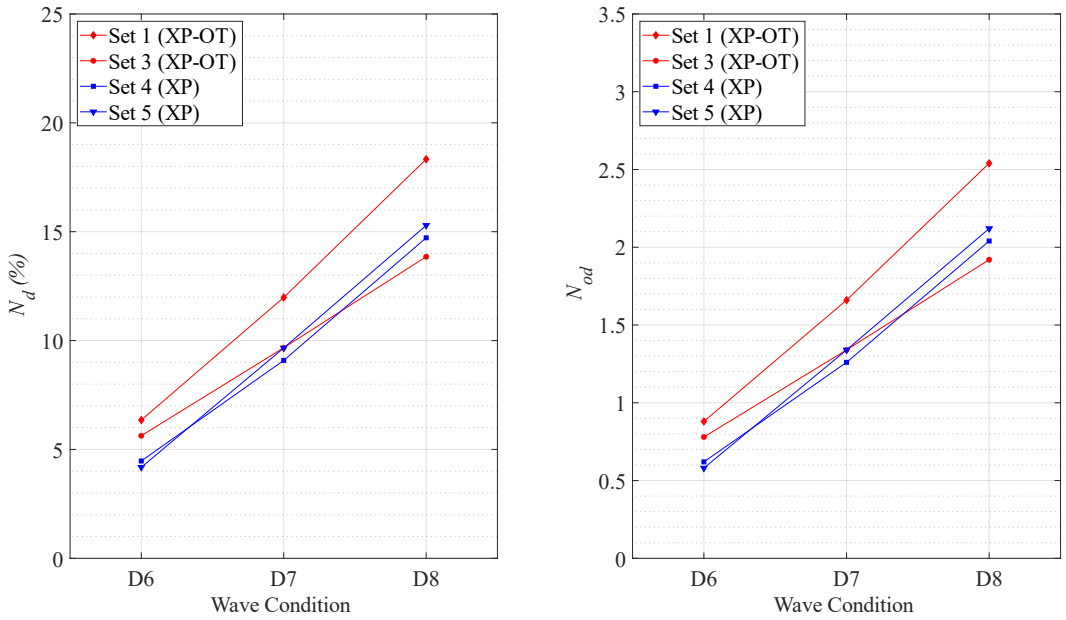

Figure 4.3. Cumulative damage results on the toe layer for Section AA2 (*D6-D8*)

Additional wave conditions for Section AA2 show similar results with design wave conditions. It is observed that implementing XblocPlusOvertop® units causes less toe stability performance.

As previously presented in Table 3.17, four sets of stability tests are conducted for Section BB using only XblocPlus® units for D1 to D7 wave conditions. Three sets of experiments are conducted using cube blocks (10 tons in prototype scale) in the toe, and one set of experiments is conducted using quarry rock (4-6 tons in prototype scale) in the toe layer. No damages are observed in the armour layer during the experiments with the design waves. Thus, stability analysis results only on the toe layer for Section BB are presented in Table 4.4, and cumulative damage results are visualized in Figure 4.4. Figure 4.4 shows the difference between the performance of toe design with quarry rock (blue curve) and cube blocks (red curves).

Table 4.4 Toe layer stability analysis results for Section BB (*D1-D5*)

Wave Cond.		D1	D2	D3	D4.1	D4.2	D5	D1-D5
N_s		1.91	2.17	2.61	2.91	2.78	3.26	-
SET 1	$N_{f,\,toe}$	5	1	3	3	2	5	19
	$N_{d,\,toe}$ (%)	1.30	0.26	0.78	0.78	0.52	1.30	4.94
	$N_{od,\,toe}$	0.15	0.03	0.09	0.09	0.06	0.15	0.57
SET 2	$N_{f,\,toe}$	5	3	3	2	1	3	17
	$N_{d,\,toe}$ (%)	1.24	0.75	0.75	0.50	0.25	0.75	4.23
	$N_{od,\,toe}$	0.15	0.09	0.09	0.06	0.03	0.09	0.51
SET 3	$N_{f,\,toe}$	22	15	42	29	18	20	146
	$N_{d,\,toe}$ (%)	3.16	2.15	6.03	4.16	2.58	2.87	20.95
	$N_{od,\,toe}$	0.48	0.33	0.91	0.63	0.39	0.44	3.18
SET 5	$N_{f,\,toe}$	6	3	12	4	3	1	29
	$N_{d,\,toe}$ (%)	1.49	0.75	2.99	1.00	0.75	0.25	7.21
	$N_{od,\,toe}$	0.18	0.09	0.36	0.12	0.09	0.03	0.87

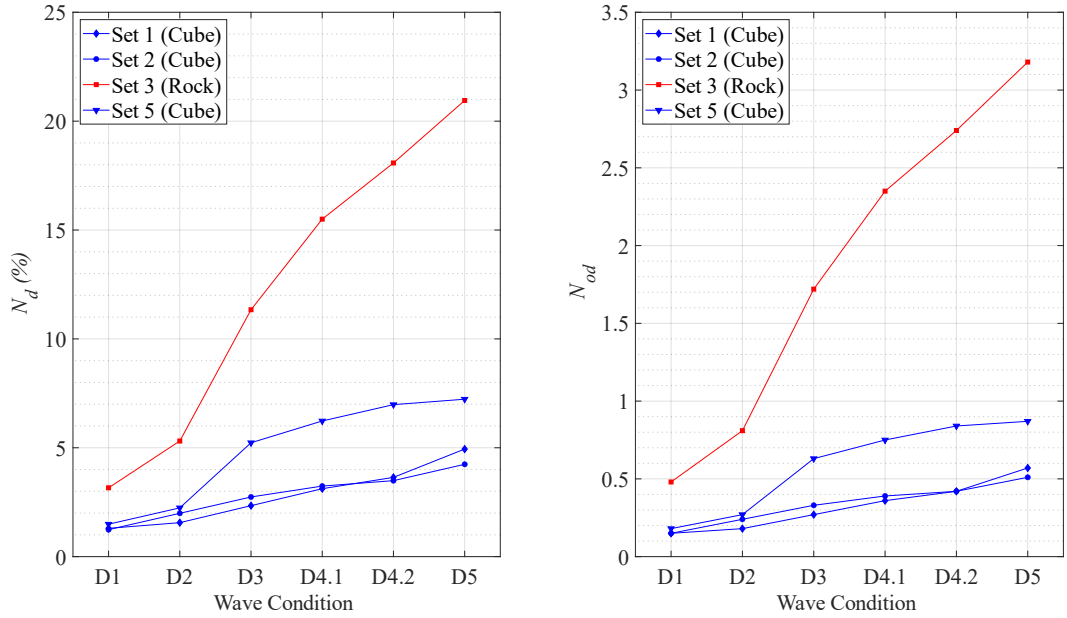

Figure 4.4. Cumulative damage results on the toe layer for Section BB (*D1-D5*)

The effect of water level on the toe layer stability and performances of different units are observed in this experimental set in Section BB. When the wave conditions are

evaluated individually, it is observed that D4.2 (HWL) caused less damage than D4.1 (LWL) for the same wave conditions (see Table 4.4). Also, on average, 283% more damage is observed for the section with quarry rocks. Due to the challenges of placing cube units in irregular patterns, deviation in the results for the cross-sections with cube units is observed for only one experimental set, as shown in Figure 4.4. On the other hand, consistent results are observed for other experiments.

Additional wave conditions (*D6, D7*) are also tested for Section BB. As stated in Chapter 3, these wave conditions are analyzed separately, and results are presented in Figure 4.5. Similarly, no damages are observed in the armour layer, and all results are presented for the toe layer.

Table 4.5 Toe layer stability analysis results for Section BB (*D6, D7*)

Wave Cond.		**D6**	**D7**	**D6-D7**
	N_s	3.26	3.62	-
SET 1	$N_{f,\,toe}$	11	6	17
	$N_{d,\,toe}$ **(%)**	2.86	1.56	2.45
	$N_{od,\,toe}$	0.33	0.18	0.51
SET 2	$N_{f,\,toe}$	10	6	16
	$N_{d,\,toe}$ **(%)**	2.60	1.56	2.31
	$N_{od,\,toe}$	0.30	0.18	0.48
SET 3	$N_{f,\,toe}$	43	22	65
	$N_{d,\,toe}$ **(%)**	6.17	3.16	9.38
	$N_{od,\,toe}$	0.86	0.44	1.30
SET 5	$N_{f,\,toe}$	3	0	3
	$N_{d,\,toe}$ **(%)**	0.78	0.00	0.43
	$N_{od,\,toe}$	0.09	0.00	0.09

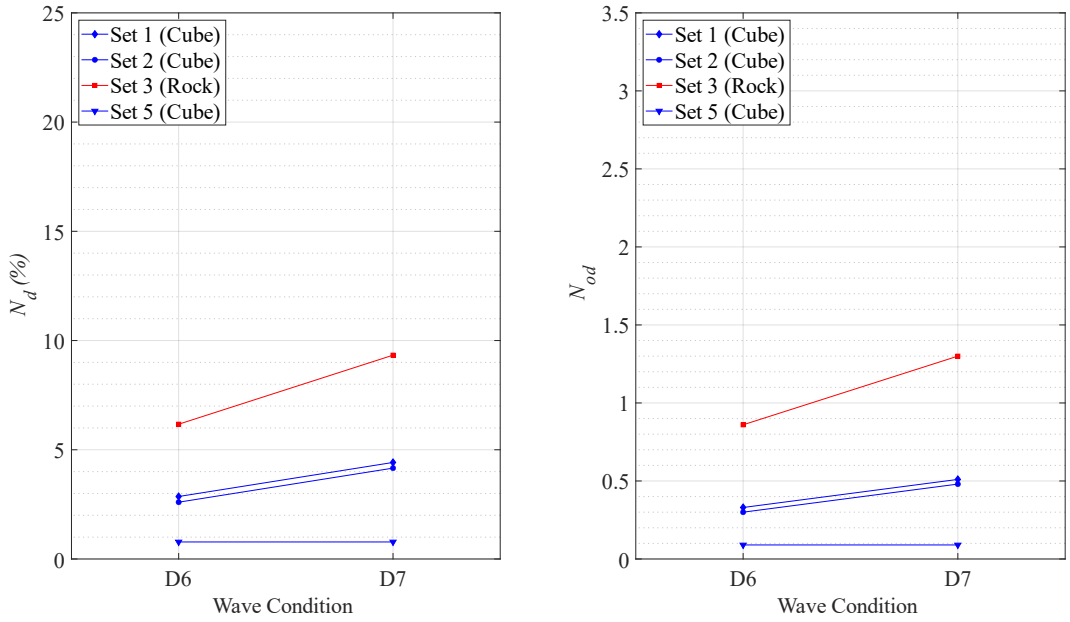

Figure 4.5. Cumulative damage results on the toe layer for Section BB (*D6, D7*)

A similar behavior is observed for additional waves (D6, D7) compared to design waves (D1 to D5). A significant increase in the damage is observed for the toe layer with quarry rocks.

Different toe stability performances are observed for the sections with and without XblocPlusOvertop® units. This difference is observed in Sections AA and AA2 and shown in Figure 4.1 and Figure 4.2. These figures show that using XblocPlusOvertop® units causes more damage at the toe layer. Damage observed in the toe section increased by 36% on average for the sections designed with XblocPlusOvertop® units except for the small wave height conditions (D1 and D2). This result is explained based on the different run-down processes of the waves for the cases with and without XblocPlusOvertop® units. The difference in the run-down process of the waves is shown in Figure 4.6.

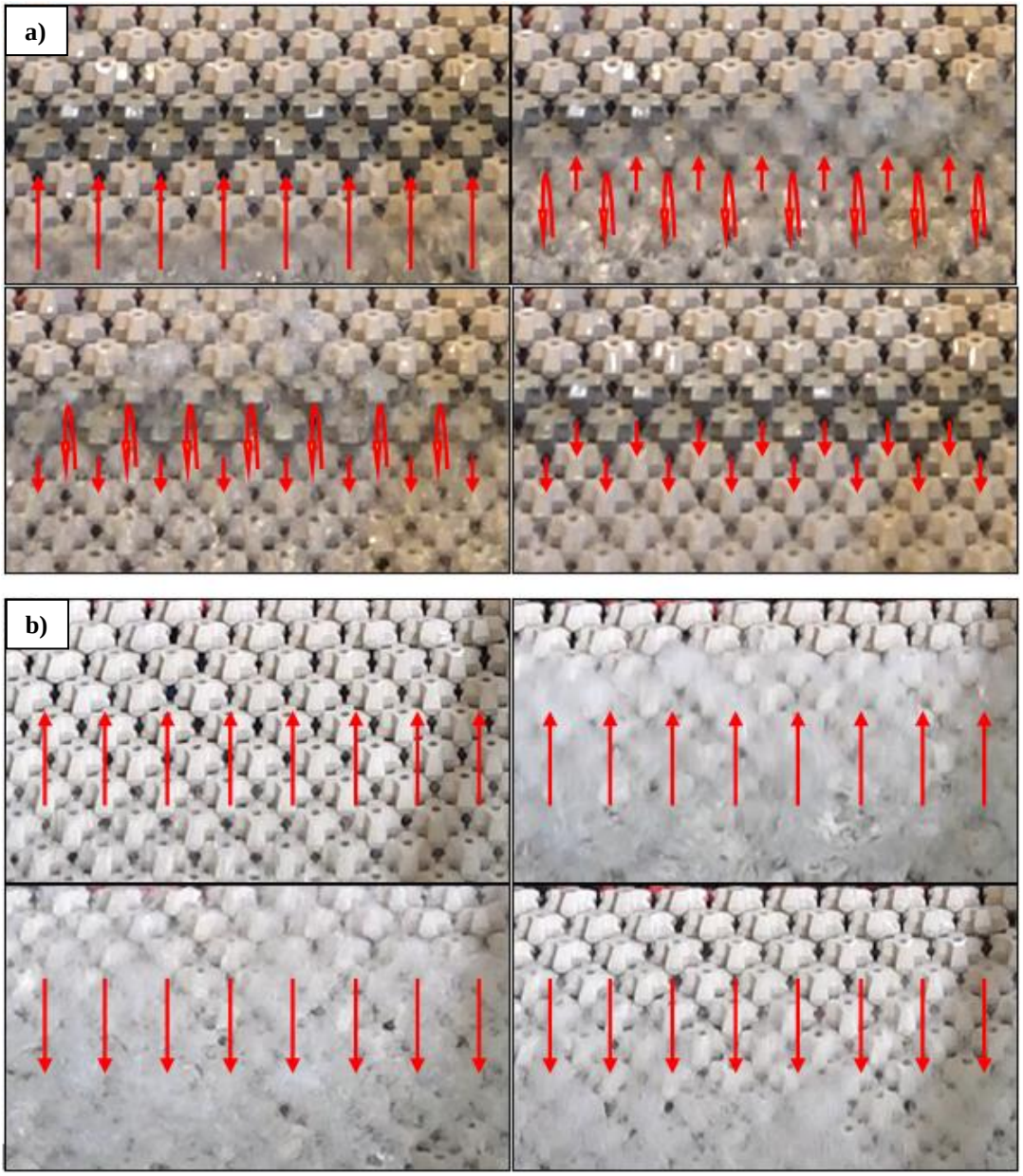

Figure 4.6. Difference in run down process; a) with XblocPlusOvertop® units, b) without XblocPlusOvertop® units. (Dark grey units in (a) are XblocPlusOvertop® units.)

Figure 4.6a shows that incident waves are reflected and run down towards the toe region very quickly, without losing their energy, as the run-up process is not completed. Similar instants from the experiments are visualized in Figure 4.6b for the case where only XblocPlus® units are used in the cross-section, and it is seen that

the run-down process starts after the run-up process is completed, where more wave energy is dissipated without any reflection as in the case where the XblocPlusOvertop® units are in place. Bakker et al. (2022) also observed this difference in the run-down patterns, where a similar mechanism to bullnose structures is identified when XblocPlusOvertop® units are used in the tested cross-sections. This situation also explains the similar results between the sections constructed with XblocPlus® and XblocPlusOvertop® units together with the sections with only XblocPlus® units for smaller wave heights. Disturbance of the run-up and run-down processes is not observed due to limited run-up heights for D1 and D2 wave conditions, and the effects of XblocPlusOvertop® units are decreased.

Additionally, the differences between the various structure depths on the stability of the toe are presented in Figure 4.7. The cases with rock units in the toe and sections without XblocPlusOvertop® units are selected. Set 2 for Section AA, Set 4 for Section AA2, and Set 3 for Section BB are plotted to present the effects of different structure depths. The green curve, red curve, and blue curve represent Section AA, Section AA2, and Section BB, respectively, for this comparison shown in Figure 4.7.

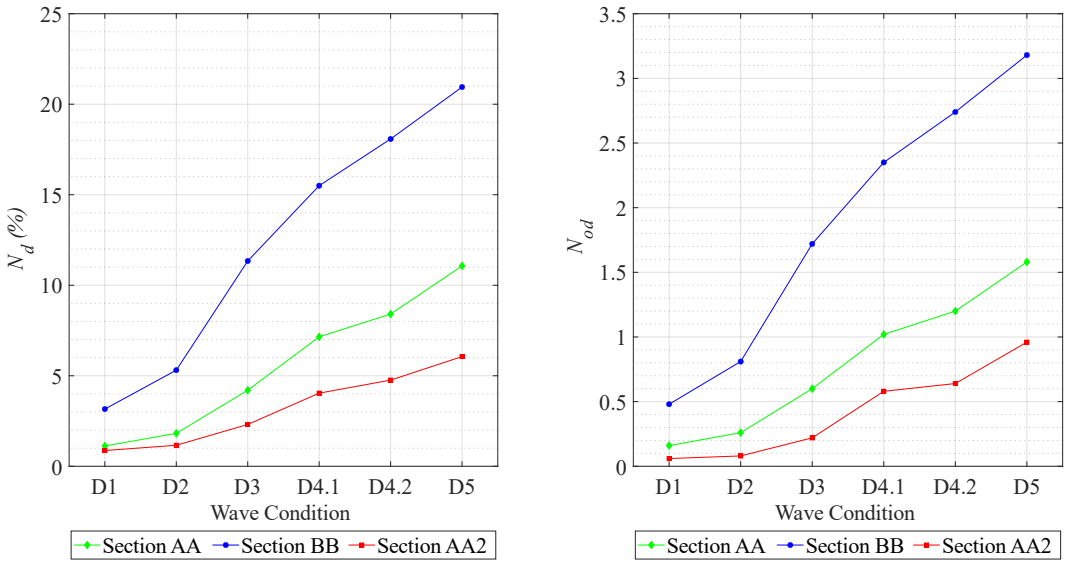

Figure 4.7. Comparison between the toe stability results of different water depths

Section BB represents the shallower, and Section AA2 represents the deeper structure depth for the coastal revetment. As expected, more critical results on toe stability are observed for the cross-section with lower toe depth. D4.1 and D4.2 wave conditions for each experimental setup also represent the effects of the different water depths and the similar observations to Figure 4.7 is presented for these two wave conditions.

In addition to the discussions above, all experimental measurements on toe stability are presented with respect to the stability number (N_s), which is shown in Equation 4.1.

$$N_s = \frac{H_s}{\Delta D_{n50}} \qquad (4.1)$$

The results of N_d and N_{od} with respect to N_s are presented in Figure 4.8 and Figure 4.9, respectively.

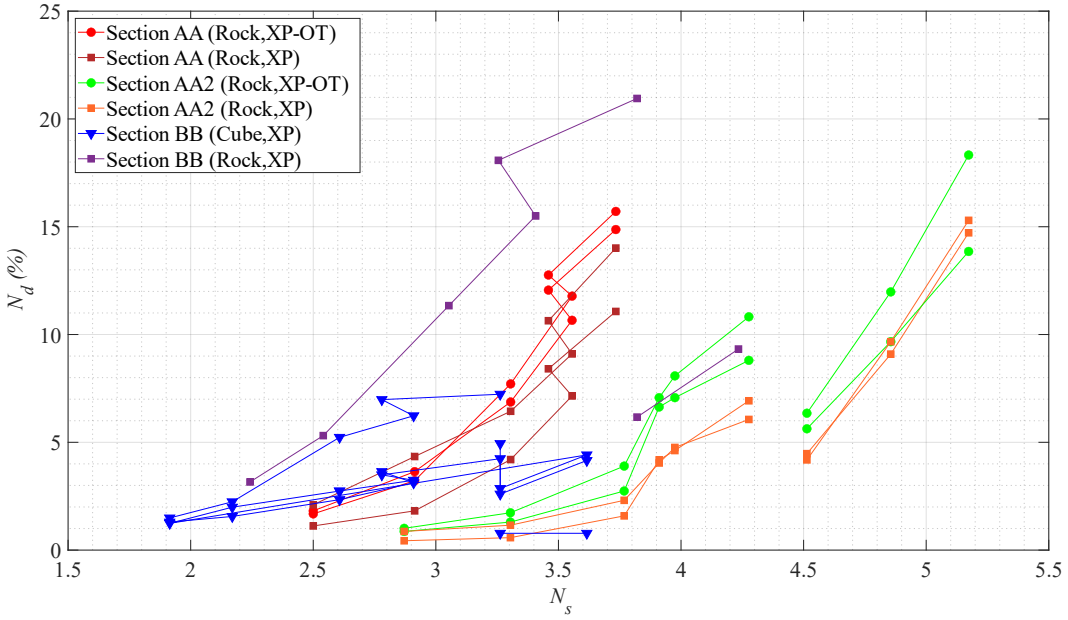

Figure 4.8. Comparison of N_d results with respect to N_s for all experiments

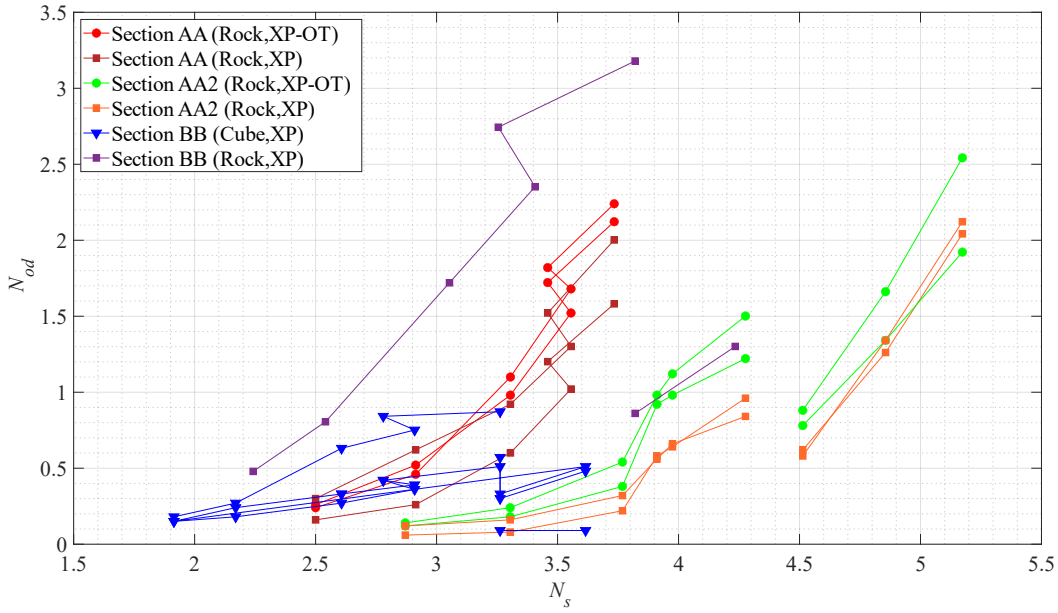

Figure 4.9. Comparison of N_{od} results with respect to N_s for all experiments

In these figures, red scatter points represent Section AA, and green scatter points represent Section AA2. Quarry rocks are used in the toe layer for these cross-sections. Blue and purple scatter points represent Section BB with cube block and quarry rock in the toe section, respectively. As shown in Figure 4.8 and Figure 4.9, the maximum damages are observed in the case with the shallowest water conditions and quarry rocks in the toe layer (Section BB), and the minimum damages are observed for the cube block units (Section BB). Section AA shows more damage on the toe layer than Section AA2 due to the toe depth variations. Moreover, for the same N_s value, the damage also shows a variation (see e.g. green scatter points for N_s=3.9). This result is most probably related to the placement of the units and blocks. However, the order of magnitude of N_d and N_{od} remains similar for the same N_s value.

As discussed above, while significant damage on the toe layer is observed, no damage is observed in the armour layer. This discussion shows that failure on the toe layer does not lead to the armour layer failure. Moreover, as Reedijk et al. (2018) and Bakker et al. (2019) presented, no damage observation for the armour layer with XblocPlus® units is expected. Bakker et al. (2019) state that no damage is observed even for the stability number N_s = 5.5 during the hydraulic stability tests of

XblocPlus® units. Similar results are observed in experiments conducted with stability numbers up to 5.2.

4.2 Forces Acting on the Crown Wall

As stated in the Chapter 3, horizontal forces acting on a crown wall are measured by pressure sensors for Section AA2 with all wave conditions from D1 to D8 and for Section BB with the wave conditions from D1 to D7. Four measurement locations are determined to place four pressure sensors. During the pressure measurements, a cross-section is constructed with XblocPlus® and XblocPlusOvertop® together, and a cross-section with only XblocPlus® units.

Measured pressure data is converted to force and momentum values by following the equations given in Section 3.2.3.2, and these results are compared with the formulas provided by Pedersen (1996) and Nørgaard et al. (2013). The performances of these formulas on this specific project are evaluated by comparing the predicted values and measured data. Moreover, differences between the methodologies suggested by Pedersen (1996) and Nørgaard et al. (2013) are presented in the results.

To enhance the prediction performances of the equations stated above, modified coefficients are suggested by conducting statistical assessments, which are explained later in this section. The experimental results of horizontal wave forces exceeded by 0.1% of the waves ($F_{H,0.1\%}$) are compared to the computations carried out with the suggested formulas by Pedersen (1996) and Nørgaard et al. (2013) in Figure 4.10.

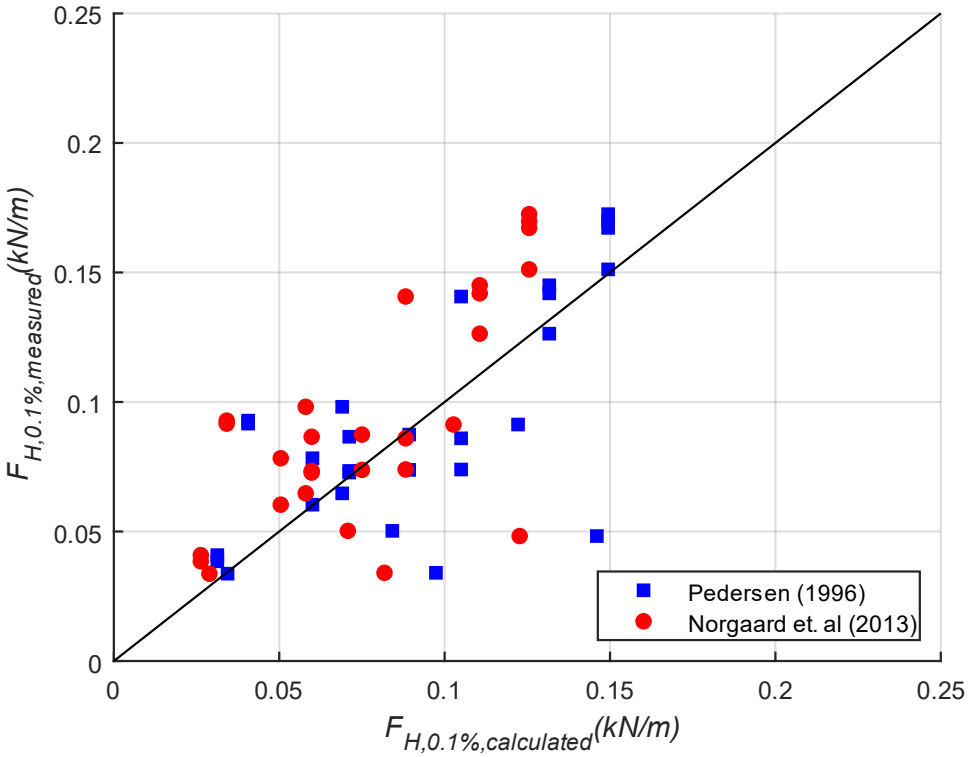

Figure 4.10. Comparison of Pedersen (1996) and Nørgaard et al. (2013) formulas with measured experimental data for $F_{H,0.1\%}$

As shown in Figure 4.10, Pedersen (1996) predict the forces acting on the crown wall slightly better than Nørgaard et al. (2013). Statistical assessments for these two different approaches are presented in Table 4.6. Statistical analysis is conducted using mean absolute error (MAE) and root mean square error (RMSE) error metrics to obtain modified coefficients that would improve the horizontal force predictions. The formulas of these error metrics are presented in Equations 4.2 and 4.3.

$$MAE = \frac{1}{n}\sum_{i=1}^{n}|p_i - O_i| \qquad (4.2)$$

$$RMSE = \sqrt{\frac{1}{n}\sum_{i=1}^{n}(p_i - O_i)^2} \qquad (4.3)$$

In these equations, predicted values are denoted by p_i, O_i represents the observed values and n represents the number of data.

Table 4.6 Statistical assessment of Pedersen (1996) and Nørgaard et al. (2013) methodology for $F_{H,0.1\%}$

	Coefficient		MAE	RMSE
Nørgaard et al. (2013)	*a*	0.210	0.0272	0.0334
	b	1.000		
Pedersen (1996)	*a*	0.210	0.0219	0.0311
	b	1.600		

As shown in Figure 4.10 and shown in Table 4.6, although both approaches show a good fit overall, Pedersen (1996) methodology shows better results in terms of MAE and RMSE by 24.2% and 7.4%, respectively. Experimental data shows slight differences between the predicted forces by following the Pedersen (1996) and Nørgaard et al. (2013) methodologies. Overall, the prediction formulas underestimate the results obtained by the pressure measurements for the tested cross-sections in the present study.

Since Nørgaard et al. (2013) modified the formula given by Pedersen (1996) for the shallow water conditions, empirical coefficients are modified to obtain a better fit between the measured data and predicted values for only the formula provided by Nørgaard et al. (2013). This formula suggests two empirical coefficients symbolized with *a* and *b*.

Although there is limited experimental data and a specific design for a consultancy project, modified *a* and *b* coefficients are determined as a=0.225 and b=1.180, which minimizes the error metrics. The comparison between the experimental measurements with the Pedersen (1996) and Nørgaard et al. (2013) formulations with modified coefficients is presented in Figure 4.11 for $F_{H,0.1\%}$.

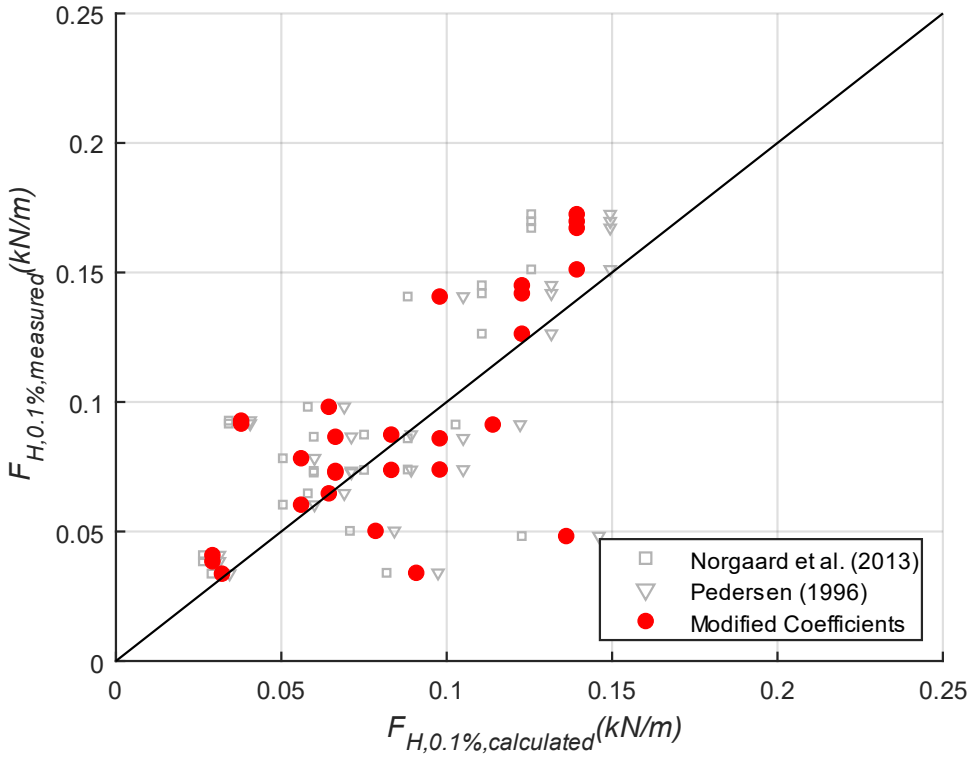

Figure 4.11. Comparison between the experimental measurements and Nørgaard et al. (2013) formulation with modified coefficients for $F_{H,0.1\%}$

As stated before, Nørgaard et al. (2013) showed a good fit overall, but slight modification in the empirical coefficients increased the accuracy, as shown in Figure 4.11. It is observed that the formula with modified empirical coefficients decreased the underestimation, and statistical assessment results are presented in Table 4.7 for modified coefficients.

Table 4.7 Statistical assessment of modified empirical coefficients for $F_{H,0.1\%}$

Coefficient		**MAE**	**RMSE**
$a_{modified}$	0.225	0.0217	0.0312
$b_{modified}$	1.180		

As presented in Table 4.7, prediction for forces acting on the crown wall by using the formula and coefficients suggested by Nørgaard et al. (2013) are improved with

modified empirical coefficients. The statistical assessment results show that the performance of the prediction formula is improved as the MAE and RMSE are decreased by 25.4% and 7.1%, respectively. These results show that the existing formulas underestimate the forces acting on the crown wall for XblocPlus® and XblocPlusOvertop® armoured coastal structures. For this specific design, it is observed that these recently developed units decrease the forces on the crown wall.

In addition to $F_{H,0.1\%}$ measurements, and analyses, moment exceeded by 0.1% of the waves ($M_{H,0.1\%}$) calculations based on experimental measurements are conducted and compared with Nørgaard et al. (2013) methodology. Similar to the force calculations, relations between the existing formulas and measured moment data are evaluated, and statistical assessments are carried out by following the formulas presented in Equations 4.2 and 4.3. As stated by Nørgaard et al. (2013) and Demir (2023), a linear relation between the behavior of $F_{H,0.1\%}$, and $M_{H,0.1\%}$, is observed in the literature. Thus, empirical coefficients in the moment prediction equation (e_1=0.95 and e_2=0.4) are not modified for the moment comparisons. All moment calculations are conducted based on the force calculations with modified *a* and *b* coefficients, as presented before. Moment comparisons using the wave force estimations with modified (present study) and suggested coefficients (Norgaard et al., 2013) are presented in Figure 4.12.

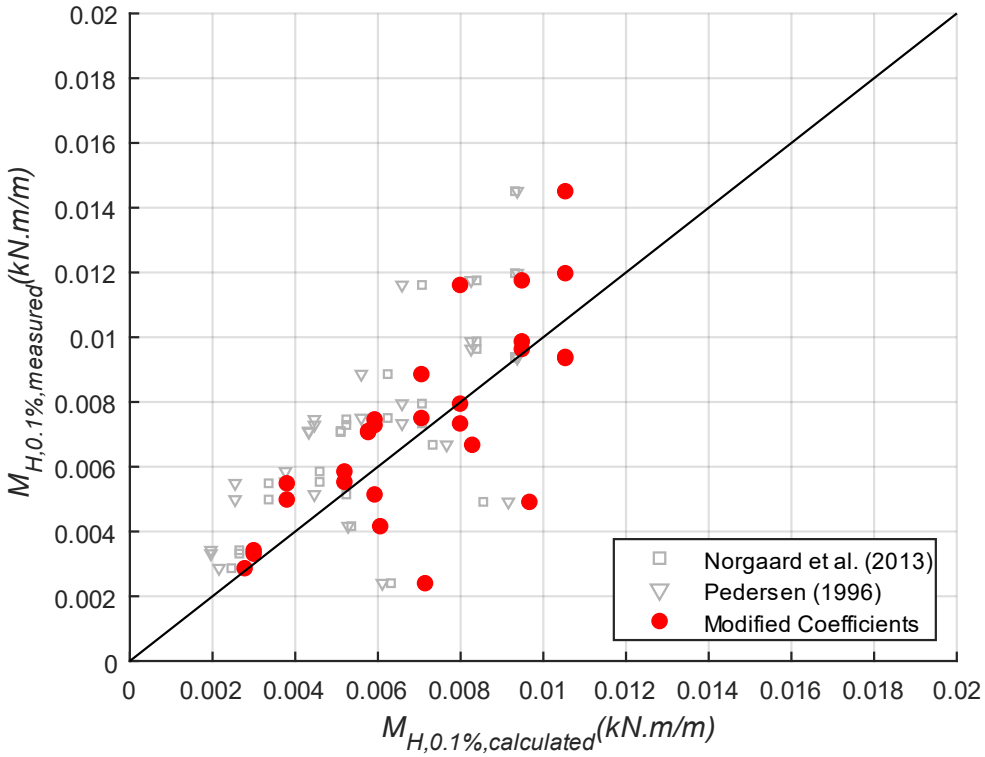

Figure 4.12. Comparison between the measured and predicted $M_{H,0.1\%}$ for modified and suggested coefficients

As shown in Figure 4.12, a good fit between the measured and calculated moment values when the modified coefficients are implemented into the equations. Statistical assessment of the coefficients is conducted for both suggested and modified values. The results of these analyses are presented in Table 4.8.

Table 4.8 Statistical assessment of suggested and modified empirical coefficients for $M_{H,0.1\%}$

Formula	Coefficient		MAE	RMSE
Nørgaard et al. (2013)	a	0.210	0.0018	0.0022
	b	1.000		
Present Study	$a_{modified}$	0.225	0.0015	0.0020
	$b_{modified}$	1.180		

As presented in Table 4.8, prediction for a moment on the crown wall by using the formula and coefficients suggested by Nørgaard et al. (2013) are improved with modified empirical coefficients. The statistical assessment results show that the performance of the prediction formula is increased by decreasing the MAE by 20% and RMSE by 10%.

In conclusion, pressure measurements are conducted to determine the forces and moments acting on the crown wall of a specifically designed coastal revetment cross-section for this case study. Although Pedersen's (1996) methodology gives better predictions for both moment and force predictions than Nørgaard et al. (2013), modifications to the empirical coefficients are conducted for Nørgaard et al. (2013) methodology due to the shallow water conditions. Slightly improved predictions can be made with the available formulas using modified empirical coefficients. Improving the prediction formulas for the forces improves the moment calculations due to the linear relationship between different formulas.

In addition to the discussions above, the effects of XblocPlusOvertop® units on the forces acting on a crown wall are evaluated by comparing the experimental measurements of $F_{h0.1\%}$ for the Sections AA2 experiments considering utilized wave conditions, where different cases with and without placing XblocPlusOvertop® units are available. The results of the comparisons are presented in Figure 4.13. In this figure, red scatter points represent XblocPlus®, and blue scatter points represent XblocPlusOvertop® units.

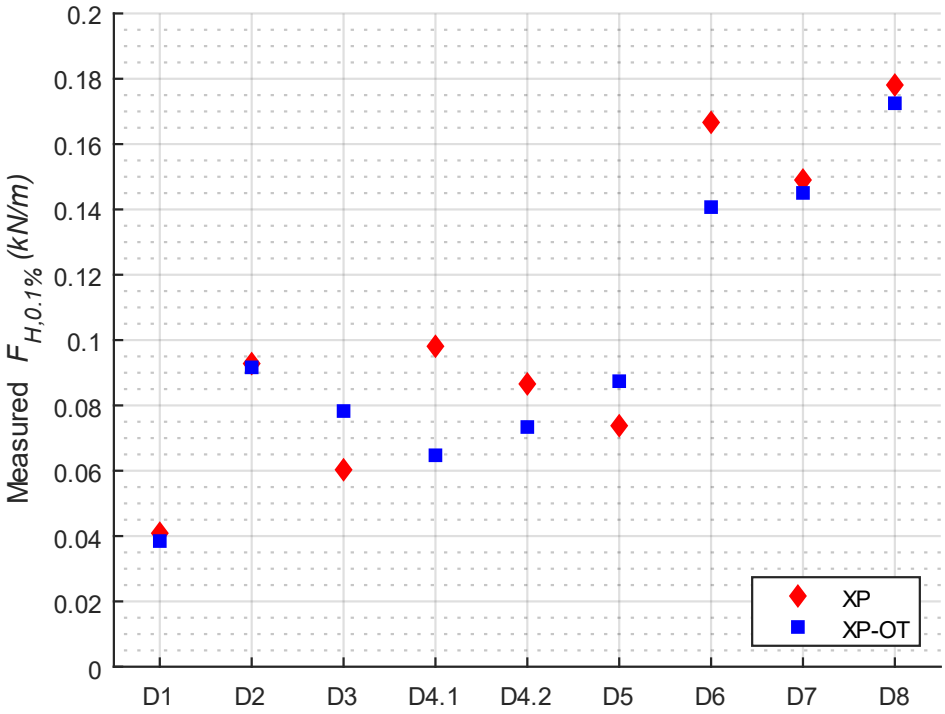

Figure 4.13. $F_{H,0.1\%}$ for XblocPlus® and XblocPlusOvertop® units

As shown in Figure 4.13, measured $F_{H,0.1\%}$ values decreased when the XblocPlusOvertop® units were placed in the armour layer. This situation is expected due to the behavior explained in Figure 4.6. XblocPlusOvertop® units disturb the run-up process of the incident waves and prevent the waves from reaching the crown wall. Thus, measured forces acting on the crown wall are decreased.

4.3 Wave Overtopping Volume

Wave overtopping measurements are conducted to test the serviceability performance of the structure. Measured overtopping volumes in the model scale are presented in Table 4.9, Table 4.10, and Table 4.11 for all cross-sections AA, AA2, and BB, respectively. Different armour layer configurations are tested without changing the toe unit and G_c for Sections AA and AA2. In Section BB, different toe units and G_c are tested.

Table 4.9 Mean wave overtopping volume results for Section AA

Wave Cond.	Armour unit	Toe Unit	G_c (m)	$q_{prototype}$ (l/s/m)
D1	XP	Rock	0.235	-
	XP, XP-OT	Rock	0.235	-
D2	XP	Rock	0.235	-
	XP, XP-OT	Rock	0.235	-
D3	XP	Rock	0.235	-
	XP, XP-OT	Rock	0.235	-
D4.1	XP	Rock	0.235	0.0796
	XP, XP-OT	Rock	0.235	-
D4.2	XP	Rock	0.235	0.2785
	XP, XP-OT	Rock	0.235	0.0398
D5	XP	Rock	0.235	1.6677
	XP, XP-OT	Rock	0.235	0.2382

Table 4.10 Mean wave overtopping volume results for Section AA2

Wave Cond.	Armour unit	Toe Unit	G_c (m)	$q_{prototype}$ (l/s/m)
D1	XP	Rock	0.235	0.0996
	XP, XP-OT	Rock	0.235	-
D2	XP	Rock	0.235	0.2954
	XP, XP-OT	Rock	0.235	-
D3	XP	Rock	0.235	1.5786
	XP, XP-OT	Rock	0.235	0.2368
D4.1	XP	Rock	0.235	3.2623
	XP, XP-OT	Rock	0.235	0.9767
D4.2	XP	Rock	0.235	5.9677
	XP, XP-OT	Rock	0.235	2.0290
D5	XP	Rock	0.235	13.8184
	XP, XP-OT	Rock	0.235	5.8768
D6	XP	Rock	0.235	30.4985
	XP, XP-OT	Rock	0.235	13.7694
D7	XP	Rock	0.235	72.2457
	XP, XP-OT	Rock	0.235	46.2957
D8	XP	Rock	0.235	155.6285
	XP, XP-OT	Rock	0.235	98.0011

Table 4.11 Mean wave overtopping volume results for Section BB

Wave Cond.	Armour unit	Toe Unit	G_c (m)	$q_{prototype}$ (l/s/m)
D1	XP	Cube	0.235	-
	XP	Rock	0.235	-
D2	XP	Cube	0.235	0.0271
	XP	Rock	0.235	-
D3	XP	Cube	0.235	0.0634
	XP	Rock	0.235	0.0634
	XP	Cube	0.120	0.2534
D4.1	XP	Cube	0.235	0.0441
	XP	Rock	0.235	0.0661
	XP	Cube	0.120	0.0661
D4.2	XP	Cube	0.235	0.1310
	XP	Rock	0.235	0.1310
	XP	Cube	0.120	0.5240
D5	XP	Cube	0.235	0.6647
	XP	Rock	0.235	0.9970
	XP	Cube	0.120	3.9214
D6	XP	Cube	0.235	2.9853
	XP	Rock	0.235	2.7432
	XP	Cube	0.120	8.7138
D7	XP	Cube	0.235	3.9828
	XP	Rock	0.235	3.9828
	XP	Cube	0.120	14.4975

The experimental results presented in the above tables are converted to mean overtopping discharges per unit length (m^3/s/m) and compared with the computed values using the mean overtopping discharge prediction equation given by Equation 2.15 (EurOtop, 2018). The roughness coefficients for XblocPlus® and XblocPlusOvertop® units in this equation are implemented as 0.45 and 0.415 based

on the formulas presented in Section 3.2.3.3. A comparison of measured data with the calculated values is visualized by non-dimensional mean overtopping discharge with respect to relative crest height and given in Figure 4.14.

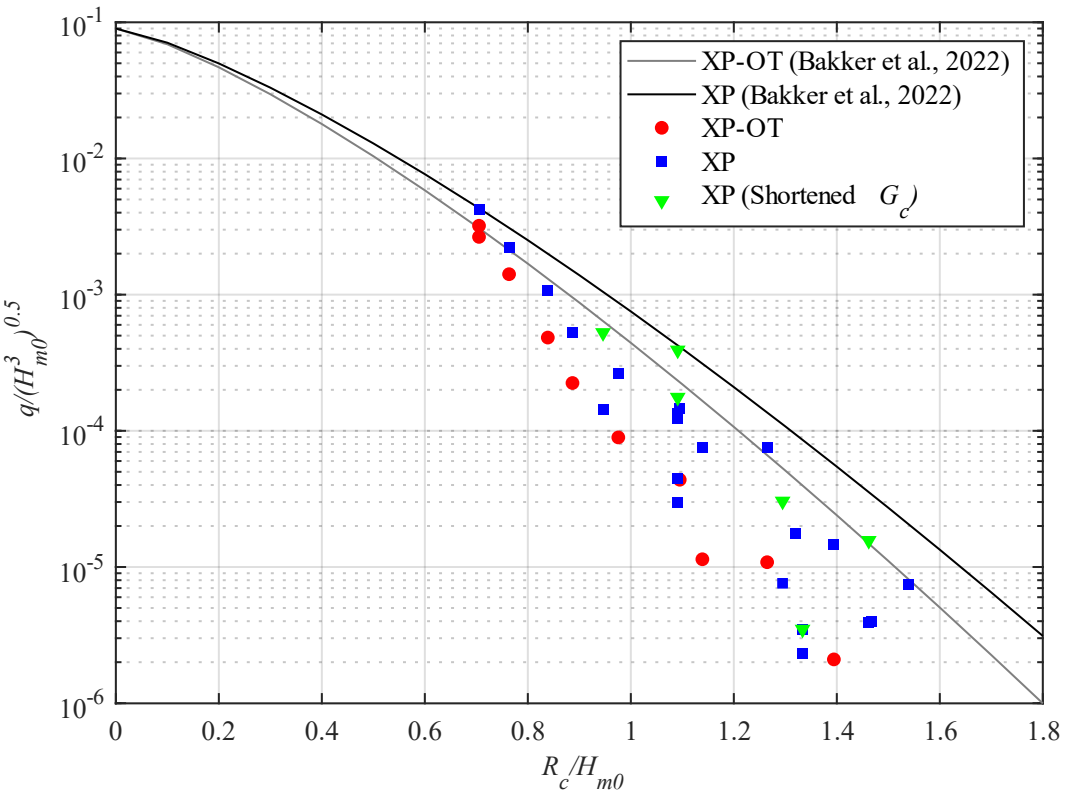

Figure 4.14. Measured mean overtopping discharges for all experiments

As shown in Figure 4.14, variations are observed between measured and calculated wave overtopping discharges. This situation is expected due to the large crest width of the coastal revetment model. A better relation between the estimated and measured discharge values is observed for the section with shortened G_c, but this crest width also causes significant variation.

The effect of a wide crest on wave overtopping is discussed in EurOtop (2018), and it is stated that this situation reduces the overtopping volumes. A reduction factor (γ_r) is suggested to represent the reduction in the wave overtopping due to the large crest widths. However, this reduction factor is applicable when A_c and R_c are equal, which is not applicable for observed cross-sections in this study. EurOtop (2018)

also states that more reduction in wave overtopping is observed for the Accropode armoured coastal structures, and this situation is similar for other single-layer armour units. Due to the limitations of the reduction factor suggested by EurOtop (2018), a new coefficient is calculated to better predict the wave overtopping discharge for this specific study. This coefficient is implemented in the wave overtopping discharge prediction formula provided by EurOtop (2018) to implement the effects of large crest widths. Non-dimensional crest widths of the model are used to determine the modification coefficient and presented in Equation 4.4 for XblocPlus® and in Equation 4.5 for XblocPlusOvertop® units.

$$\gamma_{z,XP} = \left(\frac{G_c}{N_{crest} * D_n}\right)^{0.0151} \quad (4.4)$$

$$\gamma_{z,XP-OT} = \left(\frac{G_c}{N_{crest} * D_n}\right)^{0.0325} \quad (4.5)$$

G_c represents the crest width of the experimental model, as stated previously, N_{crest} represents the number of armour units used in the crest, and D_n represents the nominal diameter of the armour unit used in the model. The modified equation for the wave overtopping discharge prediction is presented in Equation 4.6.

$$\frac{q}{\sqrt{gH_{m0}^3}} = 0.09exp\left[-\left(1.5\frac{R_c}{H_{m0}\gamma_f\gamma_\beta\gamma^*\gamma_z}\right)^{1.3}\right] \quad (4.6)$$

The performance of the formula with the coefficient of γ_z is observed and analyzed by mean absolute logarithmic error (MALE) and root mean square logarithmic error (RMSLE). The formulas to determine MALE and RMSLE are shown in Equations 4.7 and 4.8, respectively.

$$MALE = \frac{1}{n}\sum_{i=1}^{n}\left|log\left(\frac{p_i}{O_i}\right)\right| \quad (4.7)$$

$$RMSLE = \sqrt{\frac{1}{n}\sum_{i=1}^{n}\left(log\left(\frac{p_i}{O_i}\right)\right)^2} \qquad (4.8)$$

Predicted values are presented by p_i, O_i represents the observed values and n represents the number of data. These calculations are carried out for three cross-sections with limited experiments. Although the analyses are carried out with limited data, this study presents the general behavior and performance of the overtopping prediction formula for the structures studied in this thesis with large crest widths.

A comparison of measured mean overtopping discharges with the modified formula for all experiments is presented in Figure 4.15.

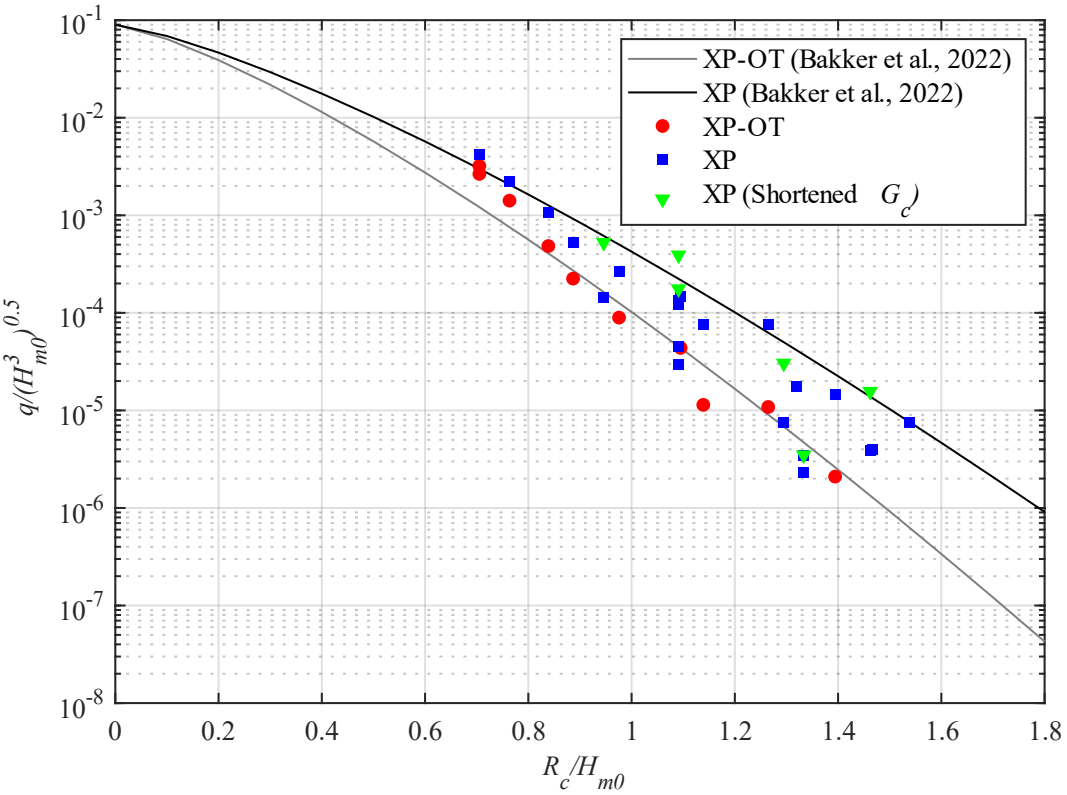

Figure 4.15. Measured mean overtopping discharges with modified roughness coefficients for all experiments

As presented in Figure 4.15, a better fit is obtained between the measured and predicted wave overtopping discharges with the modified formula. However, this coefficient is suggested for this specific design and should be studied further. It can be seen that more error is observed when the R_c/H_{m0} value is smaller than 0.8. The statistical analysis results for modified and original formulas are presented in Table 4.12.

Table 4.12 Statistical assessment of suggested and modified roughness coefficients

Unit	γ_z	MALE	RMSLE
XblocPlus®	$\gamma_{z,XP} = 1.0000$	0.9982	1.2675
	$\gamma_{z,XP} = 0.9158$	0.7294	0.9493
XblocPlusOvertop®	$\gamma_{z,XP\text{-}OT} = 1.0000$	1.3435	1.6047
	$\gamma_{z,XP\text{-}OT} = 0.8195$	0.4429	0.5567

Table 4.12 presents the MALE and RMSLE values for with and without the suggested coefficient. It is shown that the modified formula improves the prediction by decreasing the MALE by 36.9% and RMSLE by 33.5% for XblocPlus® units. 203.3% and 188.3% of reductions for the MALE and RMSLE are obtained for the XblocPlusOvertop® units. According to these results, it is observed that the XblocPlus® units show a better fit with respect to XblocPlusOvertop® units without any modification in the formula. However, modification coefficients are needed for both units. Moreover, as shown in the figures above, shortened G_c decreases the variation between the measured and predicted mean overtopping discharge values.

As presented in the tables and figures above, using XblocPlusOvertop® units causes a significant reduction in mean overtopping discharges. This result is expected due to the run-down process that occurs on the armour units explained in Figure 4.6. On average, a 63% reduction in wave overtopping discharge is observed when the XblocPlusOvertop® units are placed. As shown in Figure 4.15, the maximum difference between the measured wave overtopping discharge with the section constructed by XblocPlusOvertop® units and the section with only XblocPlus® units

is 31.6%. On the other hand, the maximum difference is observed as 599%. As a result, smaller reductions are observed for the lower relative freeboard values, and similar to Bakker et al. (2022), the change in the wave overtopping discharge increased for the sections with and without XblocPlusOvertop® units when the relative freeboard increased. However, Bakker et al. (2022) observed wave overtopping reduction within a range of 30% to 65%, and this result is significantly lower than the results presented in this thesis study. On the other hand, these differences are expected due to the large crest width of the present specific design in this project. A significantly wide crest decreases the collected water via a chute implemented in the experimental setup. Moreover, the ratio between the wave height and the structure depth implemented in this study is relatively high, and this situation affects the H_{max}. Nørgaard et al. (2014) emphasize that the highest individual wave overtopping causes the greatest overtopping discharges. Therefore, it can be argued that when the maximum overtopping volume is decreased, the performance of XblocPlusOvertop® units in reducing the overtopping discharges increases. These two factors are considered as the explanation for the higher variation in the present experimental data. Moreover, the effects of different toe units on wave overtopping performance are observed, as shown in Table 4.12. No significant difference is observed for different toe units with similar toe depths. It is again stressed that these observations are limited to the scope of the present experiments.

4.4 Overtopping Induced Scour at the Lee Side of the Structure

Scour measurements are conducted for the wave conditions, where relatively high wave overtopping is observed during the experiments. Profile measurements are conducted separately for all wave conditions (D4.1 to D8 for Section AA2, D5 to D8 for Section BB) tested in the scope of the scour experiments. Profiles of the backfill area are measured by laser distance meter before and after the experiments, and the experimental setup is reset for all wave conditions. Measurement results for each

profile (see Figure 3.10) and maximum scour depths observed during the experiments are presented in Table 4.13.

Table 4.13 Scour measurement results for all profiles

Section	Wave Cond.	P1 (mm)	P2 (mm)	P3 (mm)	P4 (mm)	P5 (mm)	Maximum Scour Depth (mm)
AA2	D4.1	4.70	5.70	6.80	3.20	6.30	6.80
AA2	D4.2	10.10	11.80	11.90	11.50	10.70	11.90
AA2	D5	20.60	16.30	18.70	14.40	17.70	20.60
AA2	D6	23.90	24.00	17.30	18.30	25.80	25.80
AA2	D7	42.80	34.70	29.60	26.80	35.10	42.80
AA2	D8	57.30	51.30	51.80	50.10	53.10	57.30
BB	D5	12.00	10.70	14.20	18.70	8.10	18.70
BB	D6	12.20	9.80	9.40	11.40	15.40	15.40
BB	D7	14.50	12.70	20.10	16.90	16.50	20.10
BB	D8	18.80	17.90	25.20	25.70	27.10	27.10

Average of P1-P5 scour profile measurements before and after each wave condition are presented for all wave conditions in Figure 4.16 and Figure 4.17. In these figures, x=0 indicates the position of the crown wall, and the distance between the measurement point and the crown wall is identified in the x-axis. The measured scour depths are presented in the y-axis. In addition, individual initial and final profile measurements for all wave conditions are presented in Appendix C.

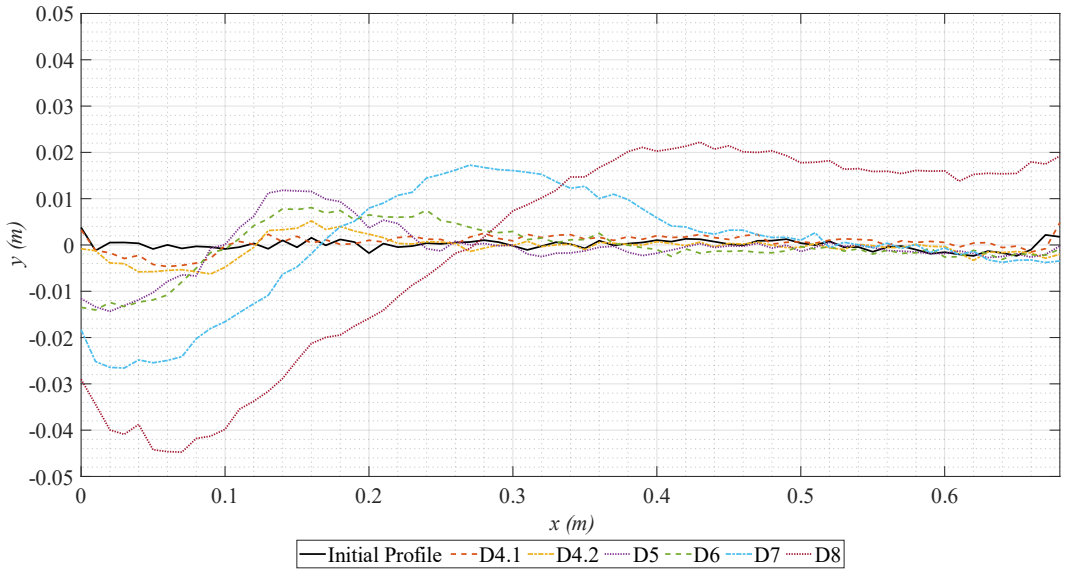

Figure 4.16. Average initial and final scour measurements for Section AA2

As presented in Figure 4.16, the maximum scour depth is observed for D8, which is the wave condition with a maximum wave height among the experiment set. The maximum accretion is also observed for the D8 wave condition. Measured scour depths and accretion height are decreased from D8 to D4.1, as expected. This situation is expected due to the wave overtopping volumes measured in this thesis study and presented in Section 4.3. Increasing the wave overtopping volumes causes larger scour depths, as presented in the figure above.

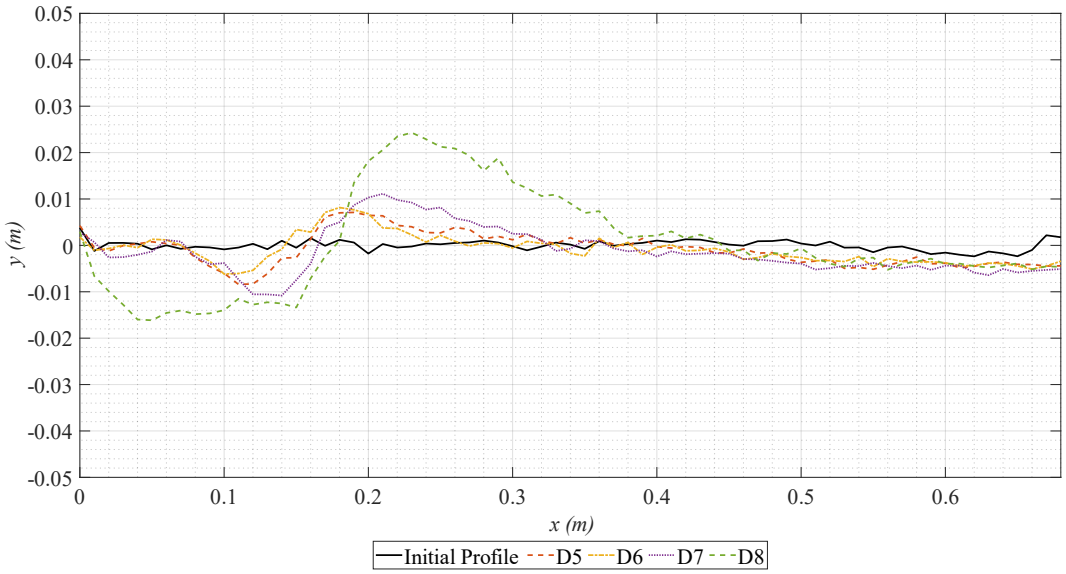

Figure 4.17. Average initial and final scour measurements for Section BB

As presented in Figure 4.17, the maximum scour depth is observed for D8, which is the wave condition with a maximum wave height among the experiment set. The maximum accretion is also observed for the D8 wave condition. Measured scour depths and accretion height are decreased from D8 to D5, similar to Section AA2.

Scour depths for different experimental setups are predicted using the formula provided by Yıldırım et al. (2024), given in Equation 3.10. In the development of this formula, the densimetric overtopping discharge range is given as 0.00243 – 21342.74. In the present experiments, some cases are out of the range of Yıldırım et al. (2024). The comparison graph is presented in Figure 4.18, indicating the data points in the range and out of the range of Yıldırım et al. (2024).

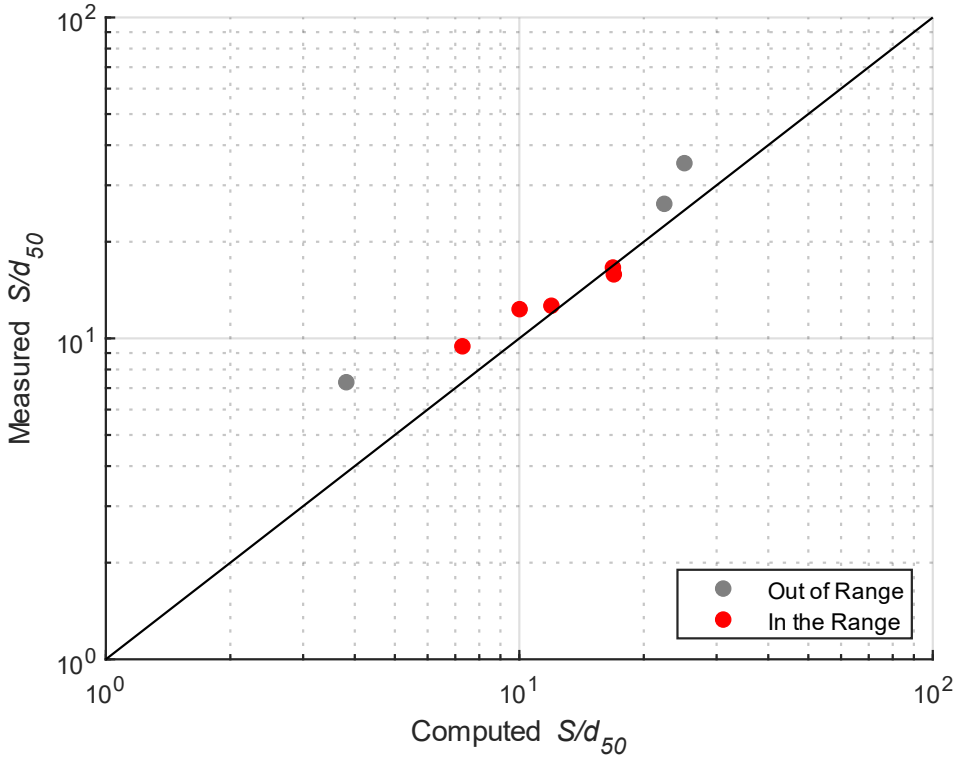

Figure 4.18. Measured and calculated scour depths

In the comparison between the measured scour depths with the cross-sections with an L-shaped crown wall and an I-shaped crown wall, differences are expected to be observed. However, as shown in Figure 4.18, overall a good fit is observed between the measured scour depths and calculated scour depths by Equation 3.10. However, significant deviations are observed for the cases where the densimetric overtopping discharge is out of the range of Yıldırım et al. (2024), which is expected. The maximum variation between the predicted and measured data in the range of the formula provided by Yıldırım et al. (2024) is determined as 29.73%, and the minimum difference is observed as 1.29%. On average, a 13.36% difference is calculated between the experimental data and the predicted scour depth values.

Yıldırım et al. (2024) investigated the I-shaped crown wall and proposed a formula based on experimental studies using this type of crown wall structure. However, the L-shaped crown wall design is implemented in this thesis study. Experimental results

show that the measured scour at the lee side of a coastal revetment is predicted well when the L-shaped crown wall is used instead of the I-shape. However, this observation is completely limited to the scope of the present experiments. Further investigations should be carried out to generalize this observation.

CHAPTER 5

CONCLUSION

In this study, the hydraulic performance of an XblocPlus® armoured coastal revetment is tested. A total of 127 experiments are carried out in this thesis study. The stability of the armour layer and toe section is evaluated by visual inspection methods. Different cross-sections are tested by changing the armour configuration, relative freeboard, structure depth, and toe units. Cross-sections with and without XblocPlusOvertop® units are constructed. Three different relative freeboards and structure depths are implemented, and quarry rock and cube block units are used as toe units for different cases. Moreover, pressure sensors are used to measure forces acting on the crown wall to evaluate the effects of different cross-sections. Measured forces acting on the crown wall are compared with the formulas proposed by Pedersen (1996) and Nørgaard et al. (2013). The overtopping performance of the structure is also tested in the scope of this thesis study. A gutter and overtopping box are installed to measure the mean overtopping volumes. Measured wave overtopping discharges are compared with the formula and roughness coefficients explained by Bakker et al. (2022). Finally, wave overtopping induced scour at the lee side of the coastal revetment is measured in several experimental cases. Effects of different crown wall shapes are evaluated by comparing the measurement results with the formula provided by Yıldırım et al. (2024), based on the limited data. The main findings of these observations are listed as follows:

- Armour and toe stability measurements are conducted for Section AA for wave conditions from D1 to D5, for Section AA2 for wave conditions from D1 to D8, and for Section BB for wave conditions from D1 to D7. According to the results, no damage is observed on the XblocPlus® and XblocPlusOvertop® units used in the armour layer for all experiments. However, significant damage is observed in the toe layer constructed using

quarry rocks. The experimental studies show that XblocPlusOvertop® units increase the damage on the toe layer by 36% on average due to the run-down processes observed when the XblocPlusOvertop® units are placed.

These results show that recently developed armour units that are investigated in this thesis study performed well in terms of armour stability by no damage performance. On the other hand, a negative impact on the toe stability is observed when the XblocPlusOvertop® units are placed.

- Forces acting on the crown wall are measured and evaluated with the formulas suggested by Pedersen (1996) and Nørgaard et al. (2013). According to the experimental studies, modified empirical coefficients are suggested, and a 25.4% better correlation between the prediction formula and measured data is obtained. Due to the linear relationship between $F_{H,0.1\%}$, and $M_{H,0.1\%}$, the performance of the prediction formula of $M_{H,0.1\%}$, is increased by 20% with the modified coefficients.
- Performance of the XblocPlusOvertop® units is evaluated with the XblocPlus® units in this study. It is shown that $F_{H,0.1\%}$, and $M_{H,0.1\%}$ values decrease due to the effects of XblocPlusOvertop® units.
- The effect of XblocPlusOvertop® units on mean overtopping discharges are investigated based on the experiments carried out for Section AA, Section AA2, and Section BB for all wave conditions. An average of 63% reduction in the mean overtopping discharge is observed when the XblocPlusOvertop® units are placed at the armor layer of the structure. However, this result is provided within the limited data and specific design condition limitations.
- Comparisons between the overtopping discharge prediction methods and measured wave overtopping discharges show variance. It is stated that the large crest width values implemented in this study caused these differences, and a new modification coefficient is suggested for the prediction formula by considering the crest width effects. Implementing the modification coefficient enhanced the performance of the prediction formula by 36.9%

and 203.3% for XblocPlus® and XblocPlusOvertop® units in terms of the mean absolute logarithmic error, respectively.

- It is emphasized that XblocPlusOvertop® units reflect the waves as bullnose structures. This behavior starts the run-down process before the run-up process is finalized. Thus, XblocPlusOvertop® units increase the wave-overtopping performance of the structure and decrease the forces and moments acting on the crown wall. On the other hand, a quick run-down process without losing energy causes more damage to the toe layer.
- According to the experimental studies, measured scour at the lee side of the coastal revetment is compared with the prediction formula provided by Yıldırım et al. (2024). A good fit between the measured and predicted scour depths is observed within the range of the formula by Yıldırım et al. (2024). The comparisons show that an L-shaped crown wall has no significant effect compared to I-shaped crown walls within the scope of the present experiments.

All experimental studies discussed in this thesis study are carried out within certain limitations. The most important limitation is that cross-sections tested during the physical model experiments are designed for a specific project. Thus, all results and observations are applicable to these cross-sections, and further investigations on the findings presented in this study should be considered for different designs.

All investigations are completed in this study with the limited dataset in terms of number of experiments, and experimental conditions. All findings give insight into the performance of XblocPlus® and XblocPlusOvertop® units, and further investigations should be conducted on the subjects discussed in this thesis study. In this scope, further recommendations are listed as follows:

- Further investigations should be carried out to increase the data on pressure measurements. Moreover, vertical forces acting on the bottom of the crown wall structure can be investigated in addition to horizontal forces acting on the front face of the crown wall.

- Additional experimental studies on wave overtopping discharges should be conducted with different G_c and different numbers of armour units on the crest to investigate the modification coefficient proposed in this study. Moreover, limitations due to the limited data should be eliminated by improving the dataset.
- The effects of different crown wall shapes on the wave overtopping induced scour at the lee side of a coastal revetment should be further investigated with a larger dataset.

REFERENCES

AYGM. (2016). *Kıyı Yapıları Planlama ve Tasarım Teknik Esasları*. T.C. Ulaştırma, Denizcilik ve Haberleşme Bakanlığı, Altyapı Yatırımları Genel Müdürlüğü.

Bakker, P., Jacobs, R., Van De Koppel, M., Reedijk, B., & Muttray, M. (2019). Hydraulic Stability and Practical Application of XblocPlus Breakwater Armouring. *Coastal Structures*. https://doi.org/10.18451/978-3-939230-64-9_011

Bakker, P., Ruwiel, T., Van De Koppel, M., Yang, Z. Q., & Donnelly, J. (2022). Wave Overtopping Reduction by Modular Concrete Armour Units. *Coastal Engineering Proceedings*, 44–44. https://doi.org/http://dx.doi.org/10.9753/icce.v37.papers.44

Baldock, T. E., & Simmonds, D. J. (1999). Separation of incident and reflected waves over sloping bathymetry. *Coastal Engineering*, *38*, 167–176. www.elsevier.comrlocatercoastaleng

Bomers, A., Aguilar Lopez, J. P., Warmink, J. J., M H Hulscher, S. J., Bomers abomers, A., P Aguilar Lopez jpaguilarlopez, utwentenl J., J Warmink, tudelftnl J., & M H Hulscher sjmhhulscher, S. J. (2018). Modelling effects of an asphalt road at a dike crest on dike cover erosion onset during wave overtopping. *Natural Hazards*, *93*, 1–30. https://doi.org/10.1007/s11069-018

Bradbury, A. P., Allsop, N. W. H., & Stephens, R. V. (1988). *Hydraulics Research Hydraulic Performance of Breakwater Crown Walls*.

Broos, J. W. M. (2019). *Stability of the First Row of an Xblocplus Armour Layer a Physical Model Study Using Digital Displacement Analysis* [TU Delft]. http://repository.tudelft.nl/.

Calvin, K., Dasgupta, D., Krinner, G., Mukherji, A., Thorne, P. W., Trisos, C., Romero, J., Aldunce, P., Barrett, K., Blanco, G., Cheung, W. W. L., Connors, S., Denton, F., Diongue-Niang, A., Dodman, D., Garschagen, M., Geden, O., Hayward, B., Jones, C., … Ha, M. (2023). *IPCC, 2023: Climate Change 2023: Synthesis Report. Contribution of Working Groups I, II and III to the Sixth Assessment Report of the Intergovernmental Panel on Climate Change [Core Writing Team, H. Lee and J. Romero (eds.)]. IPCC, Geneva, Switzerland.* (P. Arias, M. Bustamante, I. Elgizouli, G. Flato, M. Howden, C. Méndez-Vallejo, J. J. Pereira, R. Pichs-Madruga, S. K. Rose, Y. Saheb, R. Sánchez Rodríguez, D. Ürge-Vorsatz, C. Xiao, N. Yassaa, J. Romero, J. Kim, E. F. Haites, Y. Jung, R. Stavins, … C. Péan, Eds.). https://doi.org/10.59327/IPCC/AR6-9789291691647

CERC. (1977). *Shore Protection Manual* (Vol. 1).

CERC. (1984). *Shore Protection Manual* (4th ed., Vol. 2).

CIRIA, CUR, & CETMEF. (2007). *The Rock Manual. The use of rock in hydraulic engineering* (2nd ed.). C683, CIRIA.

Demir, F. (2023). *Effects of Antifer Placement Methods on Wave Loads Acting on Crown Walls in Shallow Water*. METU.

Erler, B. (2023). *Effect of Different Antifer Unit Placement Methods on Wave Overtopping*. METU.

EurOtop. (2018). *Manual on wave overtopping of sea defences and related structures. An overtopping manual largely based on European research, but for worldwide application* (J. W. van der Meer, N. W. H. Allsop, T. Bruce, J. De Rouck, A. Kortenhaus, T. Pullen, H. Schüttrumpf, P. Troch, & B. Zanuttigh, Eds.; 2nd ed.). www.overtopping-manual.com

Goda, Y., & Suzuki, Y. (1976). Estimation of Incident and Reflected Waves in Random Wave Experiments. *Coastal Engineering*, 828–845.

Hofland, B., Houtzager, D., Caldera, G., Antonini, A., Van Gent, M., Bakker, P., & Van der Lem, C. (2023). Rocking of single-layer armour units measured by embedded sensors. *Journal of Coastal and Hydraulic Structures*, *3*. https://doi.org/10.59490/jchs.2023.0028

Hughes, S. A. (1993). *Physical Models and Laboratory Techniques in Coastal Engineering* (Vol. 7). WORLD SCIENTIFIC. https://doi.org/10.1142/2154

Jacobs, R., Bakker, P., Vos-Rovers, I., & Reedijk, B. (2018). Xblocplus Development of a Regular Placed Interlocking Armour Unit. *Coastal Engineering*.

Janssen, D. (2018). *Stability analysis of XblocPlus crest element* [TU Delft]. https://doi.org/10.4121/uuid:c65df664-f905-49c0-a47b-eae5682c0d6b

Koosheh, A., Etemad-Shahidi, A., Cartwright, N., Tomlinson, R., & van Gent, M. R. A. (2022). Distribution of individual wave overtopping volumes at rubble mound seawalls. *Coastal Engineering*, *177*. https://doi.org/10.1016/j.coastaleng.2022.104173

Lamberti, A., Martinelli, L., Gaeta, M. G., Tirindelli, M., & Alderson, J. (2011). Experimental spatial correlation of wave loads on front decks. *Journal of Hydraulic Research*, *49*(SUPPL.1), 81–90. https://doi.org/10.1080/00221686.2011.636933

Martin, F. L., Losada, M. A., & Medina, R. (1999). Wave loads on rubble mound breakwater crown walls. In *Coastal Engineering* (Vol. 37). www.elsevier.comrlocatercoastaleng

Molines, J., Herrera, M. P., Gómez-Martín, M. E., & Medina, J. R. (2019). Distribution of individual wave overtopping volumes on mound breakwaters. *Coastal Engineering*, *149*, 15–27. https://doi.org/10.1016/j.coastaleng.2019.03.006

Möller, J., Weissmann, R., Schüttrumpf, H., Grüne, J., Oumeraci, H., Richwien, W., & Kudella, M. (2002). Interaction of wave overtopping and clay properties for seadikes. *Coastal Engineering Proceedings*, *2*, 2105–2115.

Moreno, A. J. (2017). *Experimental Study on the Wave Overtopping Performance of XBLOC+ Armour Unit*. https://www.ntnu.edu/studies/mscomem

Nørgaard, J. Q. H., Andersen, T. L., & Burcharth, H. F. (2013). Wave loads on rubble mound breakwater crown walls in deep and shallow water wave conditions. *Coastal Engineering*, *80*, 137–147. https://doi.org/10.1016/j.coastaleng.2013.06.003

Nørgaard, J. Q. H., Lykke Andersen, T., & Burcharth, H. F. (2014). Distribution of individual wave overtopping volumes in shallow water wave conditions. *Coastal Engineering*, *83*, 15–23. https://doi.org/10.1016/j.coastaleng.2013.09.003

Pedersen, J. (1996). Wave Forces and Overtopping on Crown Walls of Rubble Mound Breakwaters: an Experimental Study. In *Aalborg: Aalborg Universitetsforlag. (Series Paper* (Issue 12).

Pillai, K., Etemad-Shahidi, A., & Lemckert, C. (2017). Wave overtopping at berm breakwaters: Experimental study and development of prediction formula. *Coastal Engineering*, *130*, 85–102. https://doi.org/10.1016/j.coastaleng.2017.10.004

Reedijk, B., Eggeling, T., Bakker, P., Jacobs, R., & Muttray, M. (2018). Hydraulic Stability and Overtopping Performance of a New Type of Regular Placed Armour Unit. *Coastal Engineering Proceedings*, 111–111. https://doi.org/http://dx.doi.org/10.9753/icce.v36.structures.54

Ruwiel, T. (2020). *Crest stability of XblocPlus armoured low crested breakwaters* [TU Delft]. http://repository.tudelft.nl/.

Schoonees, T., Kerpen, N. B., & Schlurmann, T. (2021). Full-scale experimental study on wave overtopping at stepped revetments. *Coastal Engineering*, *167*. https://doi.org/10.1016/j.coastaleng.2021.103887

Senturk, B. U., Guler, H. G., & Baykal, C. (2023). Numerical simulation of scour at the rear side of a coastal revetment. *Ocean Engineering*, *275*. https://doi.org/10.1016/j.oceaneng.2023.114092

van den Berg, I., Hofland, B., & Reedijk, B. (2020). Influence of irregularities in the rock underlayer on the stability of XblocPlus. *Coastal Engineering*, *157*. https://doi.org/10.1016/j.coastaleng.2020.103637

Van Der Meer, J. W., Bernardini, P., Snijders, W., & Regeling, E. (2006). The Wave Overtopping Simulator. *Coastal Engineering*, *5*, 4654–4666.

Van Gent, M. R. A., & van der Werf, I. M. (2014). Rock toe stability of rubble mound breakwaters. *Coastal Engineering*, *83*, 166–176. https://doi.org/10.1016/j.coastaleng.2013.10.012

Xbloc. (2023). *Xbloc & Xblocplus Design Guidelines*.

Xbloc. (2024). https://www.xbloc.com

Yıldırım, M. E., Yaman, M., & Baykal, C. (2024). Scour at the rear side of rubble mound revetments due to random wave overtopping: Laboratory experiments. *Ocean Engineering*, *309*. https://doi.org/10.1016/j.oceaneng.2024.118401

APPENDICES

A. Wave Height Distributions

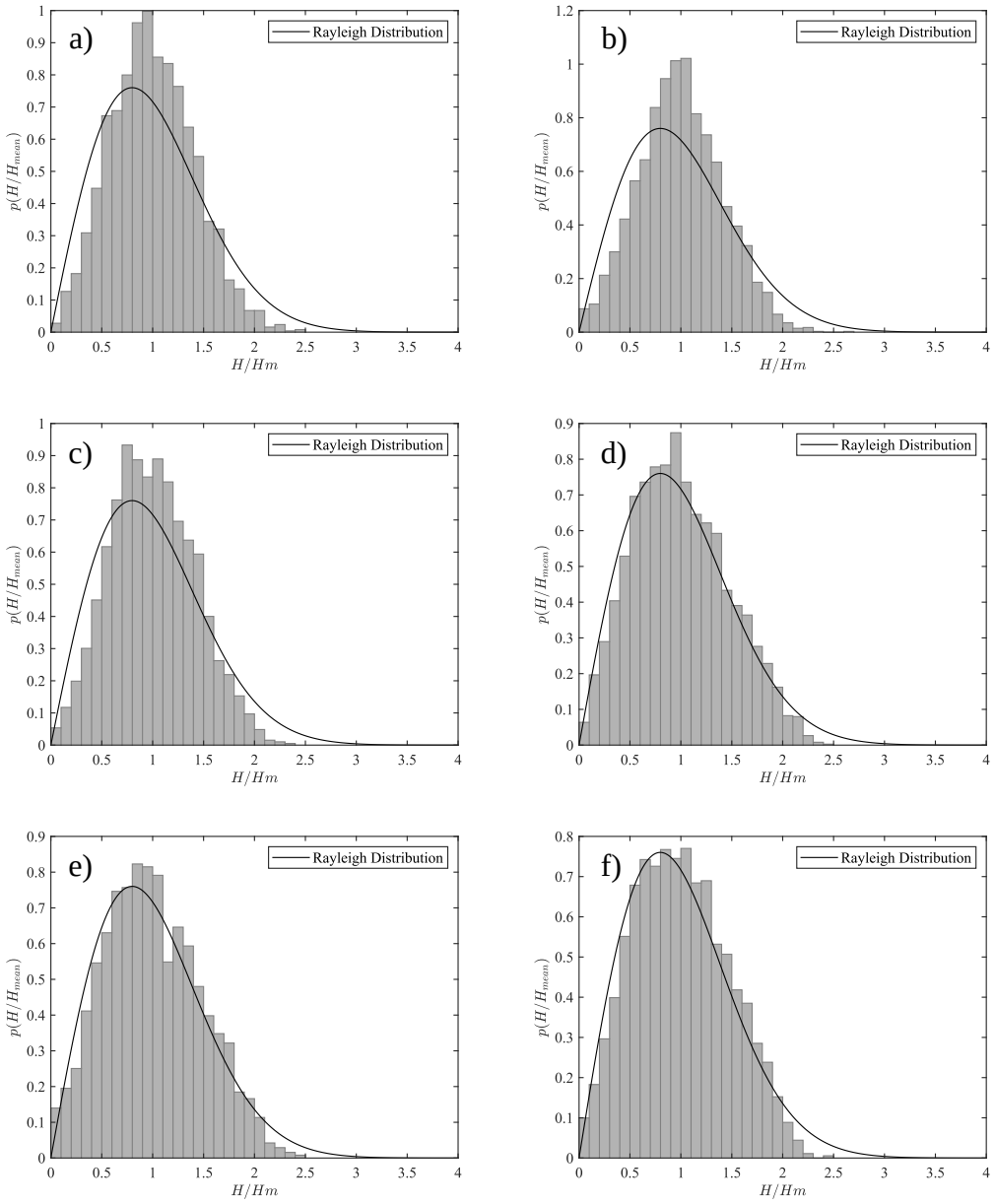

Figure A.1. Non-dimensional histogram, Section AA; a) *D1*, b) *D2*, c) *D3*, d) *D4.1*, e) *D4.2*, f) *D5*

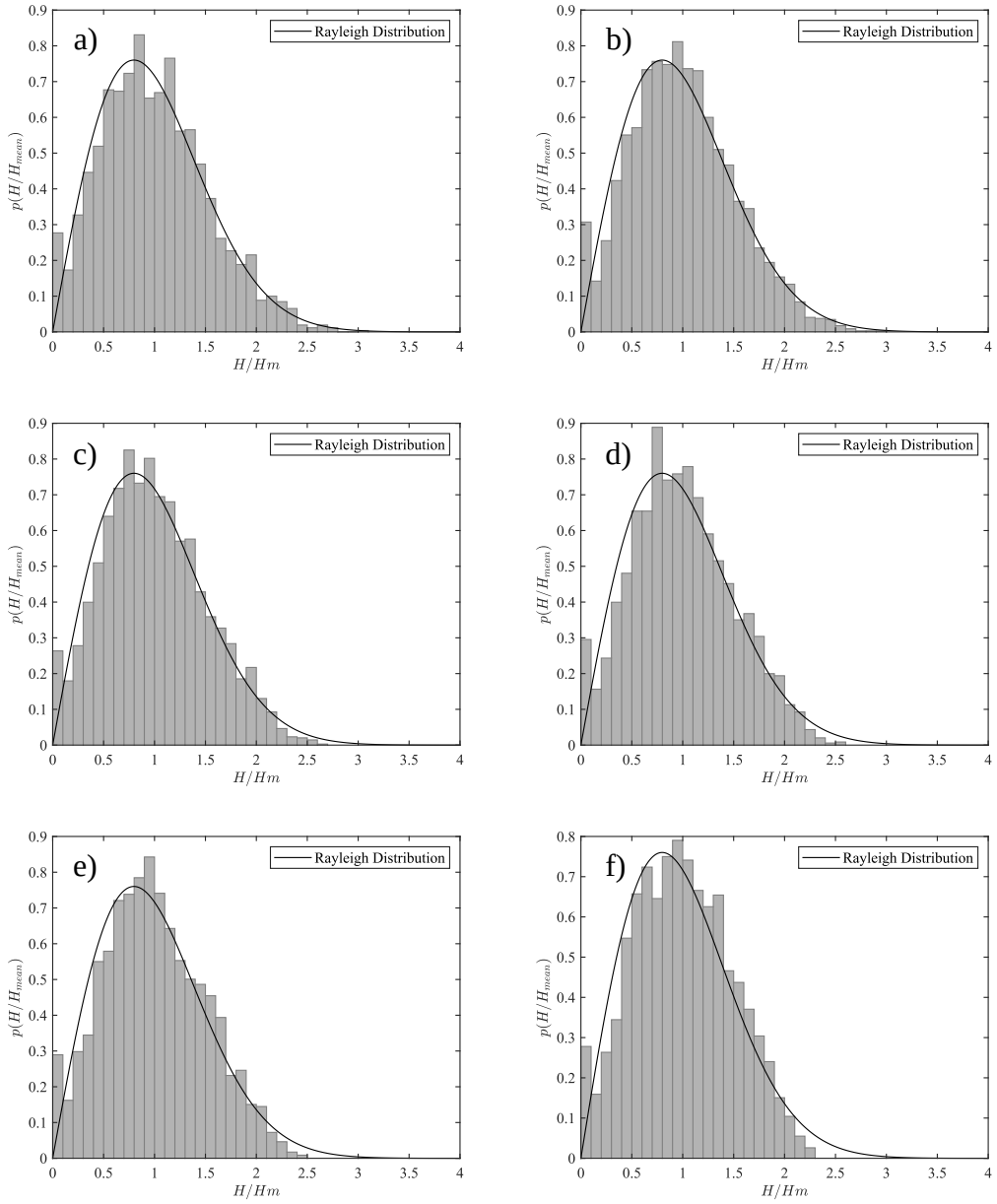

Figure A.2. Non-dimensional histogram, Section AA-2; a) *D1*, b) *D2*, c) *D3*, d) *D4.1*, e) *D4.2*, f) *D5*

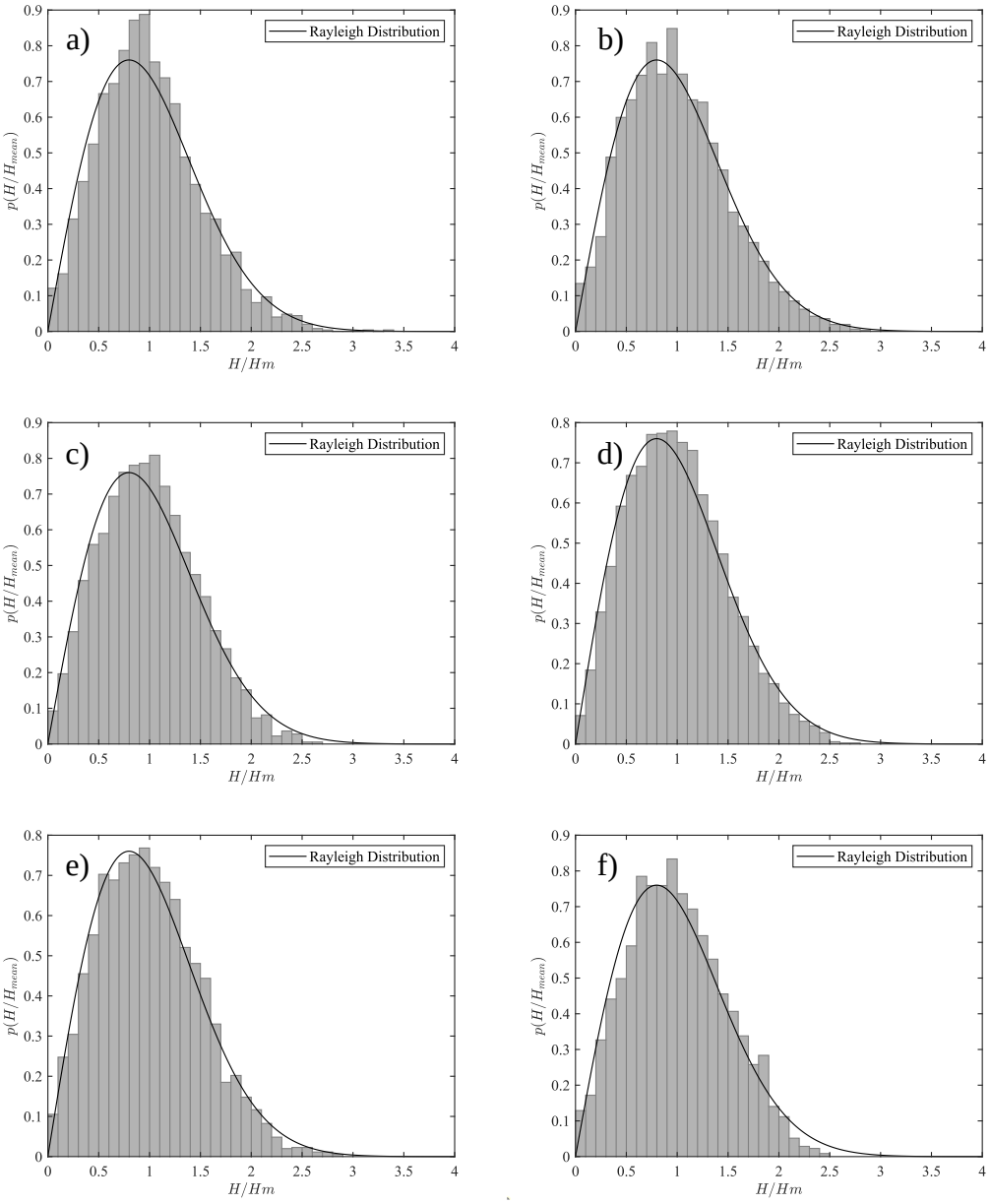

Figure A.3. Non-dimensional histogram, Section BB; a) *D1*, b) *D2*, c) *D3*, d) *D4.1*, e) *D4.2*, f) *D5*

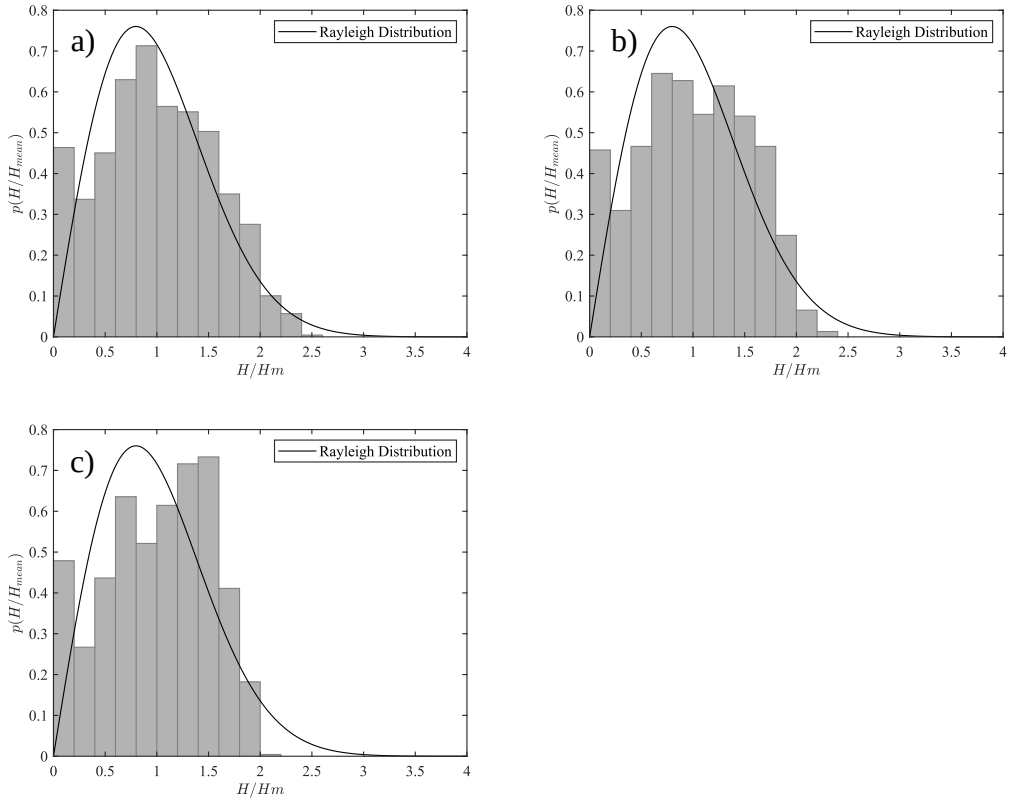

Figure A.4. Non-dimensional histogram for additional waves, Section AA-2; a) *D6,* b) *D7*, c) *D8*

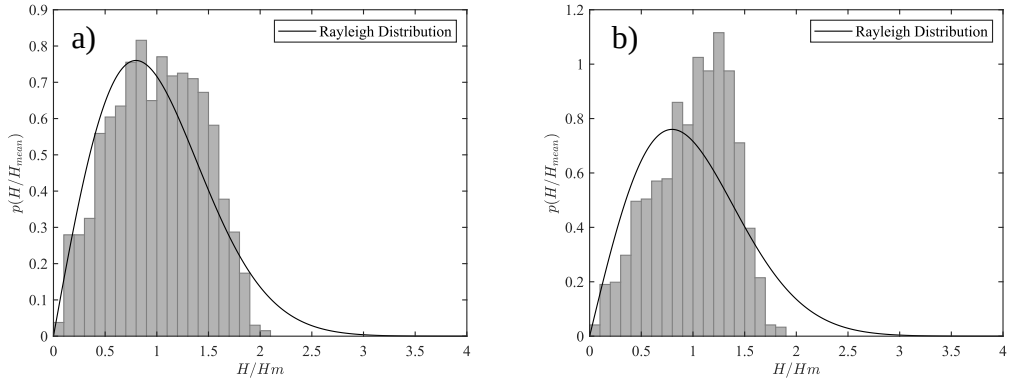

Figure A.5. Non-dimensional histogram for additional waves, Section BB; a) *D6*, b) *D7*

B. Cross-sections of Different Experimental Cases

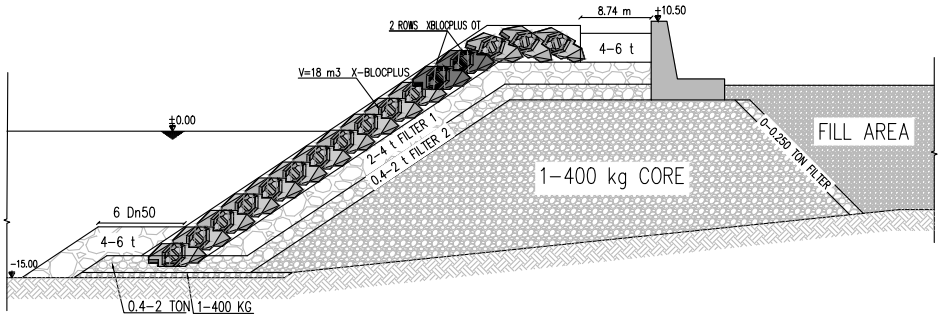

Figure B.1. Section AA with XblocPlusOvertop® units

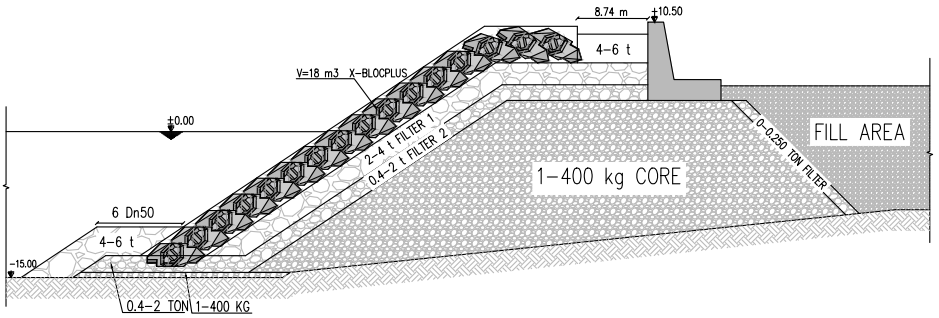

Figure B.2. Section AA without XblocPlusOvertop® units

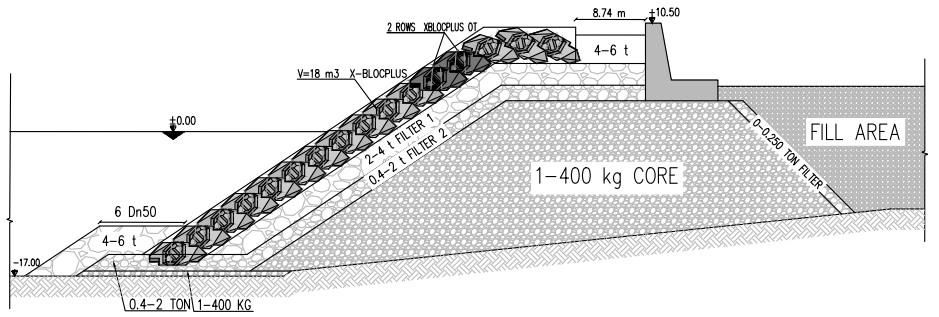

Figure B.3. Section AA-2 with XblocPlusOvertop® units

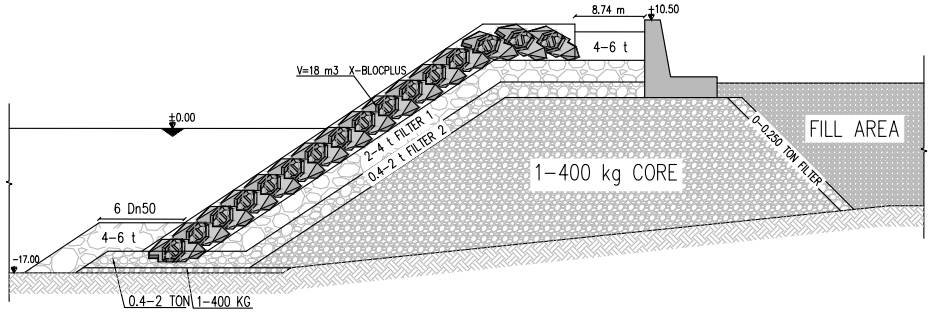

Figure B.4. Section AA-2 without XblocPlusOvertop® units

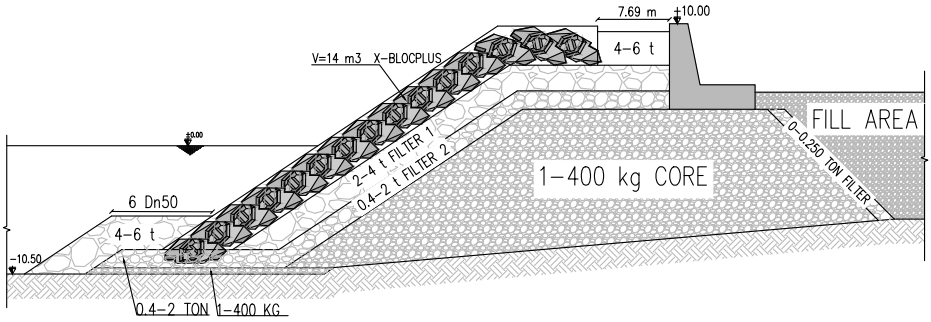

Figure B.5. Section BB without XblocPlusOvertop® units

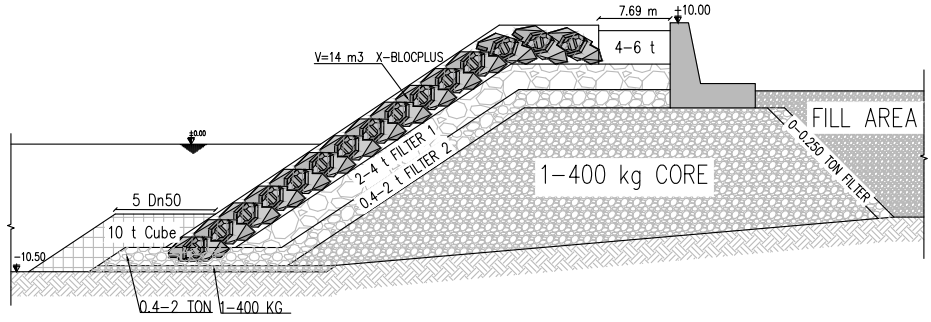

Figure B.6. Section BB without XblocPlusOvertop® units and cube blocks in the toe

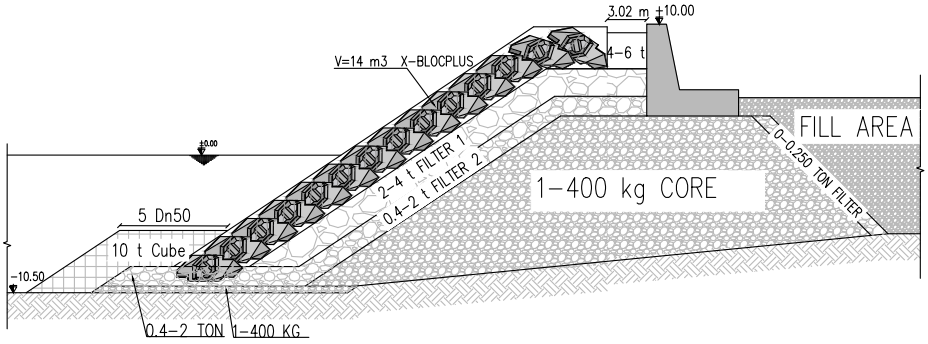

Figure B.7. Section BB without XblocPlusOvertop® units and cube blocks in the toe, shortened G_c

C. Individual Scour Measurement Results for All Profiles

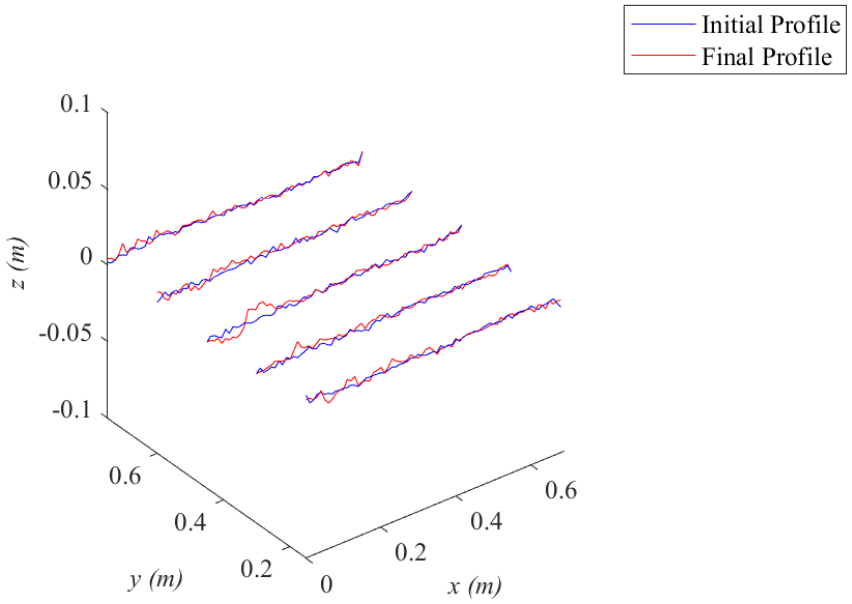

Figure C.1. Average initial and final scour measurements for Section AA2, D4.1

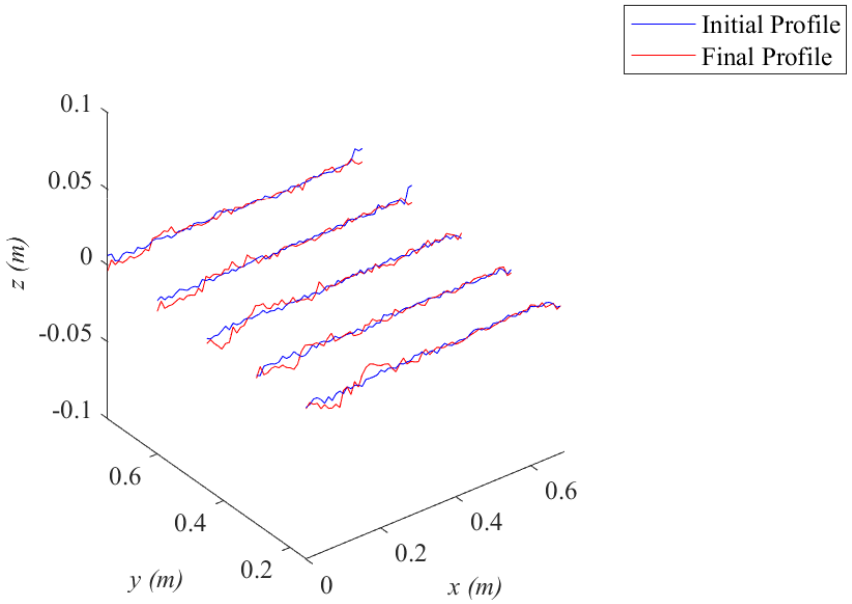

Figure C.2. Average initial and final scour measurements for Section AA2, D4.2

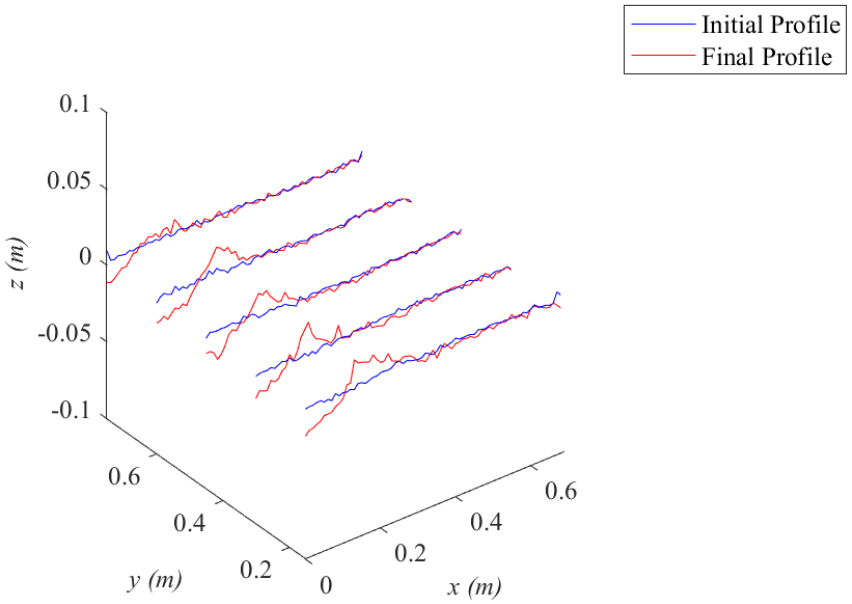

Figure C.3. Average initial and final scour measurements for Section AA2, D5

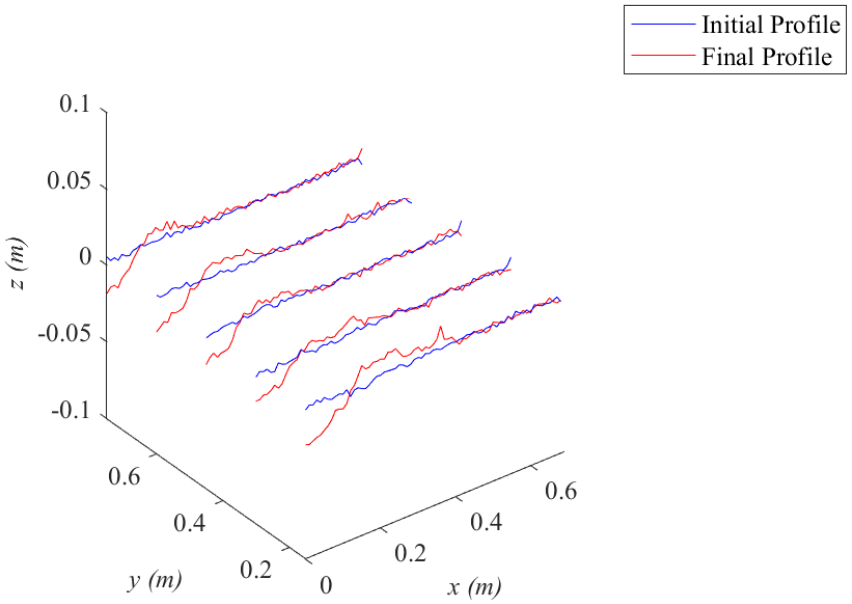

Figure C.4. Average initial and final scour measurements for Section AA2, D6

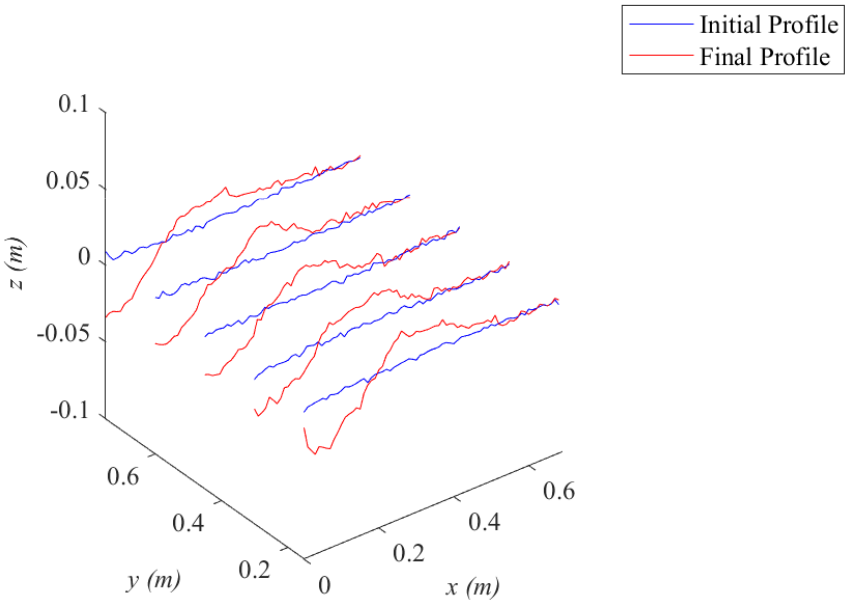

Figure C.5. Average initial and final scour measurements for Section AA2, D7

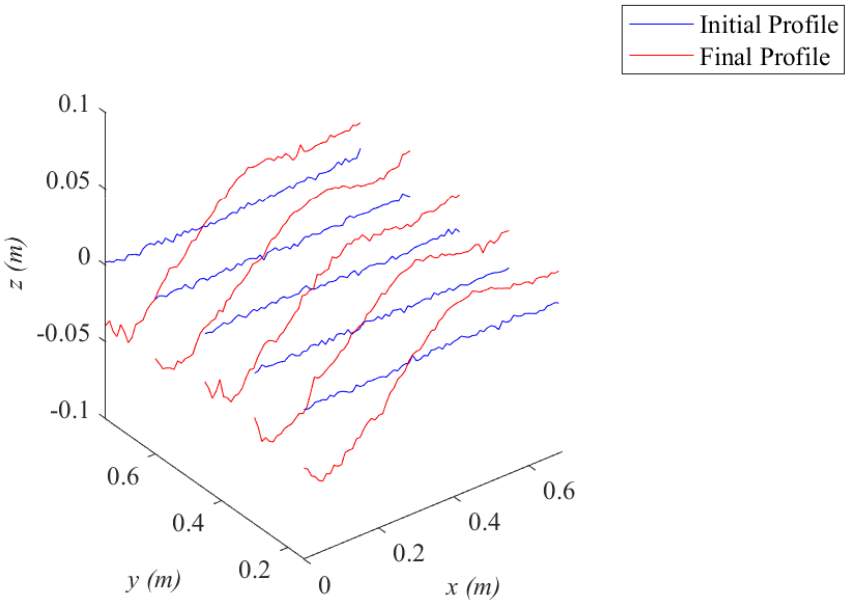

Figure C.6. Average initial and final scour measurements for Section AA2, D8

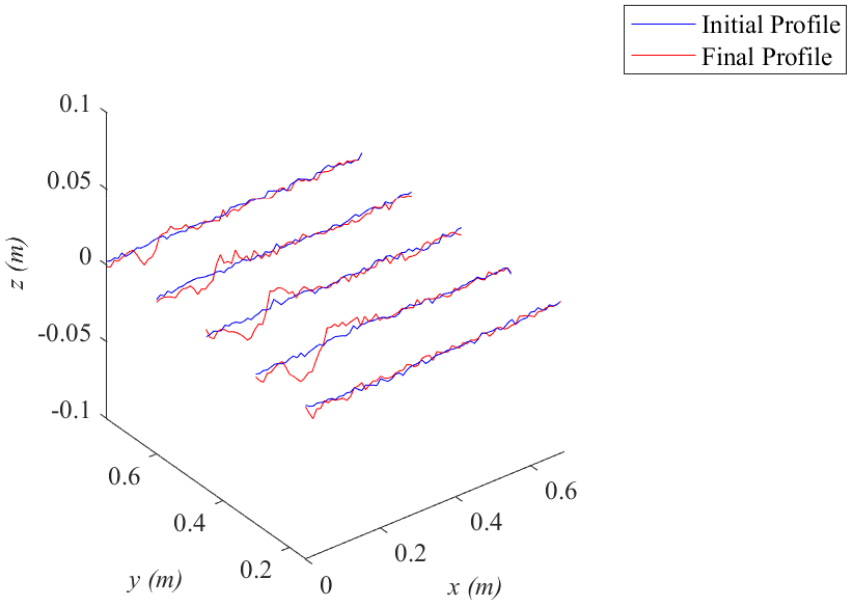

Figure C.7. Average initial and final scour measurements for Section BB, D5

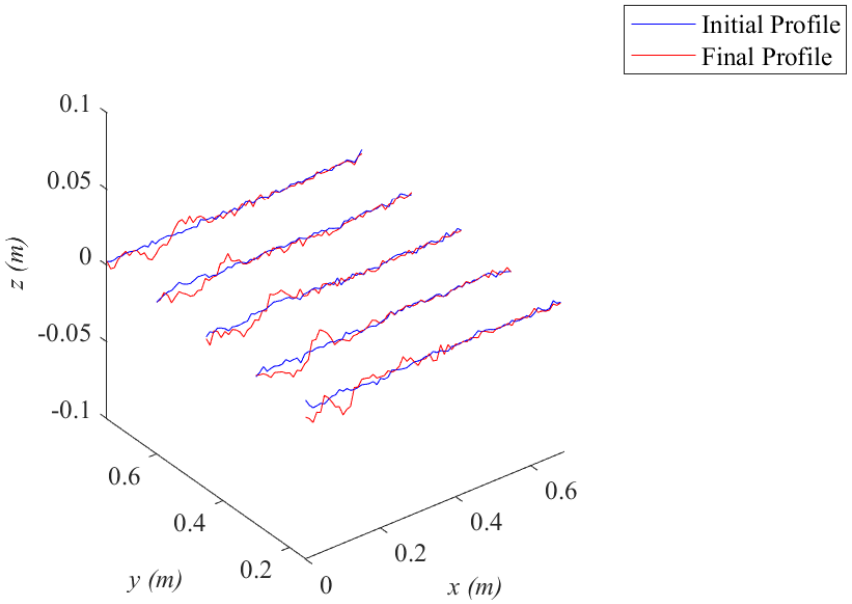

Figure C.8. Average initial and final scour measurements for Section BB, D6

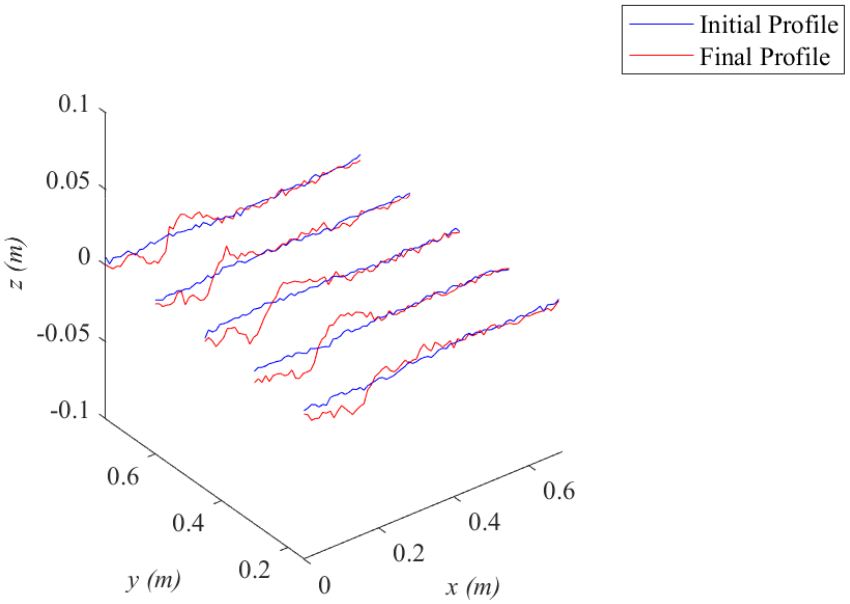

Figure C.9. Average initial and final scour measurements for Section BB, D7

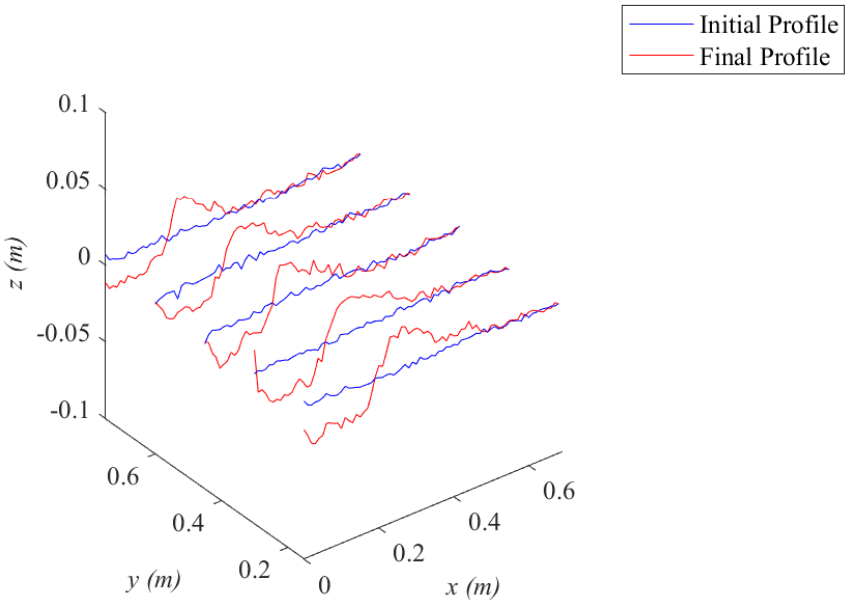

Figure C.10. Average initial and final scour measurements for Section BB, D8